Doctoral Dissertation

Study of Smart Antennas for High Speed Wireless Communications

（高速無線通信用スマートアンテナに関する研究）

December 21, 2001

Under the Supervision of

Associate Professor Hiroyuki Arai

Presented By

Kohei Mori

Division of Electrical and Computer Engineering
Faculty of Engineering
Yokohama National University

Abstract

In recent years, a high-speed wireless communications is strongly required. In wireless communication systems, some multipath fading, delay signal and interference signal is occurred by reflection or diffraction. In a high-speed wireless communications, it becomes an important issue to separate desired signal and delay or interference signal. Smart antenna for overcoming this problem is using high function antennas. Smart antenna solutions presented on different aspects of code technology, such as active antennas, fixed beam forming and adaptive beam forming techniques, to improve spectral efficiency and to deliver significant improvements in coverage, quality of service and capacity. This thesis describes smart antennas for high-speed wireless communications. Generally, although smart antennas show only an adaptive antenna which used adaptive signal processing, we discuss that all highly function antennas are shown to it in this thesis. We describe investigation and verification of smart antennas is performed from three different viewpoints. One is sector antenna, anther is digital beam forming array antenna, and the other is active antenna.

Sector antenna, which limit a direction of radiation by resolving directivity of antenna into sectors is one of fixed multi-beam antenna (smart antenna). We present 6-sector beam antenna using proximity coupled taper slot antenna in order to aim at low cost and simple manufacturing process of sector beam antennas. By arranging reflection board of parasitic element, side lobe level is suppressed. 6-sector beam antenna has uni-directional pattern and its half power beam width is about 60° in H plane. We also presented a delay profile is measurement by using the PCTSA sector antenna at outdoor. This 6-sector antenna used can reduce a delay spread many times than omni directional antenna used in almost fixed points and movement environment. Therefore, the sector antenna is suited for the high-speed wireless communications, because this sector antenna can reduce effectively a delay spread at outdoor.

The digital beamforming (DBF) array antenna is a kind of the smart antenna which can realize the desired beamforming and null steering by adjusting weight parameters of antenna elements using digital signal processing. In this thesis, we propose low cost DBF array antenna systems and reported its evaluation based on our experimental results. The proposed system is partially constructed by digital devices for the simplification of hardware, and employs some techniques for the resolution improvement. The system is evaluated through the DOA estimation by the MUSIC algorithm inside a radio anechoic chamber. As a result, we found that the proposed system estimates the DOA with the highest accuracy at which MUSIC algorithm could perform. Moreover, we

discusses on the estimation errors. We also found that the estimation error is particularly affected from the inaccurate element interval. This thesis also proposes the calibration method for restraint of phase and amplitude unbalance among array branches by using reference antenna. We also demonstrate near zero IF receivers. The conversion gain of this receivers is about 5 dB. We also examine this proposed receiver's ability to function as a digital beam former. As a result, we found that the ability of receiver is almost same that of common receivers using isotopic antenna.

Regarding the stability of the single active antenna, this thesis proposed an FET active antenna using a coplanar waveguide and an active antenna with a parasitic element in which a half-wave dipole parasitic resonator is placed above the gate-to-drain. By providing the parasitic resonator, the frequency stability is improved fourfold over the single oscillator and the active antenna combined with a patch antenna, without modifying the active antenna. It is confirmed that the parasitic resonator can improve the radiation pattern. This thesis also proposes the self-oscillating mixer using the active oscillator with the parasitic element of half-wavelength dipole. The IF gain of this self-oscillating mixer is increased by the parasitic element, compared only active oscillator.

The foundation materials to realize high-speed wireless communication by showing the example of these smart antennas are provided. The common point of these antennas is raising the performance of the wireless communication equipment not only combining antenna technology but also combining other technology (signal processing, microwave circuit, etc.). In order to realize high-speed wireless communications, it is indispensable to unite with two or more technologies like smart antennas.

Table of Contents

1. Introduction

1.1. Wireless communication

In connection with arrival of an information society in recent years, wireless communications prosper and that of market grow rapidly. Due to multimediaization of data, it is required that not only voice telephone calls but also any data, such as pictures and animations, is transmitted. The increasing demand for wireless communications is forcing the use of higher frequency band in order to use more channel capacity and higher-speed data transmission. The specification of the system of the wireless communications is shown in Fig. 1-1. In case of cellular phone (Cellular (PDC)), we can generally communicate without cutting off with high-speed movement, but a speed of data communications is comparatively low speed with 9600 bps (bit per second). On the other hand, in the case of wireless LAN systems used in small office, although a speed of data communications is generally high, it can communicate only in the fixed environment. Therefore, current wireless communication systems have good points and bad points. While, our requirement to realize high-speed wireless data communications with movement in the environment (the domain of the star of Fig. 1-1) rises. In case of mobile telephone service, the service of the 3rd generation (3rd G) was available at 2001. This service provided high-speed data transmission of 2 Mbps for local areas and 384kbps for global areas. After the next generation (4th G), the data speed of this system will be required to more than 20 Mbps. Furthermore, in the next generation, a super-high speed wireless data transmission equivalent to cable communications beyond 100 Mbps will be required, and it is likely that this tendency also continues in future.

In wireless communication systems, it is rare that a radio wave is received directly and a signal is received through various propagation paths, such as reflection of buildings and diffraction, etc. as shown in Fig. 1-2. This environment is called multiple path propagation. Under this propagation, some multipath fading, delay signal and interference signal is occurred by a reflection or diffraction. Wireless communication systems are limited in performance and capacity by three major impairments. The first of these is multipath fading, which cause by multiple path that the transmitted signal can take to the receive antenna. The signals from these paths add with different phases and times, resulting in a received signal amplitude and phase that vary with antenna location, directivity, and polarization. This increases the required signal power for given bit error rate (BER).

The second impairment is delay spread, which is the difference in propagation delays between paths. When the delay spread exceeds about 10 percent of symbol rate, significant intersymbol

interference can occur [1]. In case of a radio line design of data communications speed 10kbps degree, a deterioration rate of line is divided by noise and co-channel interference so that a data communications speed can almost ignore an error caused by multipath propagation. It is possible to separate between desired signals and delay signals by time difference, because a data communications speed is slower than delay times occurred by reflection or diffraction. However, for example a data communications speed is more than 1 Mbps, it is difficult to separate delay signals by time difference and it is unable to distinguish as desired signals, since a data communications speed is faster than delay times, Therefore, it becomes an important issue to separate between desired signals and delay signals.

The third impairment is co-channel interference. Cellular phone systems divide the available frequency channels into channel sets, using one channel set per cell, with frequency reuse. This results in co-channel interference, which increases as the number of channel sets decreases. For a given level of co-channel interference, a capacity can be increased by shrinking the cell size, but the cost of additional base stations rise[2].

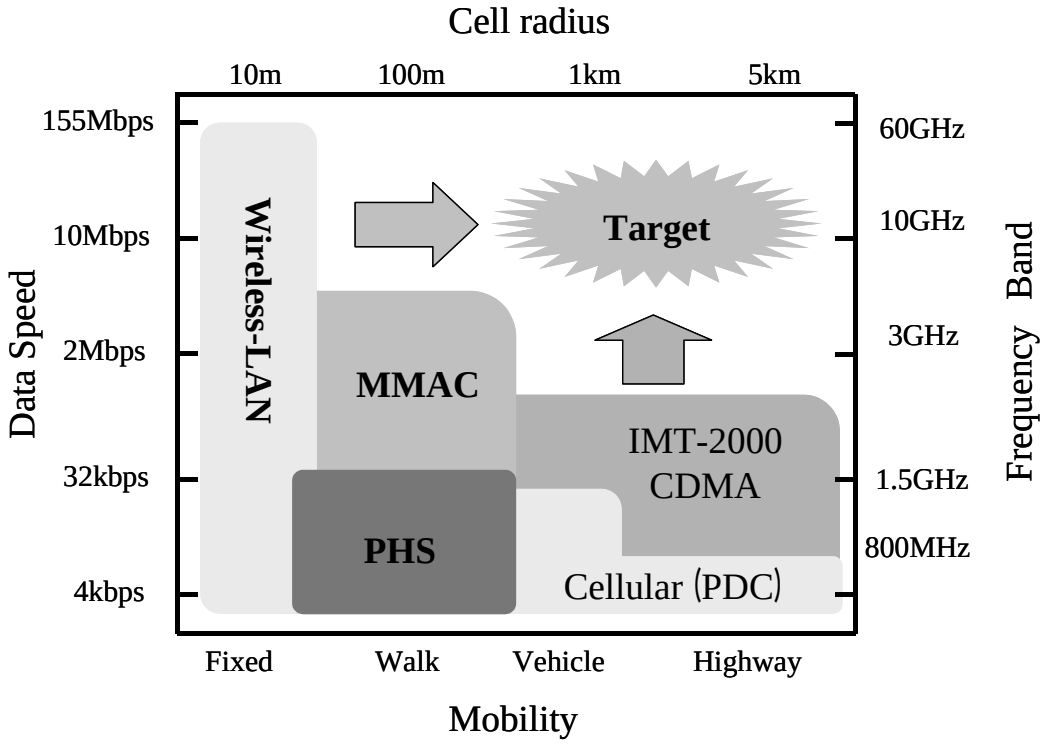

PHS: Personal Handy Phone System

PDC: Personal Digital Cellular

MMAC: Multimedia Mobile Access Communication

Fig. 1-1: Specification of system of the wireless communications

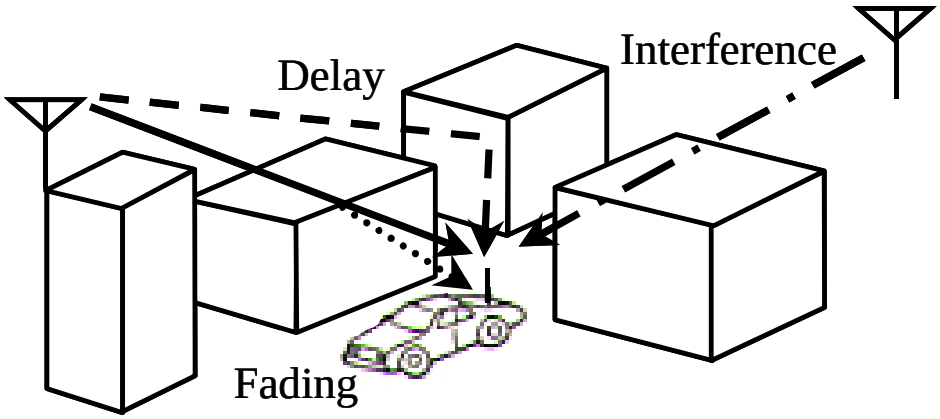

Fig. 1-2: Multiple path propagation

1.2. Smart antenna

Let us now consider some technology to overcome these impairments, thereby taking greater coverage and capacity at each base station, electric power at terminal. The technology of smart antenna technology is investigated that the C/N (carrier to noise) ratio can be increased. Moreover, it can overcome the problems in high speed mobile communication such as the limited channel bandwidth while satisfying the demand for many mobiles in a limited communication channel [3]. Smart antenna solutions presented on different aspects of code technology, such as active antennas, fixed beam forming (for example, sector antenna) and adaptive beam forming techniques, to improve spectral efficiency and to deliver significant improvements in coverage, quality of service and capacity. Therefore, smart antennas are the technology of uniting not only antenna technology but also two or more of other technology, and high function of antennas. Generally, although smart antenna shows only the adaptive antenna which used adaptive signal processing, we discuss that all highly efficient antennas are shown to it in this thesis. There are an active antenna united with microwave circuit technology and a multi-beam antenna using the directivity of an antenna. Furthermore, we can classify a multi-beam antenna roughly into a fixed beam antenna such as a sector antenna and a beam forming antenna which can scan antenna beams. In addition, we can classify above-mentioned adaptive antenna to a multi-beam antenna. This thesis discusses three kinds of smart antennas. This thesis is intended as an investigation to develop low complexity smart antenna structures for high-speed wireless communication systems. Smart antenna test beds will be developed, and various antenna configuration and algorithms will be investigated.

In addition, the following critical issues will be addressed:

- Sector antenna architectures by using PCTSA and performance
- Propagation measurements by using sector antenna and direction of arrival statistics

· Antenna configuration and calibration method development for digital beamforming

· Combination of microwave circuit and antenna technology

References

[1] P.A.Bello and B.D.Nelin, “The effect of Frequency Selective Fading on the Binary Error Probabilities of incoherent and Differentially Coherent Matched Filter Receivers”, IEEE Trans Communication System, Vol. CS-II, pp170-186, June 1963.

[2] Jack H. Winters, “Smart Antennas for Wireless System”, IEEE Personal Communications, vol.1, pp.23-27, Feb 1998.

[3] Michael Chryssomallis, “Smart Antenna”, IEEE Antennas and Propagation. Magazine, vol.42, no.3, pp.129-136, June 2000.

2. Sector Antenna

2.1. Introduction

A delay signal is occurred from multi-path propagation by reflection or diffraction. In high speed wireless data transmission, it becomes an important issue to separate delay signal and desired signal. Sector antennas can remove delay signal effectively and reduce delay spread. A delay spread is expresses dispersion of the echo of a direct wave and has a close relation to bit error rate (BER). According to [4], this problem is conquerable by using the multi-beam sector antenna according to propagation environment, in the propagation analysis using the geometric optical model. Sector antennas, which limit a direction of radiation by resolving directivity of antenna into sectors are one of fixed multi-beam antenna. For sector antenna, thin horn antenna [5], monopole Yagi-Uda arrays [6] have been suggested.

In this chapter, the sector antenna using proximity coupled taper slot antenna (PCTSA) is proposed, in order to aim at low cost and simple manufacturing process at high frequency band. This sector antenna will be mounted the roof of vehicles, and also used indoor and outdoor base station for Micro or Pico cell. However, its radiation pattern is seriously affected by the ground plane and mutual coupling between elements. This chapter presents a method of radiation pattern enhancement of 6-sector antenna using proximity coupled taper slot. Moreover, sector antenna with much number of sectors generally reduces delay spread. This chapter also presents 12-sector antenna using PCTSA. We optimize a parameter of PCTSA, and improve radiation pattern by using reflectors, to demonstrate12-sector antenna experimentally.

Moreover, in high speed wireless communications, a delay profile measurement is an important issue, in addition to a measurement of electric field strength. We need to understand the form of delay profile, in order to rake receptions for the wide-band transmission. Then, a measurement of delay profile needs to be for not only rake receptions, but also modeling of delay spread. Although studies have been made on the sector antenna in the inside such as Wireless LAN systems, there are little reports on outside environment. This chapter also presents a delay profile is measured by using the sector antenna at outdoor environment. We evaluate this delay profile measurement by using delay spread, because it is related to the transmission error rate, present the quantities of reduction of the delay spread by using 6-sector antenna. We also describe the estimation of DOA and propagation environment by using delay profile measurement.

2.2. Sector antenna using PCTSA

2.2.1. Proximity Coupled Taper Slot Antenna

The proximity coupled taper slot antenna (PCTSA) is proposed for millimeter wave applications. The PCTSA consists of two taper slots different in length. The right tapered slot is a radiation element and the left one is electromagenetically coupled exciting dipole antenna, two taper slots are connected with slot line. However, the balanced feed structure using half wave dipole antenna is not suitable for mobile antenna application. Moreover the height of the PCTSA is relatively high. The PCTSA has symmetrical structure about feeding point, then antenna mounted on the ground plane is assumed to have the identical characteristics. To separate the feeding probe from tapered slot antenna, a quarter wave monopole antenna is used to excite coupling slot shown in Fig. 2-1. The coupling parameters between exciting tapered slot and monopole antenna are LC, PL, θc, and the spacing D. The resonant frequency with exciting monopole antenna is fixed by LC, PL, and θc. The gain deviation is very small even if the spacing D is changed. Therefore, the PCTSA is tolerant in production error, which is a serious problem in high frequency region. Uni-directional radiation pattern is obtained without reflector, and its half power beam width is about 60° in H plane, and front gain is about 6 dBi. The disadvantage of proximity coupling is the frequency band limitation due to the exciting monopole characteristics. However, 3dB half-power bandwidth in antenna gain of about 50% is sufficient for mobile antenna application.

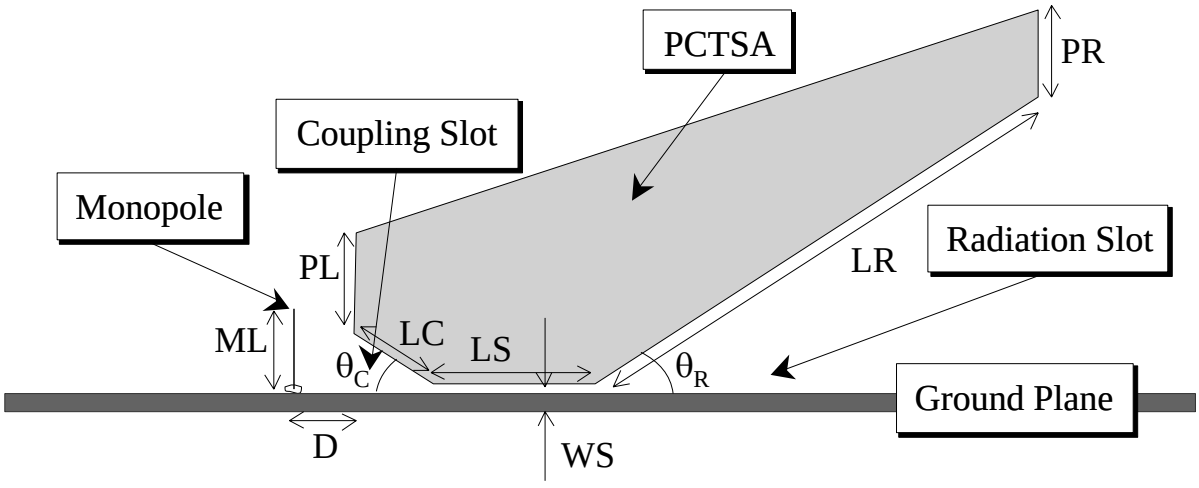

Fig. 2-1: Proximity coupled taper slot antenna (PCTSA) fed monopole antenna

2.2.2. 6-Sector antenna using PCTSA

The PCTSA has uni-directional pattern and its half power beam width is about 60° in H plane. If we make concentric array by this PCTSA, 6-sector antenna is easily obtained. The half part of taper slot made with dielectric substrate is excited by quarter wavelength monopole antenna shown in Fig. 2-1. The radiation pattern of this antenna is shown in Fig. 2-2. Its half power beam width is about 60° in this example, however side lobe level around ±90° is increased. Then, it is necessary to pattern enhancement for this model.

Fig. 2-3 shows 6-sector antenna using 6 PCTSA elements. In this array design, the PCTSA (type of Fig. 2-1) is arrayed concentrically on the circular disk ground plane. Each element is a half part of taper slot excited by quarter wavelength monopole antenna. The radiation pattern of this antenna is shown in Fig. 2-4. Its side lobe level is a little bit suppressed than that of Fig. 2-2. To suppress the side lobe level, parasitic reflectors are mounted shown in Fig. 2-5. A square parasitic reflectors ($0.56\lambda \times 0.75\lambda$) is arranged by an acute angle for PCTSA in radiation taper neighborhood of PCTSA. The radiation pattern of this sector antenna is shown in Fig. 2-6. Beam width becomes a little narrow and side lobe is decreased because parasitic elements concentrate side lobes on center. We obtain smaller side lobes rather then that without reflector, it's radiation pattern is not suitable for sector antenna. The pattern degradation is assumed to be occurred by mutual coupling between exciting probes. Then, we use partition to reduce the mutual of this array.

Fig. 2-7 shows its configuration. Excited by quarter wavelength monopole antenna that is arrayed on the circle of 50 mm in diameter, the PCTSA made by aluminum board is sustained by FRP (insulator) to make small gap between the taper slot and ground plane disk 250 mm in diameter. We use the partition for each monopole to reduce mutual coupling and also use parasitic reflectors. A dielectric substrate is not used for this prototype model, because a dielectric substrates sometimes have frequency dispersion around the antenna operating frequency 8 GHz. Fig. 2-8 shows H and E plane radiation pattern of sector1 at 8.45 GHz. Half power beam width is about 60°, and side lobe level is suppressed below –10 dB and uni-directional pattern is obtained. Fig. 2-9 also shows radiation pattern of all sectors at 8.45 GHz. A frequency characteristic of horizontal plane directivity is shown in Fig. 2-10. Even if frequency band changes, a horizontal radiation pattern is hardly changed. In a broadband of 7-9 GHz, we can obtain 6 sector beam antenna in horizontal plane. The input characteristic of each sector is shown in Fig. 2-11. The frequency bandwidth is more than 10%, and isolation among sectors is more than 30 dB. It is sufficient for high wireless communication sector antenna.

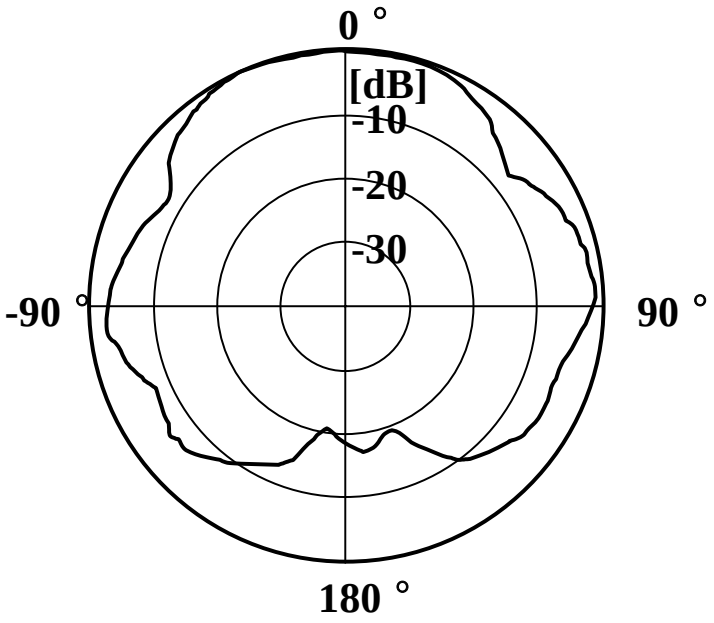

Fig. 2-2: Radiation pattern of PCTSA

LC = 17.9mm, LS = 25.7 mm, LR = 53.5 mm, $\theta_c = \theta_R = 20°$

PR = 20.9 mm, PL = 17.9 mm, WS = 0.1 mm, D = 10.0 mm

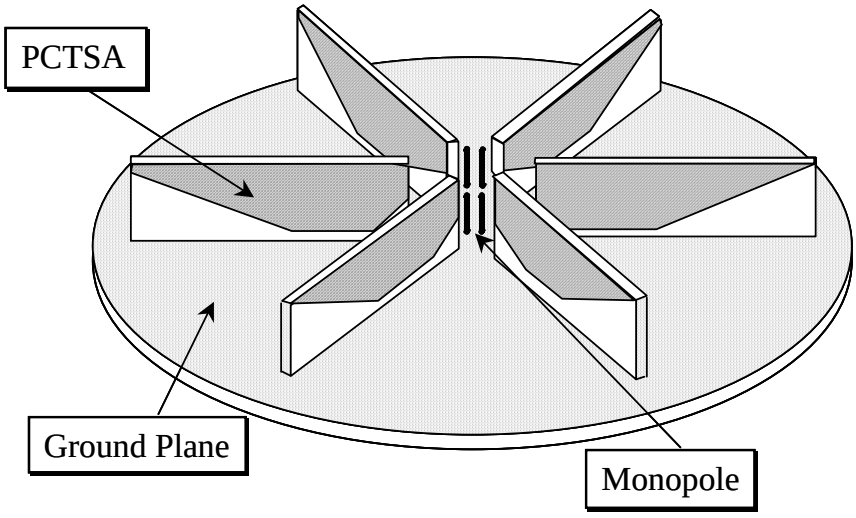

Fig. 2-3: 6-sector antenna using 6 PCTSA elements

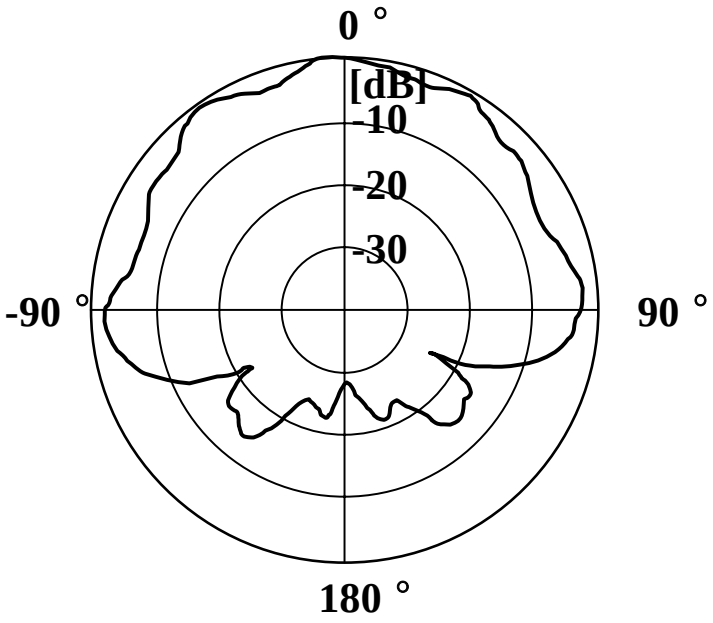

Fig. 2-4: Radiation pattern of 6-sector antenna using 6 PCTSA elements

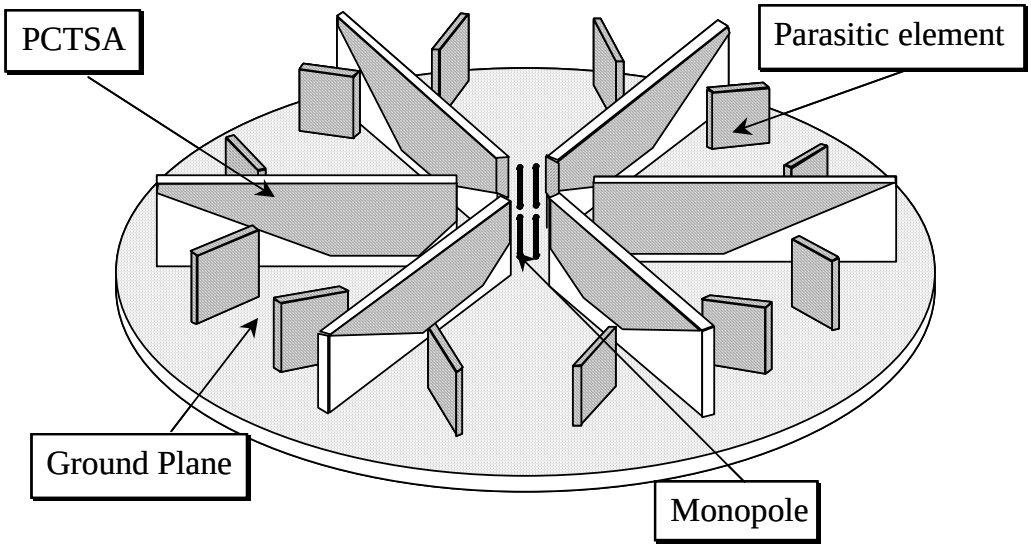

Fig. 2-5: 6-sector antenna using 6 PCTSA elements with parasitic reflectors

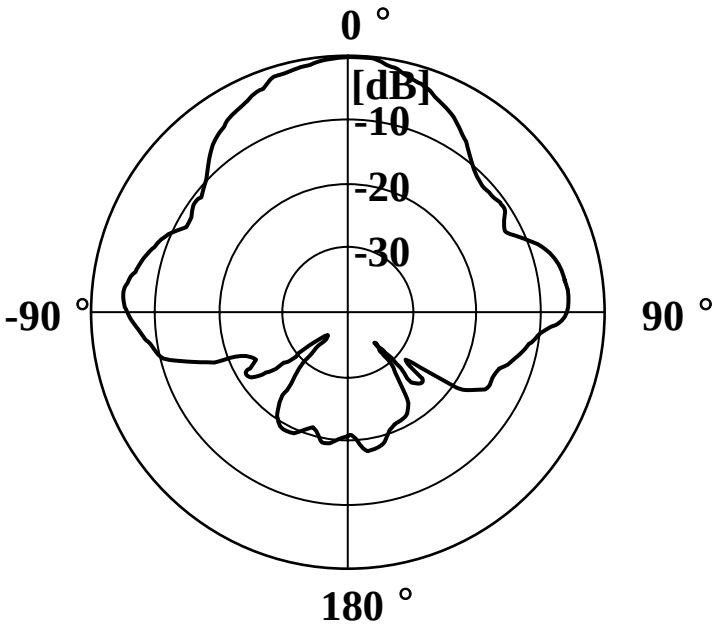

Fig. 2-6: Radiation pattern 6-sector antenna using 6 PCTSA elements with parasitic reflectors

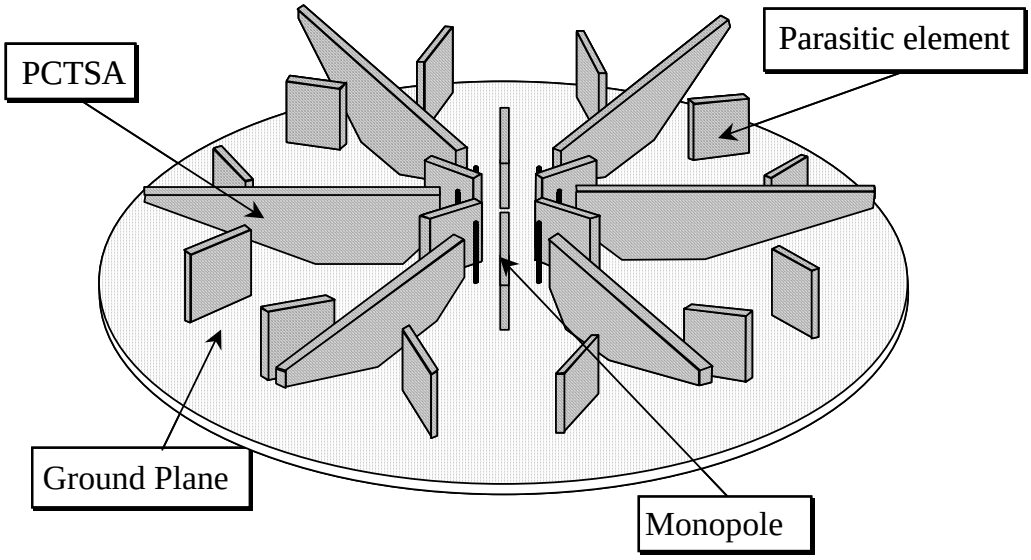

Fig. 2-7: 6-sector antenna using 6 PCTSA elements with parasitic reflectors for modified model

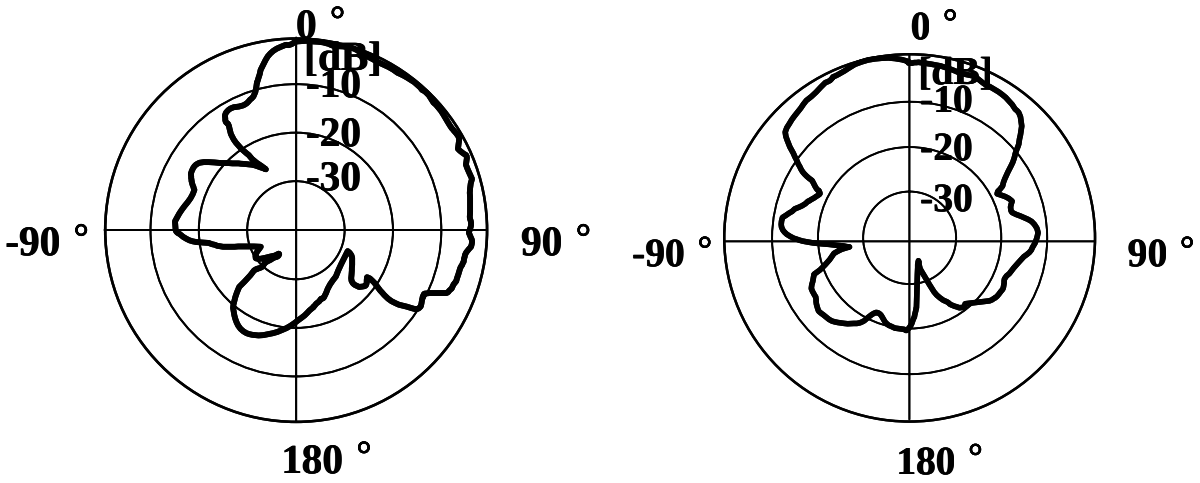

(a) E-plane (b)H-plane

Fig. 2-8: Radiation pattern 6-sector antenna at sector1
using 6 PCTSA elements with parasitic reflector for modified model

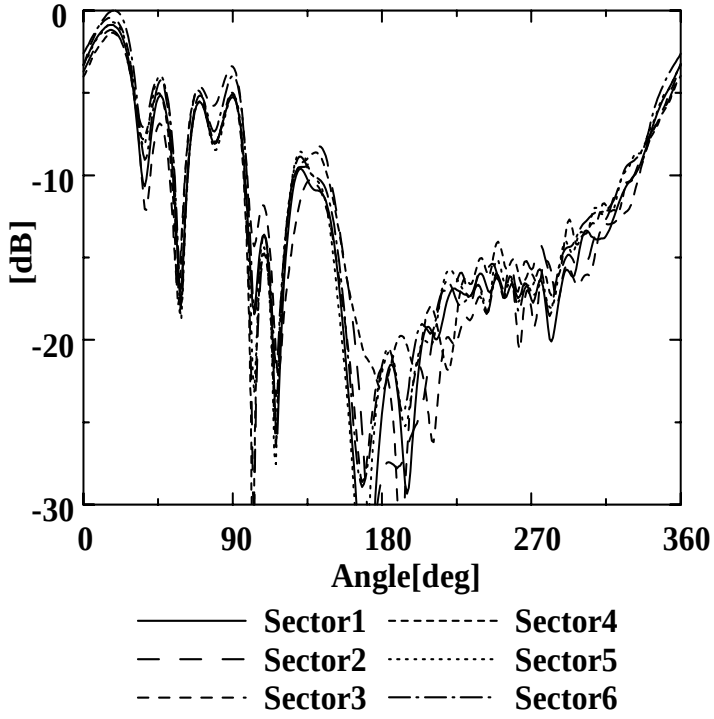

(a) E-plane

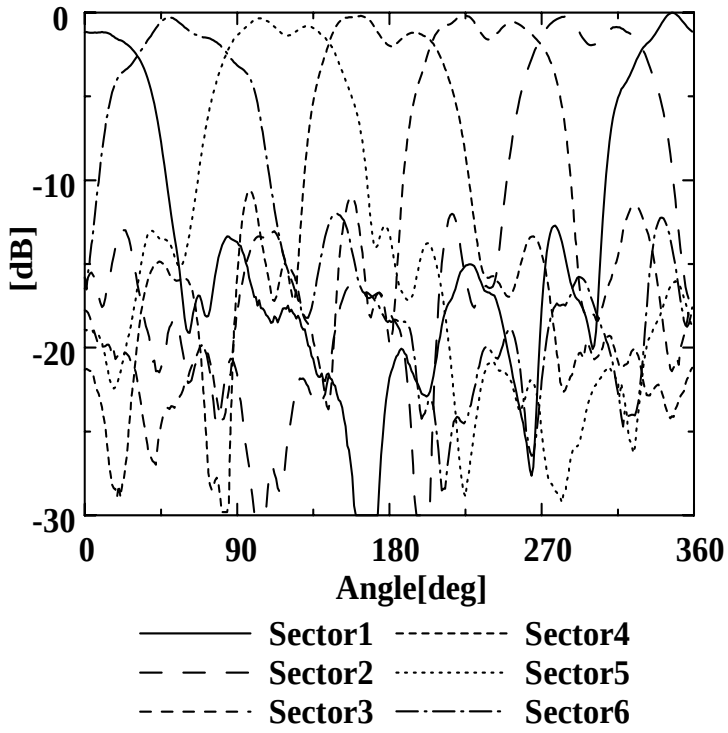

(b) H-plane

Fig. 2-9: Radiation pattern 6-sector antenna at 8.45GHz

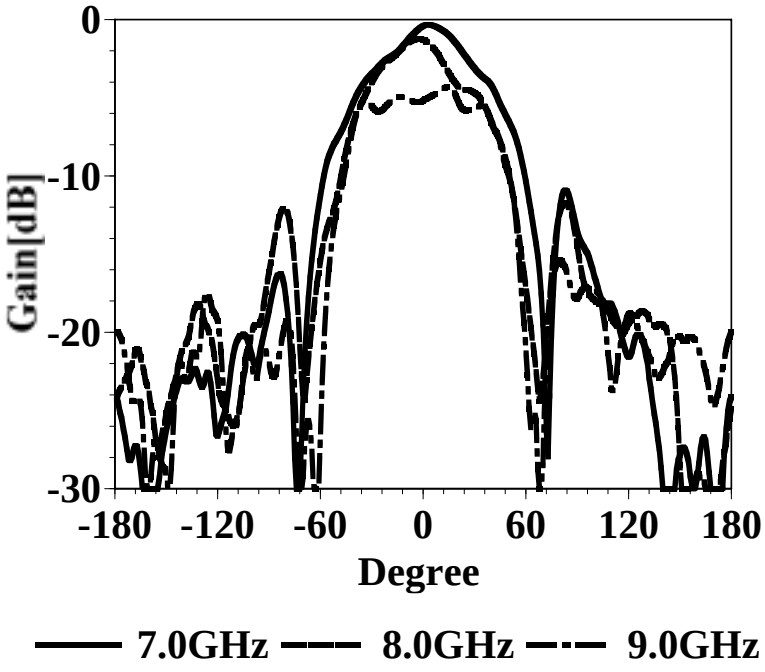

Fig. 2-10: Frequency characteristic of horizontal plane directivity

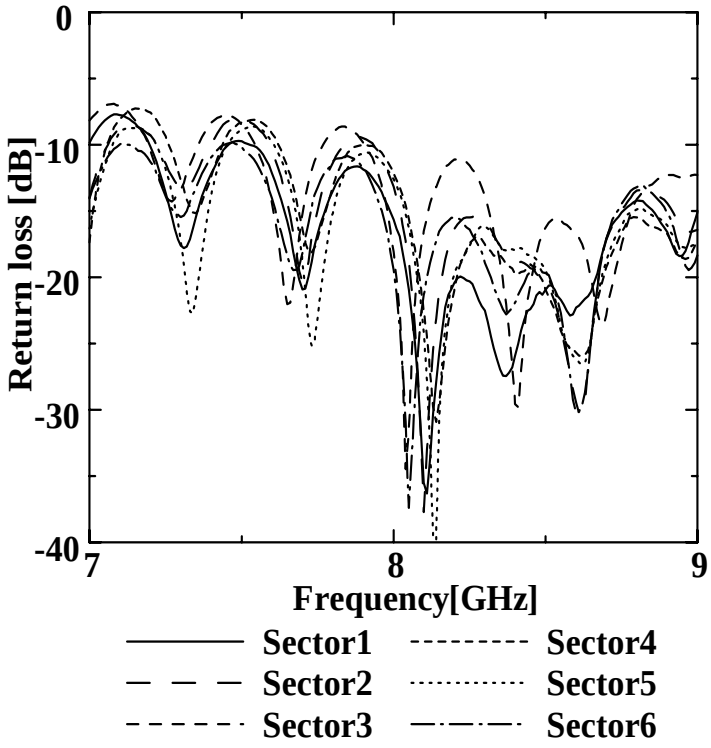

(a) Return loss each sector

(b)

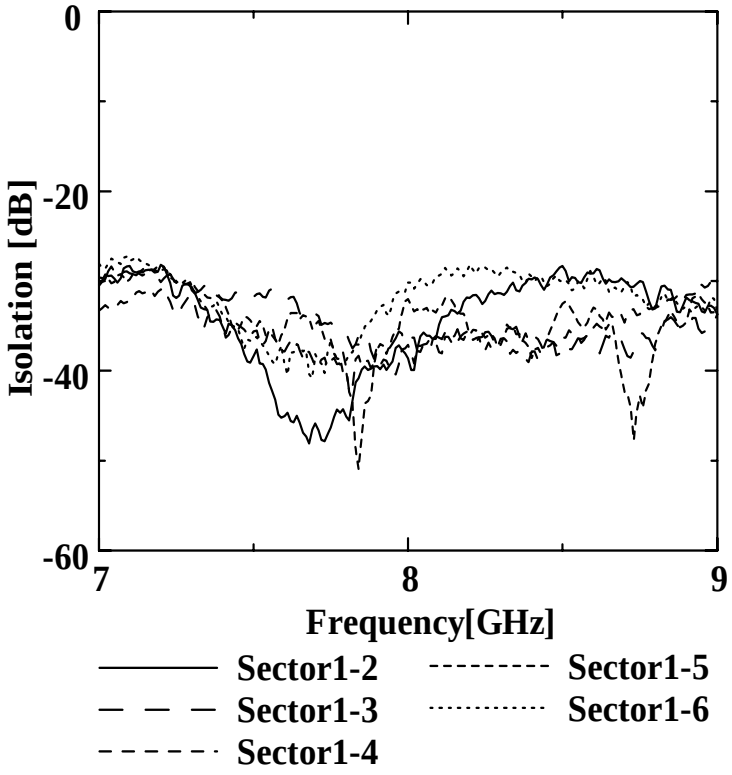

(b) Isolation among sector

Fig. 2-11: Return loss and isolation of 6-sector antenna

2.2.3. 12-sector antenna using PCTSA

2.2.3.1. Design parameters of PCTSA

The PCTSA with exciting monopole antenna has uni-directional pattern and its half power beam width is about 60° in H plane. If we make concentric array by this PCTSA, 6-sector antenna is easily obtained. However, the purpose of this section is to obtain parameters of PCTSA for 12-sector antenna. By FDTD simulation, the resonant current exists in edge of slot line and taper slot element, and a standing wave is observed along this line. Then the length of edge needs to be integer times of 1/2 wavelength in order to keep radiation condition. First, we change the parameters of coupling slot experimentally shown in Table.2-1. The parameter of III (PL = LC = 1/4λ, LS = 1/2λ) is suitable for an element for 12 sector antenna, because the half power beam width is narrow and front gain is high.

Let us change length of radiation taper slot (LR) and radiation taper slot angle (θ_R), to obtain the parameter to determine the half power beam width and front gain in H plane shown in Fig. 2-12 and Fig. 2-13. When the element length becomes longer, the half power beam width becomes narrow and front gain improves. However, the size of PCTSA becomes large, when element length becomes longer. In this section, the element length is designed to be 2λ, in order to make size of antenna small. When the radiation taper slot angle is widened, the half power beam width becomes narrow. However, we have an optimum taper slot angle to increase the front gain. The radiation taper slot angle are most suitable for 12-sector antenna in case of 20~30 degree.

Table.2-1:Front gain and a change of half power beam width by PL, LC, and LS
LR = 2λ, PR = 1/4λ,θc = θ_R = 20°, WS = 0.2 mm, D = 3mm, at f = 8.45GHz

	LC = LS = 1/4λ PL = 1/2λ (I)	PL = LS = 1/4λ LC = 1/2λ (II)	PL = LC = 1/4λ LS = 1/2λ(III)
Gain [dBi]	6.8	5.2	6.0
-3dB Beam width [Deg]	52.8	46.2	44.4

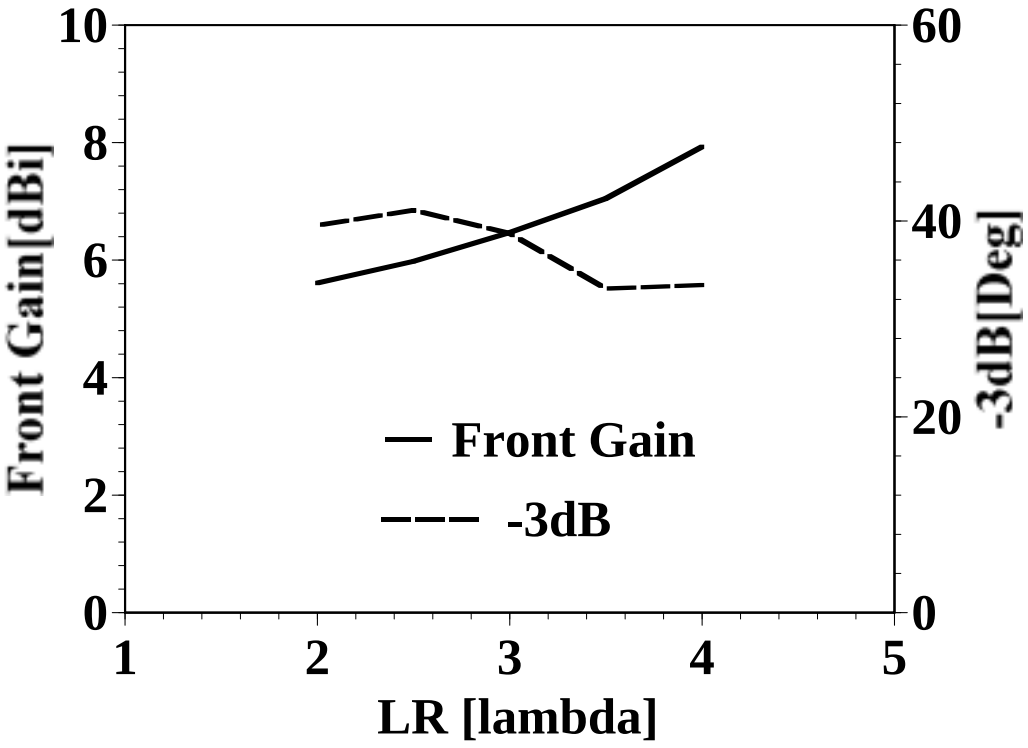

Fig. 2-12: Front gain and half power beam width by a change of LR

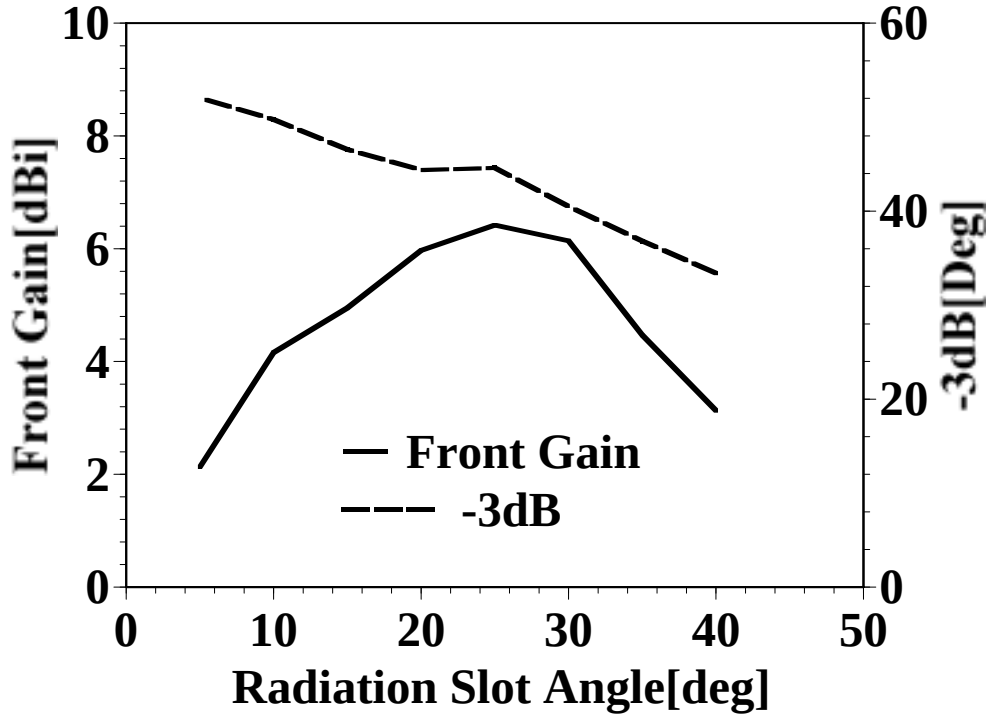

Fig. 2-13: Front gain and half power beam width by a change of θ_R

2.2.3.2. 12-sector antenna using PCTSA

Radiation pattern at 8.45 GHz, in case of PCTSA (PL = LC = 1/4λ, LS = 1/2λ, LR = 2λ, PR = 1/4λ,θc = θR = 20°, WS = 0.2 mm, D = 3 mm) is measured using the circular ground plane with a diameter of 250 mm shown in Fig. 2-14. The mutual coupling among adjacent elements increases side robe level and decreases F/B ratio, then it is necessary to improve radiation pattern by anther methods. For the radiation pattern shaping and F/B ratio improvement, there is technique to use a square parasitic element between sectors, but it is not effective for this sector model. For the radiation pattern enhancement, the cylindrical conductor (distance is 1/4 λ with monopole antenna, height = λ) behind feeding monopole antenna as reflector shown in Fig. 2-14. Because the reflector reduces back radiation from rear, then gain and half power beam width will be improved. Radiation pattern of 12-sector antenna using this cylindrical conductor is shown in Fig. 2-15. By arranging cylindrical reflector, the side lobe level is suppressed less than 15 dB. The characteristics of this sector antenna are summarized in Table.2-2. The input characteristic of sector element for 12-sector antenna is shown in Fig. 2-16. The frequency bandwidth is more than 10%, and isolation among sectors is about 20dB. It is sufficient for 12-sector antenna. Finally, we obtain PCTSA element for 12-sector antenna.

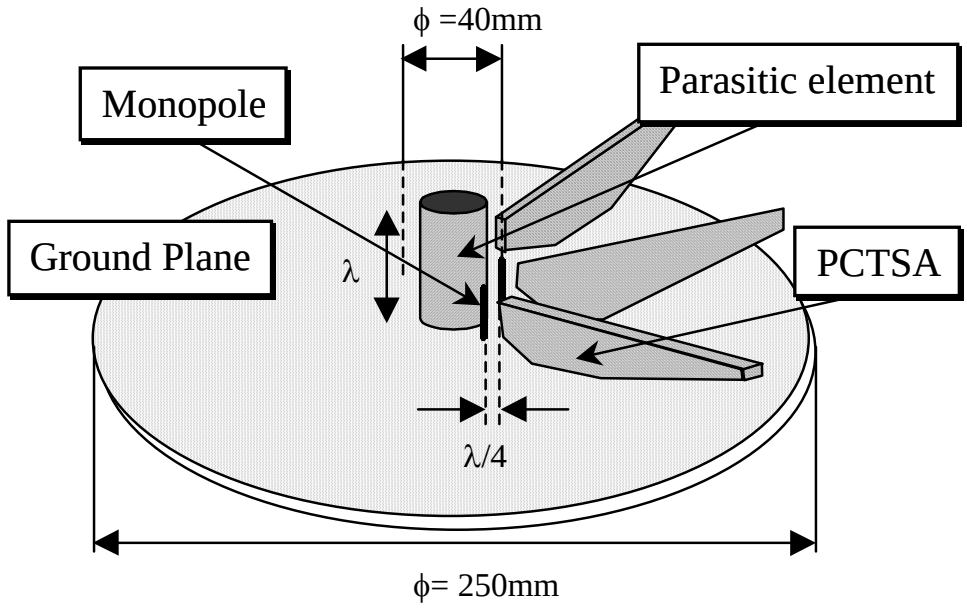

Fig. 2-14: 12-sector antenna (arranged the cylindrical parasitic element)

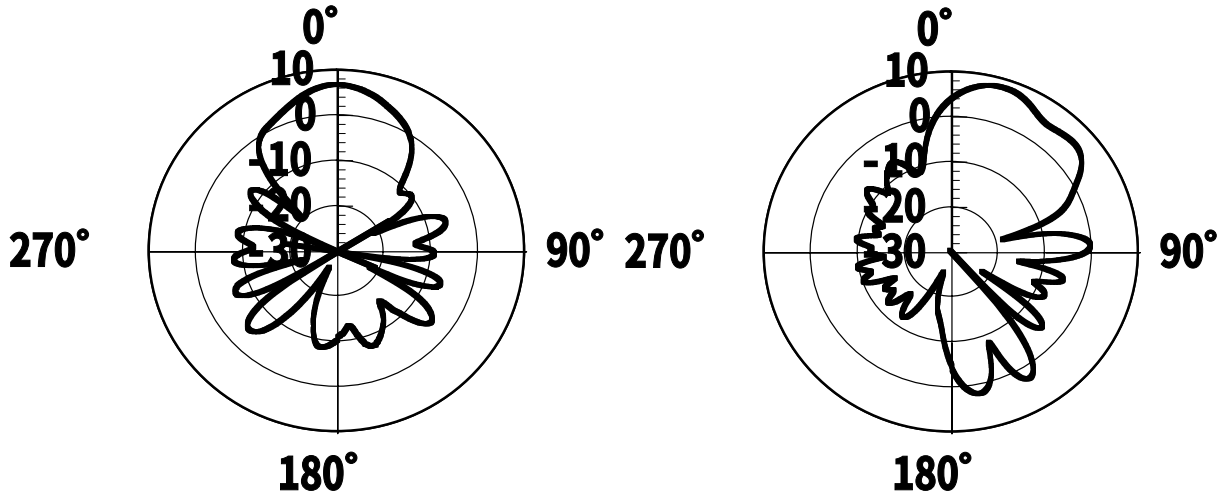

(a) E plane (b) H plane

Fig. 2-15: Radiation pattern of 12-sector antenna (at f = 8.45GHz)

Table.2-2:Characteristics of 12-sector antenna using PCTSA

LR = 2λ, PR = 1/4λ,θc = θ_R = 20°, WS = 0.2 mm, D = 3 mm, at f = 8.45 GHz

Gain [dBi]	Front Gain [dBi]	-3dB [Deg]	F/B [dB]
8.1	6.8	35.1	-17.0

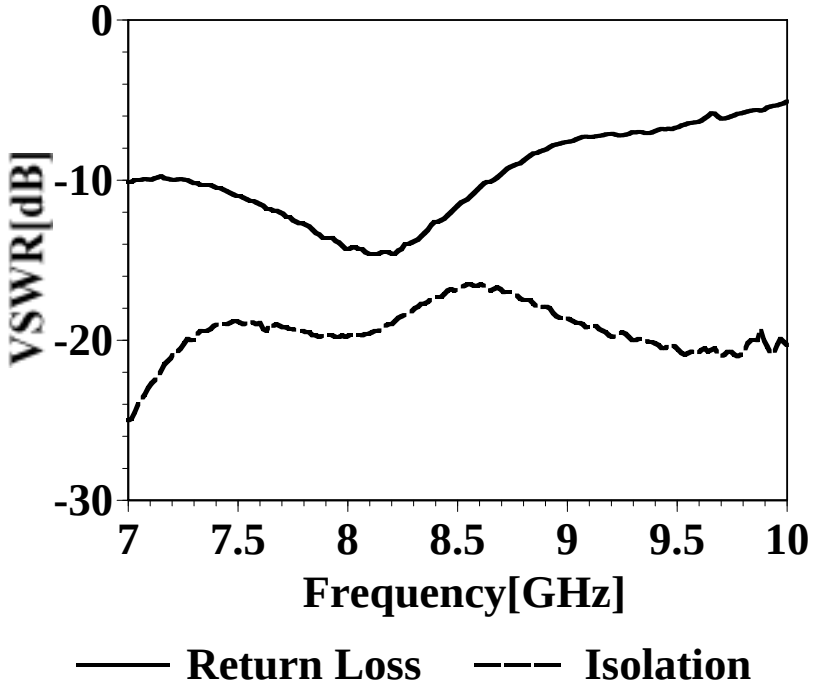

Fig. 2-16: Return loss and isolation of 12-sector antenna element

2.2.4. Summary

This section presented the 6-sector beam antenna using proximity coupled taper slot antenna. By arranging reflection board of parasitic element, the side lobe level is suppressed more than 15 dB. 6-sector beam antenna has uni-directional pattern, its half power beam width is about 60° in H plane and isolation among sector more than 30 dB.

This section also presented a 12-sector antenna using proximity coupled taper slot antenna. By optimizing the parameter of PCTSA, we demonstrated 12-sector antenna experimentally. By using cylindrical reflector, the side lobe level caused by the mutual coupling of adjacent element suppressed. This section presented that 12-sector antenna could be produced by using PCTSA. This sector beam antenna has front gain of 7 dBi and its half power beam width is about 30° in H plane.

2.3. Delay profile measurement using sector antenna

2.3.1. Delay profile measurement using sector antenna

This chapter present a delay profile is measured by using the PCTSA sector antenna at outdoor environment. Fig. 2-17 and Table.2-3 show the outline of delay profile measurement. Taking synchronism between a transmitter and a receiver by using two standard oscillators (Rubidium oscillator), a delay profile is measured at 8.45 GHz. By the data recorder, we record delay profile data (voltage value) and GPS data (time and position) in magnetic tape (DAT). The delay profile data is calculated from the voltage value in cause by calibrating data. An omni directional antenna is installed in the base station on the sixth floor of the building. Both of the omni directional antenna and the 6 PCTSA sector antenna are used for the mobile station. The delay profile is measured around Yokosuka research park (YRP). It's propagation environment is shown in Fig. 2-18. It is a suburb area surrounded fundamentally by a mountain, there is an area where a building floods, too. Therefore, it is suitable area for delay profile measurement, because it is the propagation environment that has two of suburb area and city area. The delay profile measurement is done with changing a receiving antenna (omni directional antenna and sector antenna) one after another at different propagation environment 21 fixed points (Fig. 2-18). Furthermore, moving the mobile station, the delay profile is measured at the course that are covered all 21 fixed points.

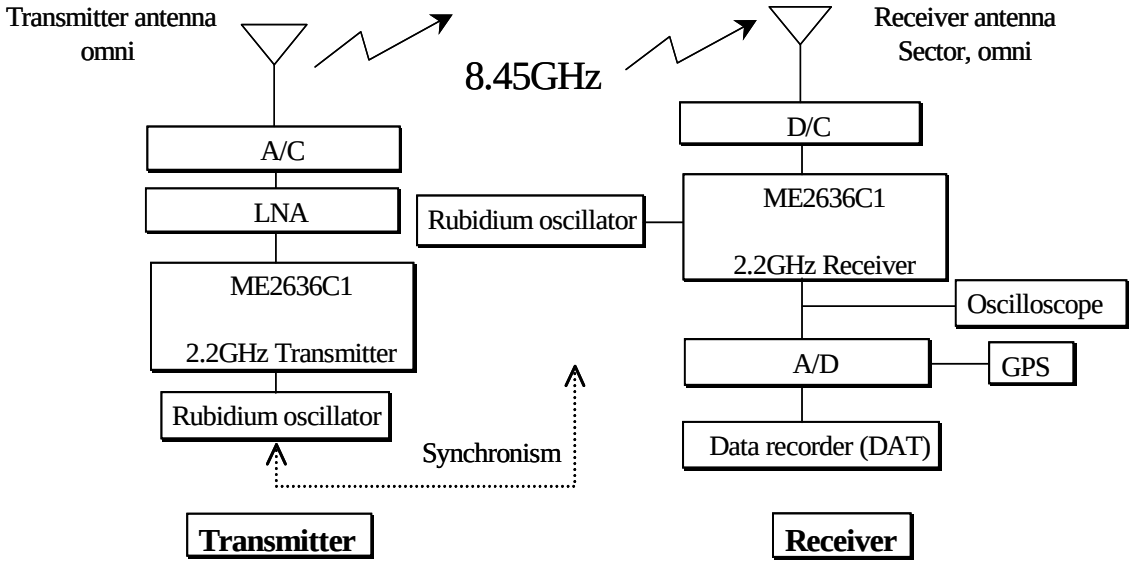

Fig. 2-17: Block dialog of delay profile measurement system

Table.2-3: Delay profile measurement system

Carrier frequency	8.45GHz
Power	+20dBm
Modulation	BPSK
Chip rate	50MHz
Tx	Omni-directional
Rx	Omni-directional, 6-Sector

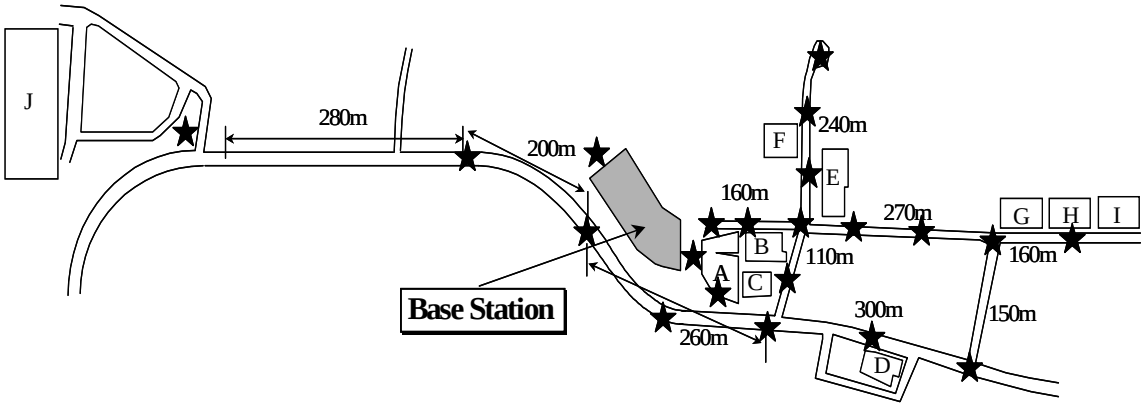

Fig. 2-18: Measurement environment (Asterisk: Measurement Point)

2.3.2. Suppressed Delay Spread By 6-Sector Antenna

We evaluate the delay profile by using the delay spread, because the delay spread is related to the transmission error rate (BER) [7]. First, we discuss the measurement at the fixed point. The fixed 21 measurement points of Fig. 2-18 contain various propagation environments (line of sight etc.). The cumulative distribution of delay spread is calculated shown in Fig. 2-19 and

Table.2-4. This delay spread is average of delay spread of 21-measurement point. The “sector n (n = 1~6)” indicates each sector of 6-sector antenna. This measurement result confirm that using sector antenna many times than by using omni directional antenna can suppress the delay spread except sector 6. Because there are almost measurement points that are not directed to base station in sector 6. However if we consider in the whole of sector antenna, the delay spread can be suppressed more than omni directional antenna. On the other hand, the delay profile is measured with the movement mobile station. The mobile station moved with the speed (about 20 Km/h) that a certain one delay profile became, the delay profile in the same point in consideration of the chip rate of this measurement. The cumulative distribution of delay spread is calculated shown in Fig. 2-20 and

Table.2-4. Same as the measurement in a fixed point, the delay spread can be suppressed more than omni directional antenna except sector 6. This reason why the beam direction of sector 6 hardly directed the direct wave direction while a base station is moved. However, if we change to the sector that the delay spread is small properly and received the desired signal, it is possible that we can get a good path.

Table.2-4: Media value of delay spread (unit [μs])

	Omni	6-sector antenna					
		1	2	3	4	5	6
Fix	0.315	0.171	0.094	0.145	0.103	0.241	0.351
Move	0.232	0.135	0.118	0146	0.07	0.139	0.283

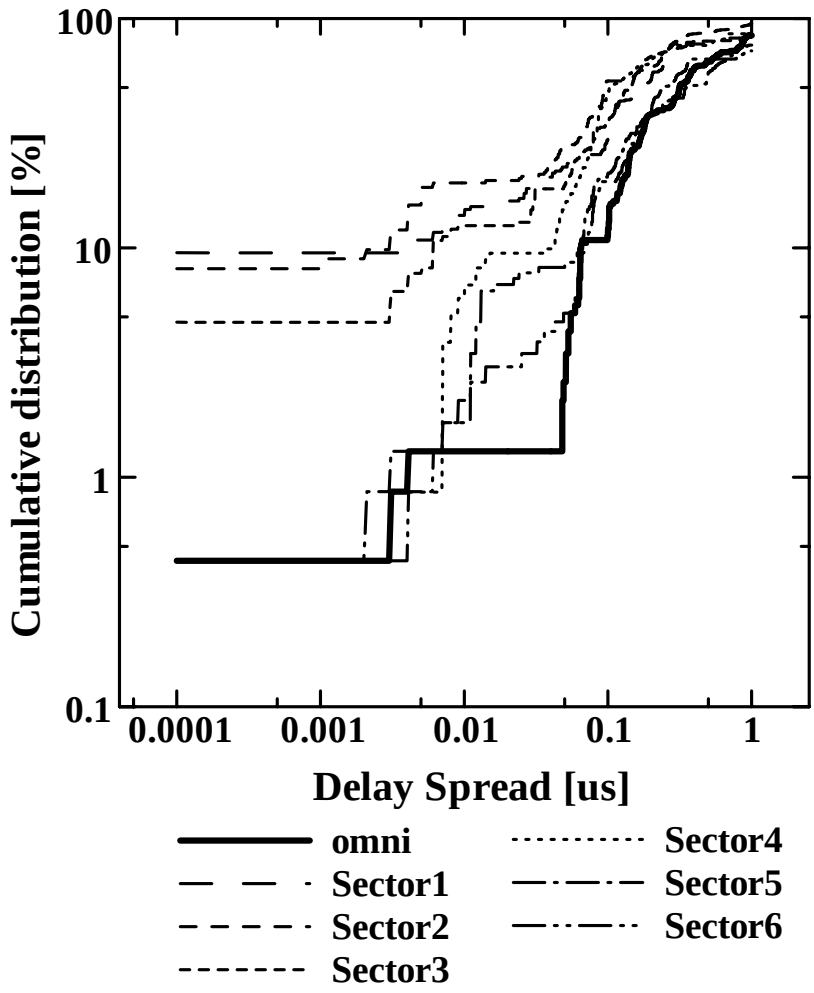

Fig. 2-19: Cumulative distribution of delay spread at Fix point

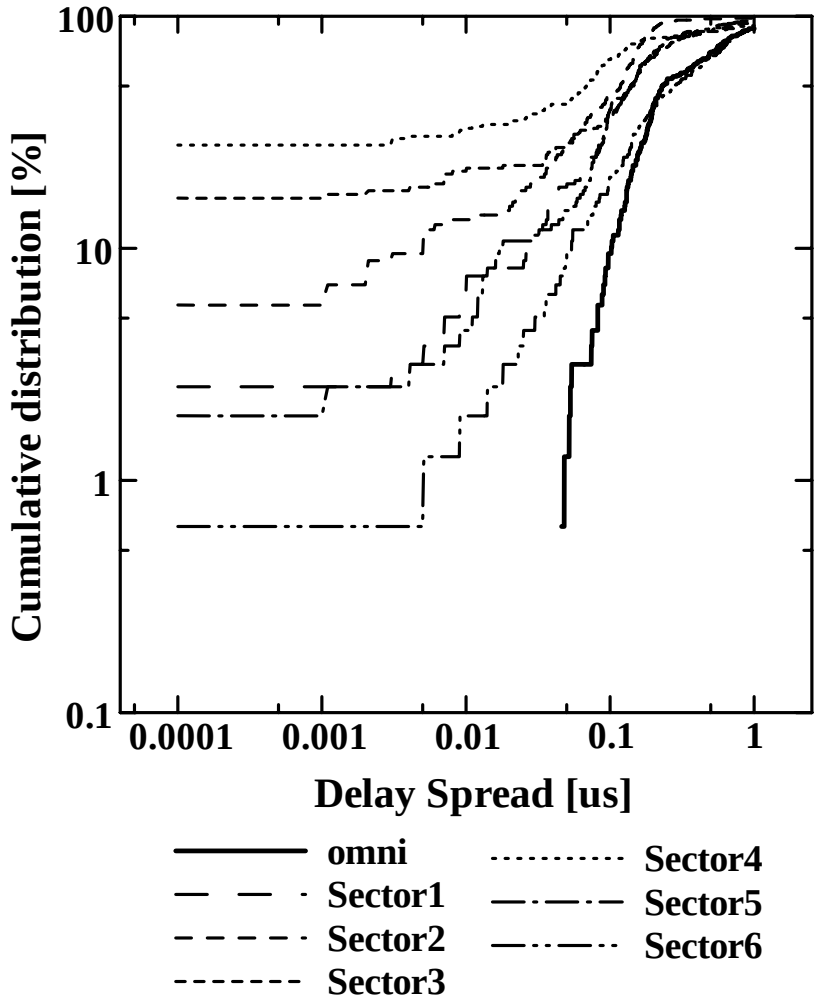

Fig. 2-20: Cumulative distribution of delay spread at movement

2.3.3. Effect of Sector antenna

The sector antenna is divided into each sector, and we consider about the case of antenna element of 60 degrees beam in the former section. We consider about the case that the measurement result of each sector is composed. To compare the effect of sector, 3-sector is combined by the PCTSA element shown in Fig. 2-21, and the antenna of 2 PCTSA elements, too. The median value of the cumulative distribution of delay spread in the movement mobile station by using each antenna is shown in Table.2-5. The delay spread can be decreased by increasing the number of sector.

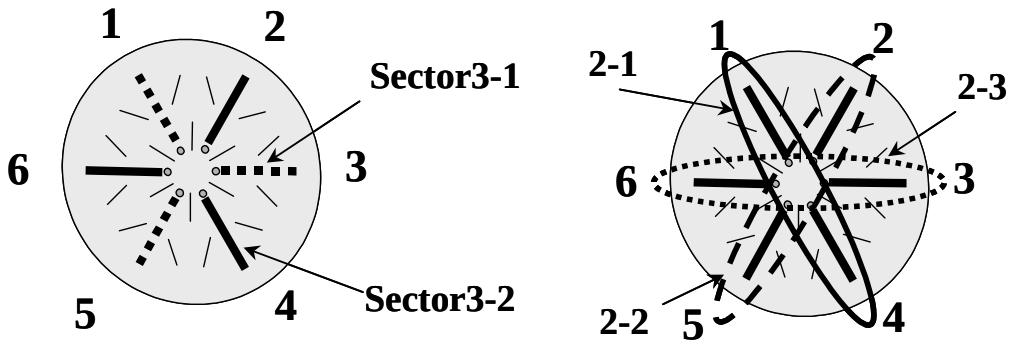

Fig. 2-21: Configuration of 3-sector antenna

Table.2-5: Median value of delay spread (unit [μs])

Omni	2 PCTSA element			Sector		
	2-1	2-2	2-3	3-1	3-2	6
0.232	0.05	0.086	0.097	0.073	0.029	0.018

2.3.4. DOA Estimation by Delay Profile Measurement Using Sector Antenna

In this section, we evaluate DOA estimation by delay profile measurement using sector antenna. The environment of delay profile measurement is shown in Fig. 2-22. The measurement result is shown in Fig. 2-23 and Fig. 2-24. The “sector n (n = 1~6)” is each sector of 6-sector antenna. At the measurement point 1, this propagation is in sight of the base station (line of sight), and this delay profile is the typical model that propagation level of direct wave decreases exponentially. Only a direct wave is received at sector 3, which is directed the base station. But the delay waves are observed at sector 6 in the opposition direction of the base station. The median value of delay spread is shown in Table. 2-6. The delay spread is the minimum at sector 3, and the maximum at sector 6. Therefore, if the minimum delay spread sector and the maximum delay spread sector are the opposite position, this propagation is in sight of the base station, and it can be estimated that the base station direction is the main beam direction of the minimum sector.

At the measurement point 2, this propagation is out of sight, and propagation level of the direct wave is low. The reflection wave (around 3 [ms]) by the building is received at sector 1, which is directed the base station. But the reflection wave is not received at sector 6. The median value of delay spread is shown in Table. 2-7. The delay spread is smaller than other sectors at sector 3,6. Therefore, we can estimate that there are few buildings (reflection thing) in the direction of sector 3,6.

The median value of delay spread at other point is shown in Table. 2-8. At the in sight of the base station, the minimum delay spread sector and the maximum delay spread sector are the opposite position, and the direction of the base station is the that of the minimum delay spread sector. On the other hand, at out of sight, the minimum delay spread sector and the maximum delay spread sector are not the opposite position. Therefore, we can estimate in sight or out of sight by the delay spread. However, although a rough direction can be grasped, exact direction of arrival cannot be performed.

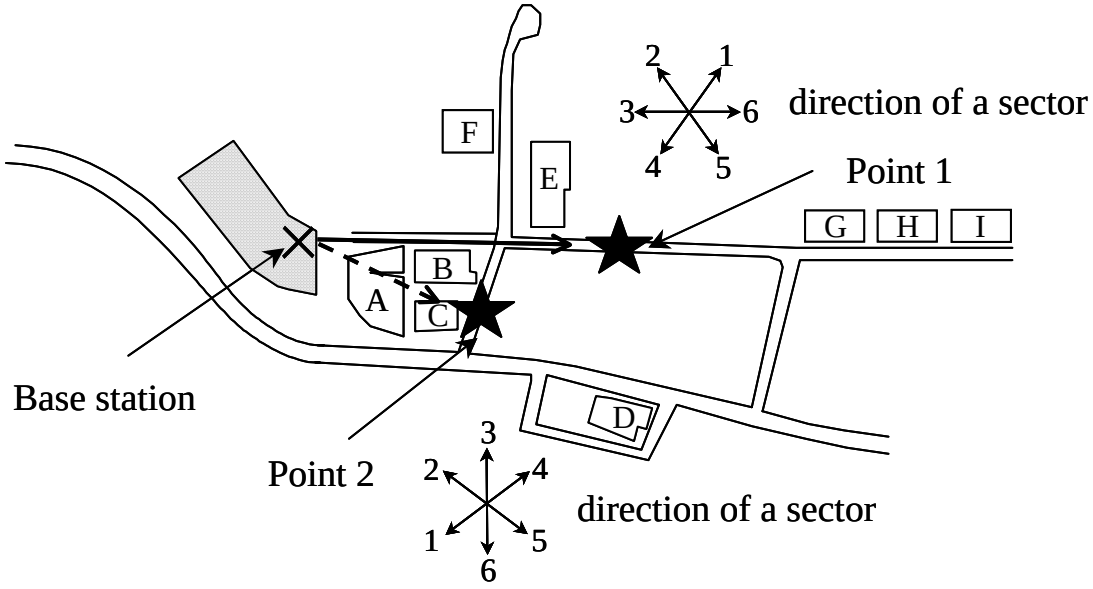

Fig. 2-22: Measurement environment

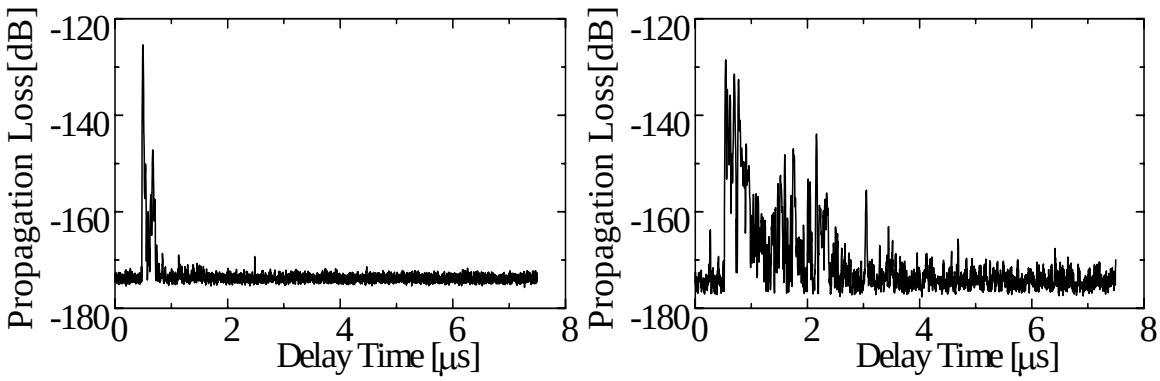

(a) Sector3 (b) sector6

Fig. 2-23: Delay profile at the Point1

Table. 2-6: Median value of delay spread at the Point1

Omni	Sector					
	1	2	3	4	5	6
0.053	0.075	0.036	0.02	0.035	0.080	0.273

Unit: [μs]

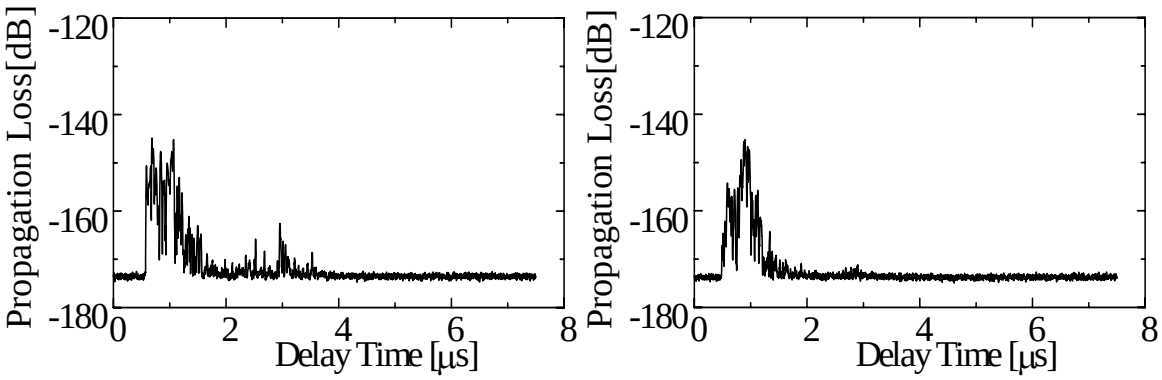

(a) Sector1 (b) sector6

Fig. 2-24:Delay profile at the Point2

Table. 2-7:Median value of delay spread at the Point2

Omni	Sector					
	1	2	3	4	5	6
0.203	0.274	0.201	0.128	0.273	0.213	0.126

Unit: [μs]

Table. 2-8:Median value of delay spread at other point

Base station direction	3	3	1-6	1-6	1-2	3	3	3	5	1
Omni	0.403	0.786	0.146	0.522	0.216	0.144	0.151	0.34	0.165	0.046
Sector1	0.195	0.28	0.12	0.328	0.435	0.142	0.208	0.05	0.207	0.028
Sector2	0.109	0.091	0.22	0.258	0.312	0.051	0.135	0.139	0.212	0.028
Sector3	0.258	0.117	0.482	0.282	0.146	0.024	0.057	0.066	0.207	0.102
Sector4	0.15	0.835	0.118	0.417	0.29	0.076	0.094	0.046	0.1	0.121
Sector5	0.128	1.796	0.104	0.652	0.44	0.119	0.225	0.094	0.126	0.07
Sector6	1.054	1.566	0.126	0.235	0.302	0.316	0.33	0.281	0.211	0.041
Min.sector	2	2	5	6	3	3	3	4	4	1,2
Max.sector	6	5	3	5	5	6	6	6	2	4
Sight	O	O	O	O	O	I	I	I	O	I

Min.sector: minimum delay spread sector, Max.sector: maximum delay spread sector,

O: out of sight, I: in sight of base station (line of sight), Unit: [μs]

2.3.5. Summary

This section presented a delay profile was measurement by using the sector antenna at outdoor environment. The 6-sector antenna used could reduce a delay spread many times than omni directional antenna used in almost fixed points and movement environment. Therefore, the sector antenna is suited for high-speed wireless data transmission, because this sector antenna can reduce effectively the delay spread at outdoor.

This section also presented that the estimation of DOA and propagation environment by using delay profile measurement. The delay profile and the delay spread in each sector are verified; we can estimate the propagation environment (in sight or out of sight) and the direction of the base station by the position of the sector. However, although a rough direction can be grasped, exact direction of arrival cannot be performed.

References

[4] K.Uehara, T.Seki, K.Kagoshima, “Indoor Propagation Calculation Considering Antenna Patterns Using Geometrical Optics Method”, IEICE Trans Japan, vol. J78-B-II, no. 9, pp.593-601, Sep 1995.

[5] J.E.Mitzlaff, “Radio Propagation and Anti-Multipath Techniques in the WIN Environment”, IEEE Network Magazine, vol.5, no.6, pp21-26, Nov.1991.

[6] T.Maruyama, K.Uehara, K.Kagoshima, “Design and Analysis of Small Multi-Sector Antenna for Wireless LANs Made by Monopole Yagi-Uda Array Antenna”, IEICE Trans Japan, vol. J80-B-II, no. 5, pp.424-433, May 1997.

[7] Chuang J.C-I, “Simulation of digital modulation on portable radio communication channels with frequency-selective fading”, IEEE Globcom’86, pp.31.6.1-31.6.7, Dec 1986.

3. Digital beam forming array antenna

3.1. Introduction

Adaptive array antenna is one of multi-beam antenna by using adaptive signal processing. In recent years, the technology of the adaptive array antenna has been greatly advanced, and applied to mobile communications systems [3]. The digital beamforming (DBF) array antenna is a kind of the adaptive array antenna which can realize the desired beamforming and null steering by adjusting weight parameters of antenna elements using digital signal processing shown Fig. 3-1. Therefore, the DBF array antenna can be investigated to increase the C/N (carrier to noise) ratio. The antenna beam forming is also deeply related with the directions-of-arrival (DOA), because the angular spread is a very important factor in the adaptive array antenna. Therefore, we have to develop hardware and algorithm which accurately estimates the DOA. Many researches have been already made on the algorithm itself and the hardware implementation of the DBF array antenna [8]. However, such DBF array antennas are very complicated and expensive, because they are implemented by application-specific integrated circuits (ASICs) and high-cost RF module. To avoid such costly situation, some low-cost adaptive antennas have been recently proposed [9]. This system achieved low-cost implementation by using digital signals, array signal processing, and demodulation on PC. However, this paper particularly described the constitution of hardware, and didn’t discuss the experimental results including errors and calibration method among branches.

This chapter proposes a 2.6GHz low cost DBF array antenna system. The reason why we chose 2.6GHz band is that this band has very wide availability. It is close to the IMS band used in the wireless LAN (2.45GHz), the IMT2000 band (2.1GHz), and the 3GHz band which is assumed to be used in the next generation mobile communication. Fortunately, low cost RF modules are easily available in this band. The proposed system is partially constructed by digital devices for the simplification of hardware and employs some techniques in order to improve the resolution and eliminate the error by noise and distortion of cause of low cost RF modules. The proposed system estimates the DOA by the multiple signal classification (MUSIC) algorithm [10] inside a radio anechoic chamber. Moreover, this section discusses the estimation errors. In order to specify the factor of the estimation errors, we evaluate the system in case of one transmission source.

In another section, we describe calibration method of phase and amplitude unbalance among the branches using 8.45 GHz DBF receiver. We also demonstrate near zero IF receiver with calibration circuit for DBF at 8.45 GHz. This band is a candidate of frequency band of next generation wireless

telecommunication in Japan also 3.0 GHz and 5.4 GHz in Japan. We describe active patch antenna with low noise amplifier and near zero IF mixer for this receiver. We also examine this proposed receiver's ability to function as a digital beam former.

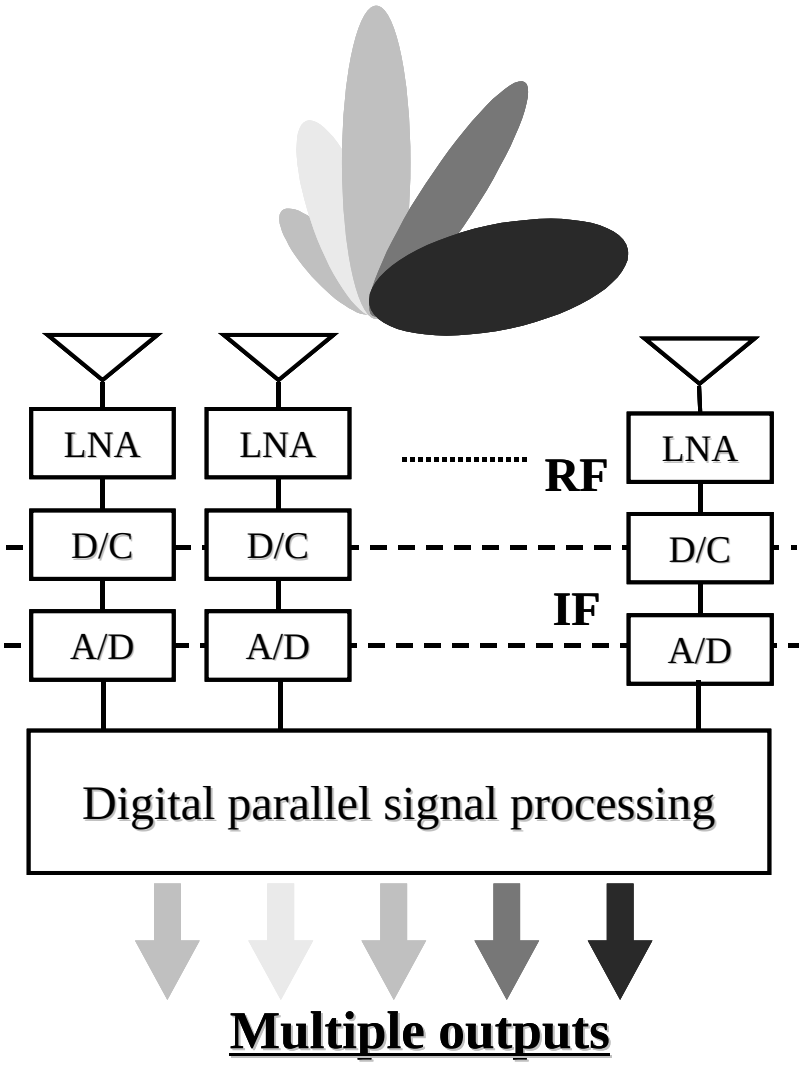

Fig. 3-1: Receiving digital beamforming

3.2. Doa estimation using receiving Digital beam forming at 2.6 GHz

3.2.1. Construction of the DBF Array Antenna System

3.2.1.1. Construction of Hardware

The construction and specifications of the proposed DBF array antenna system in case of 4 antenna elements are shown in Fig. 3-2. We made the DBF receiver of 4 elements, because it is difficult to make a divider circuit which is required in case the number of antenna elements is not 2^n. In addition, the number of elements can be more than 4, such as 8 or 16 elements by using 4 elements prototype. In order to evaluate the performance of this prototype receiver, we used a linear array of omni directional antennas with the half wavelength interval that is generally used in the adaptive array antenna.

An RF signal passes through three steps of frequency conversion in Fig. 3-2 at which the converters and filters are constructed by generally used low cost RF modules. At the 400MHz IF part (second step), this system have the gain and phase adjustment circuit with variable gain amplifier (VGA) and phase shifter (PS), in order to eliminate the correlation between channels by noise and distortion of cause of a low cost RF device, because calibration is an important aspect of performance of any adaptive array system. In another section, we discuss calibration method in detail. Furthermore, if we change a local oscillator for external reference oscillator, we can synchronize between transmitter and receiver by locking the PLL oscillator.

The obtained IF signals are sampled by the A/D converter board on a PCI bus in sync and are kept in the memories of a PC. Therefore, various algorithms can be examined by off-line digital signal processing by a PC with some common program languages. Fig. 3-3 shows the input power from RF port versus IF power from A/D converter. From Fig. 3-3, we can see that the dynamic range of this system becomes around 30 dB with the 12 bit A/D converter.

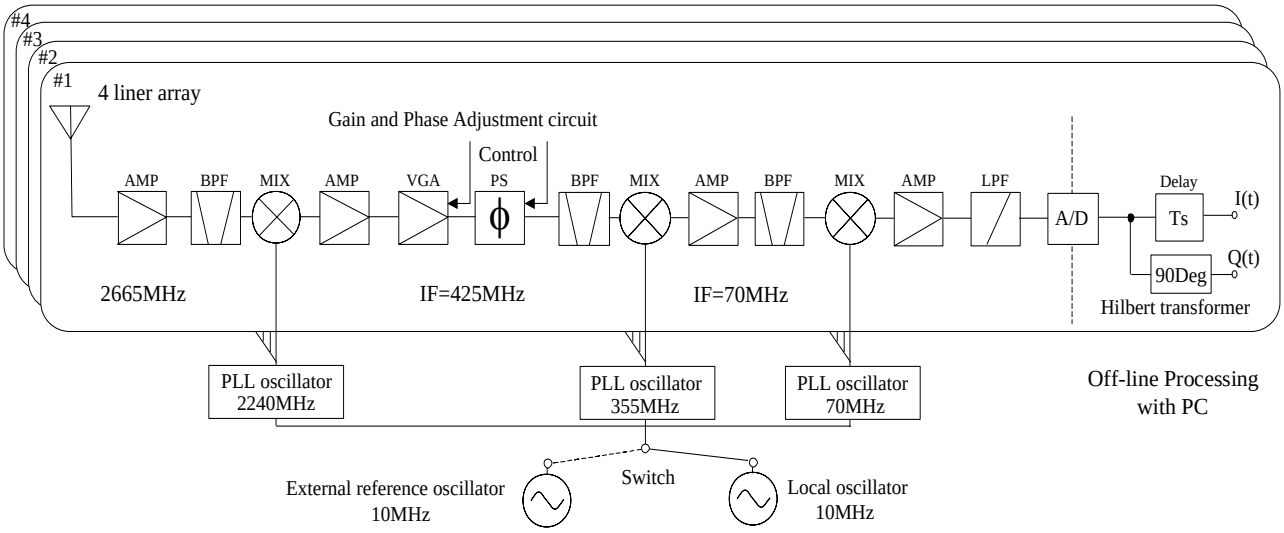

Fig. 3-2: Black diagram of the DBF receiver at 2.6 GHz

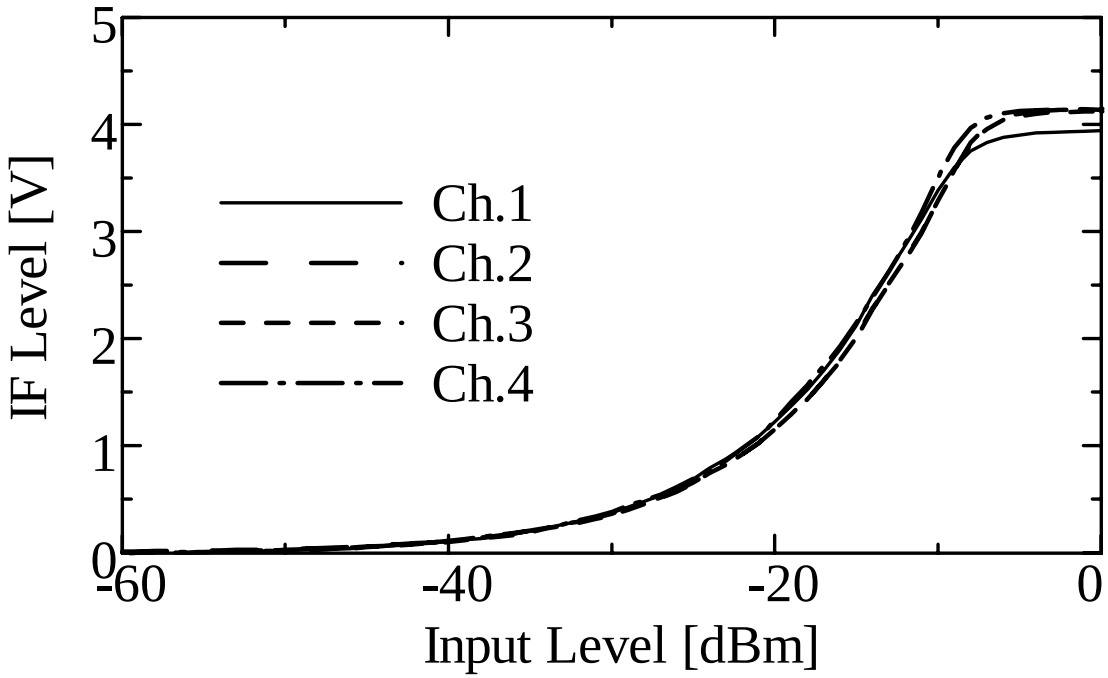

Fig. 3-3: Input power versus IF power

3.2.1.2. Quadrature Hybrid using Hilbert Transformer

General receivers divide the received signal into I and Q signals by using a quadrature hybrid, generally implemented by analog circuits in order to obtain phase information. However, in this case, it is difficult to make the orthogonal detection precisely, and the phase error causes the DOA estimation error. Particularly, the phase noise occurs in low cost RF modules. To simplify the hardware construction and improve the accuracy of the DOA estimation, this system utilize the Hilbert transformer which can be implemented as a FIR digital filter which has antisymmetrical impulse response [11] instead of the analog orthogonal detector. Also, in case of general digital hybrid, LPF is necessary for both I and Q components. However, quadrature hybrid using Hilbert Transformer can be implemented by only one FIR digital filter and the order of this filter can be less than that of LPF for digital hybrid. An IF signal is divided into 2 signals: one is the I (In-phase component) inputted to the delay circuit (T_s), and another is the Q (Quadrature-phase) component of which the phase is delayed 90 degrees by a Hilbert Transformer are shown in Fig. 3-2. Generally, FIR filters of which the impulse response is asymmetrical work as 90 degrees phase shifter. The number of tap of this filter is $N = 100$ to have an almost ideal characteristics. The impulse response $\{h(n)\}_{n=0}^{N-1}$ is given by

$$h(n) = -\frac{2\varpi(n)}{\left(\frac{N-1}{2} - n\right)\pi} \sin^2\left[\frac{\left(\frac{(N-1)}{2} - n\right)\pi}{2}\right] \qquad (3.1)$$

$n = 0,1,...,N-1.$

where $\varpi(n)$ denotes Kaiser's window function [11] of $\alpha = 3.0$. In case of more than $f \geq 0.005/T$, the amplitude error is reduced within 3%, and it can almost be regarded as an ideal characteristics.

3.2.1.3. Increasing the Number of Elements

Basically, the number of the estimated arrival waves depend on that of array element. To be able to increase the number of the estimated arrival waves, we try to receive signal data by virtual 7 elements using the proposed 4 elements DBF array antenna. We can evaluate whether the resolution of DOA estimation is improved by increasing the number of elements by virtual 7 elements, without adding a new receiver.

We rotate the array antenna elements 180 degrees around the edge element of the array antenna, and then increase the number of the antenna elements virtually as shown in Fig. 3-4. This rotation can be done by the rotator that can gives a precise angle. The phase of array element is adjusted based on the center element of the rotation by using the following method.

Two received IF voltage data by before and after the rotation are respectively denoted by $V_1(k)$ and $V_2(k)$, where k is the sampling number. Besides, denotes the phase difference between the center element of the rotation on $V_1(k)$ and $V_2(k)$. The phase of $V_1(k)$ and $V_2(k)$ can be compared by δ, and then the phase of $V_2(k)$ is delayed. The delayed data $V_2^{'}(k)$ can be written as

$$V_2^{'}(k) = V_2(k)e^{j\delta} \tag{3.2}$$

Based on the phase difference δ we can line up and exchange data of $V_2(k)$ and connect with data of $V_1(k)$. Therefore, We can virtually have the DBF array antenna system with 7 elements from that of 4 elements by rotation.

In other words, we can obtain almost the double resolution by only the original number of the array elements.

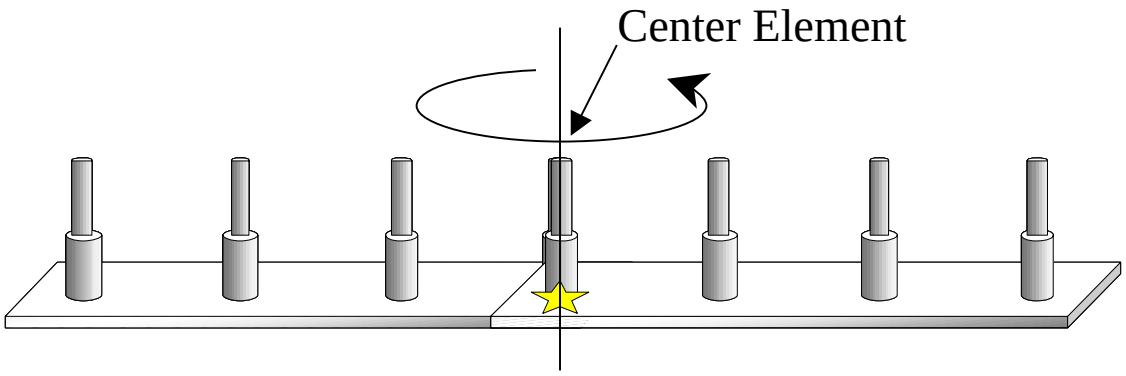

Fig. 3-4: Increasing the number of elements by rotation

3.2.2. DOA Estimation by MUSIC Algorithm

In this section, the proposed system is evaluated through DOA estimation by MUSIC algorithm inside a radio anechoic chamber. In the DOA estimation, this algorithm is very general, can get a super-resolution, and is suitable for evaluating the prototype receiver. Moreover, as for this algorithm, the mode vector (direction vector) is necessary to calculate a MUSIC spectrum compared with the ESPRIT algorithm is the same super-resolution method. Therefore, the factor of error can be evaluated, if the mode vector including some error is used. The construction of the experimental environment and the measurement setup are shown in Fig. 3-5 and Table. 3-1, respectively. A signal of continuous wave (CW) from a signal generator (SG) is transmitted from a sleeve antenna through a high power amplifier (HPA) and a 4-way divider (unused terminal is terminated). The proposed system estimates the DOA from the received RF signals.

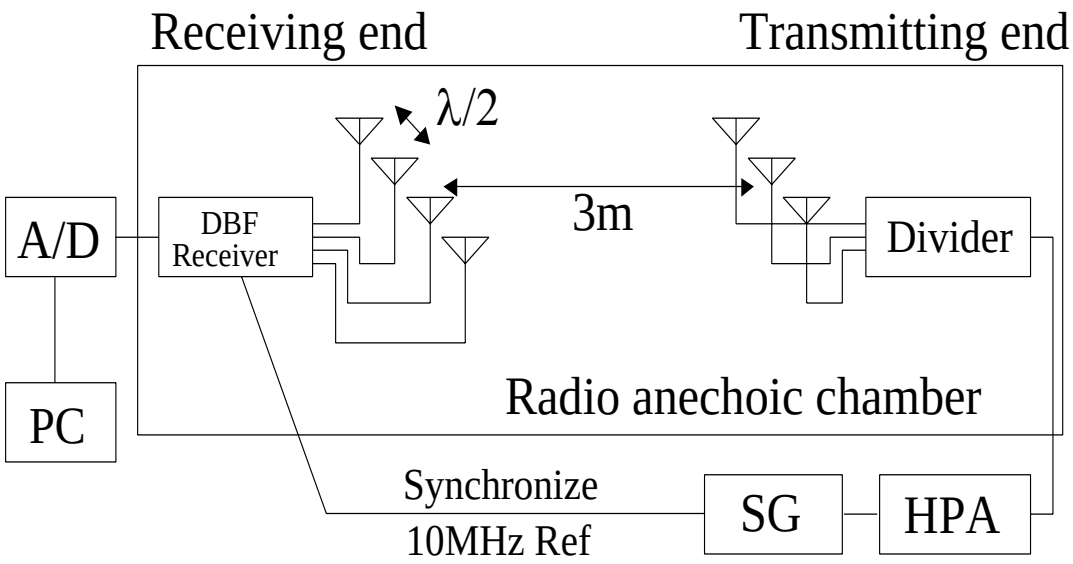

Fig. 3-5: Construction of the experimental environment

Table. 3-1: Specification of the system and measurement setup

Transmitting and Receiving antenna	Sleeve antenna*
The number of array element	4 linear array**
Transmitting power	-12dBm
Amplifier Gain	+40dB
Distance between transmit and receiver	3m
A/D converter	12bit, 250KS/s
IF frequency	25kHz
The number of snapshot	500

*The antenna gain is about 2 dBi.

**The distance of each antenna is λ/2.

Let θ_t and θ_r respectively denote the direction of the transmitting antenna and the angle of the rotator as shown in Fig. 3-6. The transmitting antenna is installed 3 m far from the center of the receiving array antenna. The direction of arrival to the receiving array antenna can be given by $\theta_t - \theta_r$. The experiments of the DOA estimation can be summarized as the following three steps.

First we calibrate the amplitude and phase of each element at IF band by using adjustment circuit and digital oscilloscope. A transmitting antenna is installed in front of receiving array antenna ($\theta_t = \theta_r = 0$ deg) at the anechoic chamber. Here we assume that all the arriving waves are plane ones. The dispersion of each antenna elements, cables and low cost RF circuits can be restrained by this procedure.

Then the DOA is estimated using 4 antenna elements. The transmitting antennas are installed at desired positions, and the angle θ_r of the receiving array is set by rotating. The received IF signals are sampled simultaneously by the A/D converter on PC. The DOA is estimated by MUSIC algorithm by off-line processing.

Furthermore, the DOA is also estimated by 7 antenna elements. The receiving array antenna is re-installed so that either of the edge elements of the receiving array is placed at the center of the rotation to be virtual 7 elements. The received IF signals at the angle θ_r are sampled and keep the sample values in the PC memory. Then, the receiving array is rotated 180 degrees ($\theta_r + 180^o$) and we sample the IF signals again. We adjust the phase characteristics of the array elements based on the center of virtual 7 elements, and estimate the DOA by using the data of 7 elements.

Because the arrival waves are coherent in our experimental system, the cross-correlation of the

arrival waves is suppressed by spatial smoothing [12]. Accordingly, the number of the array elements must be more than twice against that of the arrival waves for the accurate DOA estimation by MUSIC algorithm with spatial smoothing. Therefore, the maximum numbers of arriving waves is 2 in cases of 4 elements, and 3 in case of 7 elements, because the number of subarray becomes 3 in case of 4 elements, 5 in case of 7 elements.

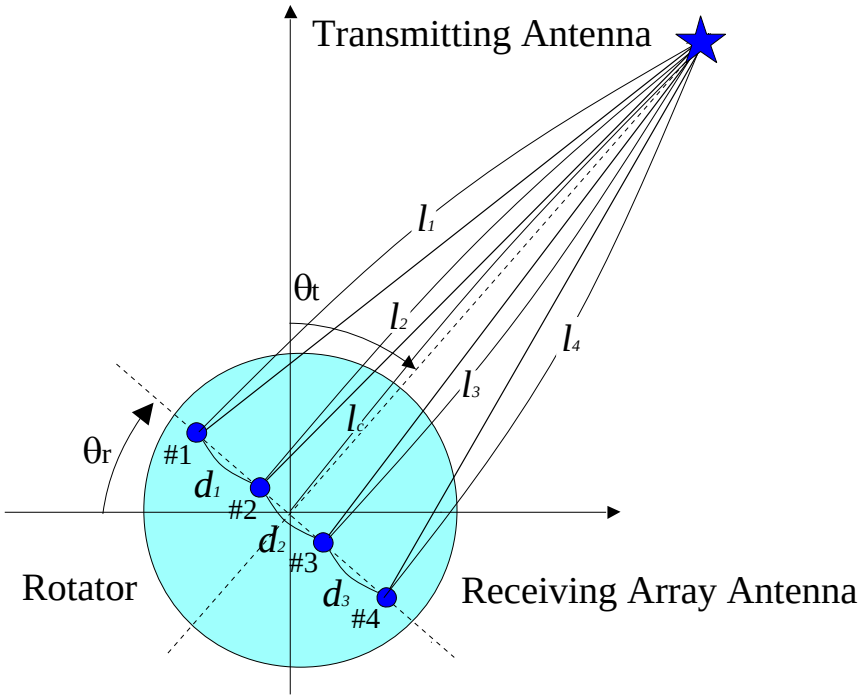

Fig. 3-6: Arrangement of lengths and distances between antennas

3.2.2.1. Result of the DOA Estimation

First, we describe the results of the DOA estimation in case of 4 array elements. Three transmitting antennas are installed so that the angle of the receiving array is 0, ±30 degree. The estimation result in case of one wave source shown in Fig. 3-7. From Fig. 3-7, we can observe that estimation error is almost ±0 degree. In case of two wave source, we tested 2 combinations of the angles θ_t: (1) θ_t = 0, 10deg and (2) θ_t = 0, 20deg. The results of the DOA estimation are depicted in Fig. 3-8 and Fig. 3-9. From Fig. 3-8 and Fig. 3-9, we can see the followings: When the arrival wave is close to the front direction of the receiving array, in other words, $\theta_t - \theta_r$ is nearly equal to zero, the estimation error is almost ±0 degree. However, the DOA is inaccurately estimated when the angle $\theta_t - \theta_r$ gets close to ±90 degree. In either of the cases, the DOA is estimated as the opposite direction around 0 degree (Fig. 3-8 θ_r = ±30 deg,. Fig. 3-9 θ_r = 30 deg). Besides, from

Fig. 3-8, the estimation error becomes larger as the transmitting antennas are more adjacently installed (1ess than 10 degree). As a result, if the transmitting antennas are in the front direction (less than ±20 degree), we can accurately estimate the direction of 2 arrival waves by 4 antenna elements.

We also investigate the results of the DOA estimation in case of 7 array elements (by rotation). The estimation result in case of one wave source shown in Fig. 3-10. From Fig. 3-10, we can observe that the DOA can be estimated very accurately. Moreover, the MUSIC spectrum became more sharpened (50% below 3dB) in comparison with that in case of 4 elements. Fig. 3-11 and Fig. 3-12 illustrate the estimation result in case of two wave sources. The same angles as the case of 4 elements are chosen. As seen in Fig. 3-11, the MUSIC algorithm still cannot distinguish 2 waves from the sources adjacently installed with the distance of only 10 degrees. However, as seen from Fig. 3-12, the estimation error is almost ±0 degree. In case of three wave sources, the estimation result is shown in Fig. 3-13 and Fig. 3-14. Still the problem occurs when the sources are adjacently installed with the distance of only 10 degrees. From Fig. 3-13, the arrival waves could not be classified to 3 waves similarly to the case of two wave sources in Fig. 3-11.

From the above experiments, we found that the DOA of up to 2 wave sources could be accurately estimated in case of 4 elements, and that of up to 3 wave sources also could in case of 7 elements (by rotation). We confirmed that the accuracy of the DOA estimation could be improved by increasing the number of array elements. However, the estimation error became larger when the wave sources were adjacent (the distance of only 10 degrees).

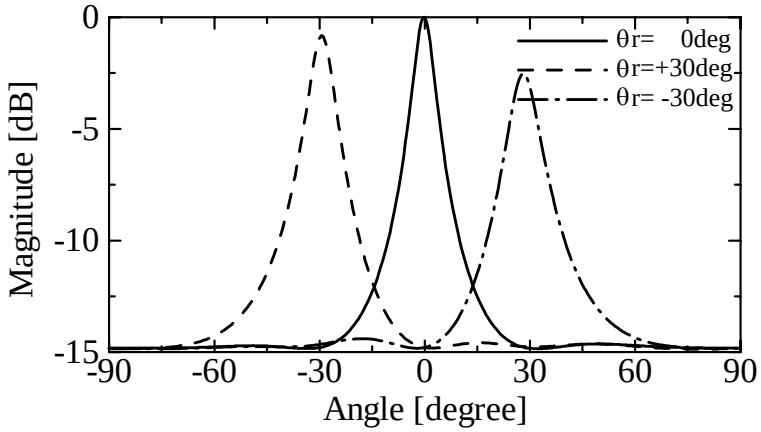

Fig. 3-7: MUSIC spectrum versus θ_r in case of 4 elements (θ_t = 0deg: 1 wave source)

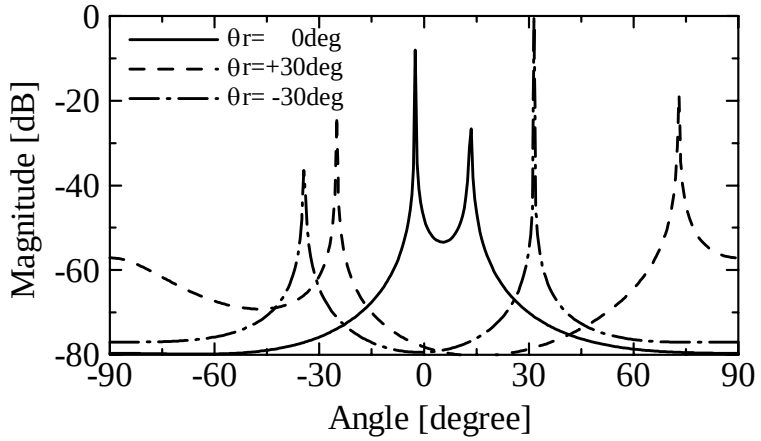

Fig. 3-8: MUSIC spectrum versus θ_r in case of 4 elements

(θ_t =0, 10 deg: 2 wave source)

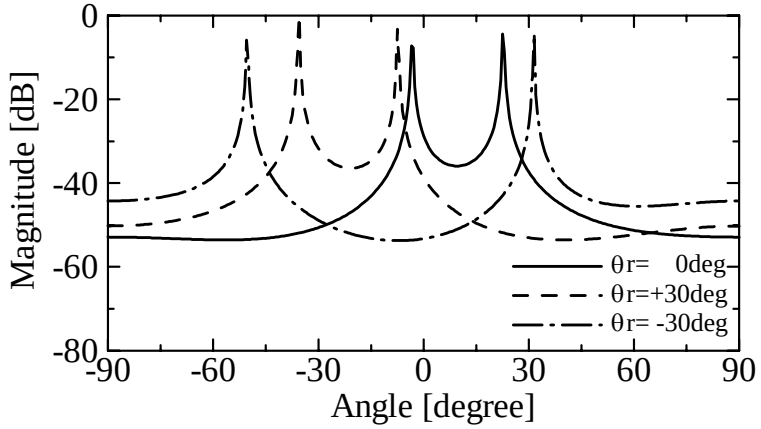

Fig. 3-9: MUSIC spectrum versus θ_r in case of 4 elements

(θ_t =0, 20 deg: 2 wave source)

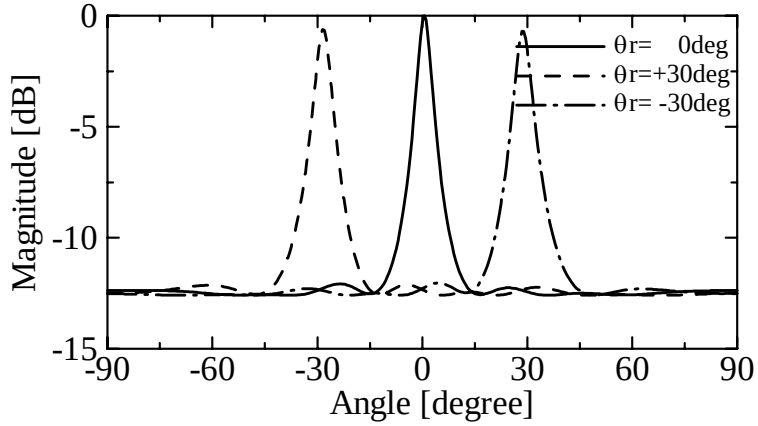

Fig. 3-10: MUSIC spectrum versus θ_r in case of 7 elements

(θ_t = 0 deg: 1 wave source)

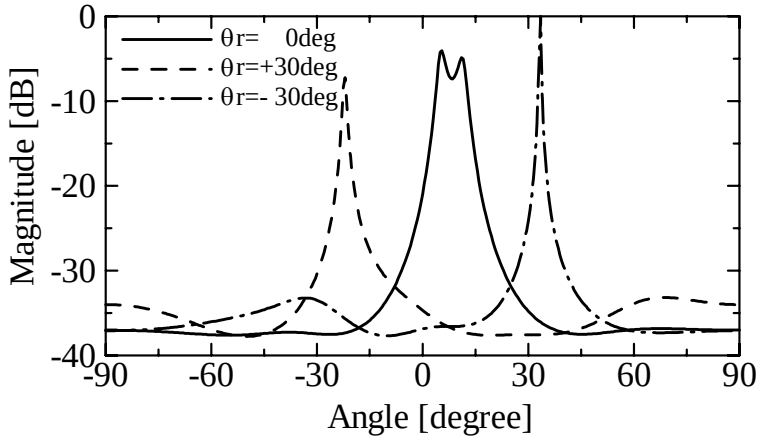

Fig. 3-11: MUSIC spectrum versus θ_r in case of 7 elements

(θ_t = 0, 10 deg: 2 wave source)

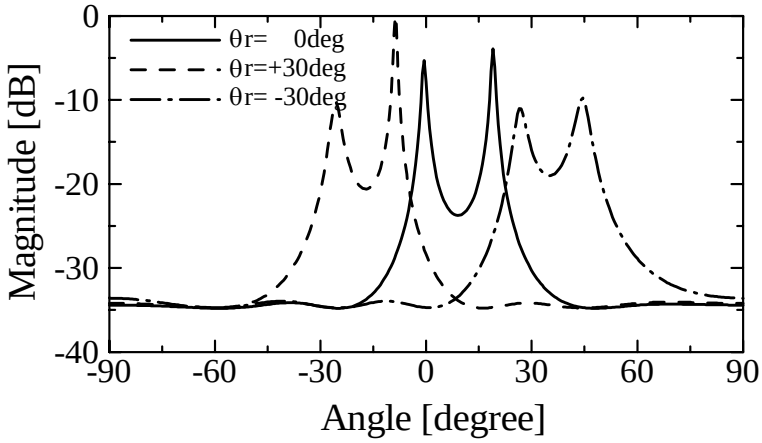

Fig. 3-12: MUSIC spectrum versus θ_r in case of 7 elements

(θ_t = 0, 20 deg: 2 wave source)

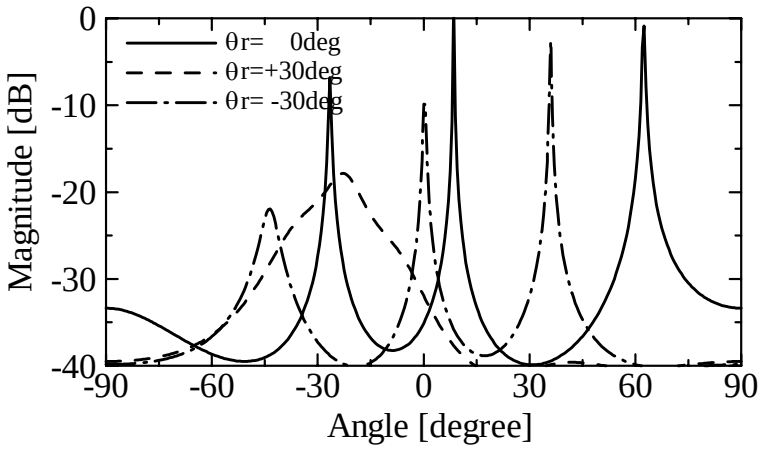

Fig. 3-13: MUSIC spectrum versus θ_r in case of 7 elements
(θ_t = –30, 0, 10 deg: 3 wave source)

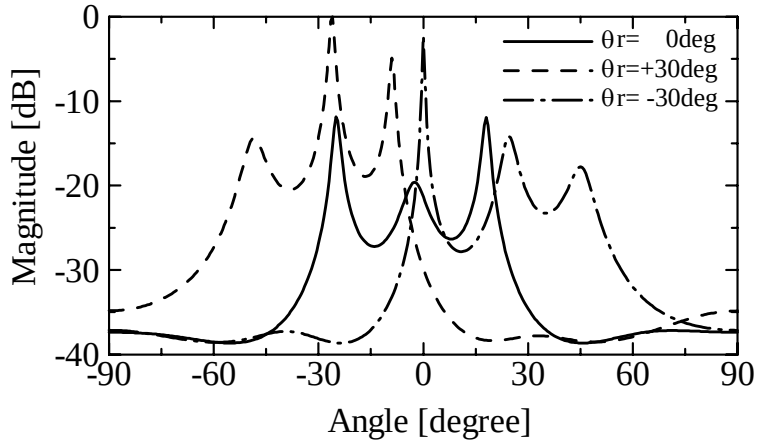

Fig. 3-14: MUSIC spectrum versus θ_r in case of 7 elements
(θ_t = –30, 0, 20 deg: 3 wave source)

3.2.3. Estimation Error Analysis in One Transmission Source

We again analyses the 4 elements model with one transmission source installed in front of the array (θ_t = 0 deg), in order to examine the estimation error in detail and specify error factors. The relation between the transmitted direction θ_r and the estimation error is shown in Fig. 3-15, while the angle θ_r is varied at every 10 degrees. From Fig. 3-15, the estimation error seems to become larger as the absolute of the arrival angle $|\theta_t - \theta_r|$ gets larger. It would be caused by either of probable error factors: the inaccurate interval of elements, the phase difference of each array element, and the difference of propagation loss due to the proximity between the transmitting and receiving antennas. In addition, in case of virtual 7 elements, the error by center of turn and angle of rotation make the inaccurate interval of elements, too. The arriving waves are usually dealt with plane waves in the DOA estimation, that is, the distance between the transmitting and receiving antennas is assumed to be sufficiently large. The distance in the proposed system is only 3 m long, and this may be one of error factors. Therefore, we newly evaluate the DOA estimation while considering either of the above-mentioned factors, in order to specify the true error factor. The IF signals in the proposed system can be modeled as a pure sine wave $G_i(t)$:

$$G_i(t) = A_i \cos(\omega_{IF} t + \delta_i), \quad i = 1, 2, 3, 4, \tag{3.3}$$

where A_i, δ_i and $\omega_{IF} = 2\pi f_{IF}$ denote the amplitude, the phase difference, and the oscillating angular frequency of $G_i(t)$, respectively. The waves $G_i(t)$ of Equation (3.3) differ from each other since the distances between the transmitting antenna and each receiving antenna element is also different from each other. The amplitude A_i becomes the propagation loss which is obtained from transmission formula:

$$A_i = \frac{\lambda_{RF}}{4\pi |l_i - l_c|} \tag{3.4}$$

where λ_{RF} is wavelength at RF. The distances l_i and l_c represent that between the transmitting antenna and i-th receiving array antenna element, and that between the transmitting antenna and the center of the receiving array antenna, respectively, as drawn in Fig. 3-6. Moreover, δ_i can be written in a form

$$\delta_i = \frac{2\pi \left| l_i - l_c \right|}{\lambda_{RF}} \tag{3.5}$$

Equation (3.4) and (3.5) denotes the difference of the propagation loss and the phase difference between array elements, respectively, due to the proximity between the transmitting and receiving antennas. The ideal intervals between array elements is a half wavelength $\lambda_{RF}/2$, however there exists slight inaccuracy. The errors of the intervals are as follows:

$$d_1 - \lambda_{RF}/2 = -0.971\%\left(0.546mm\right)$$
$$d_2 - \lambda_{RF}/2 = -0.260\%\left(0.146mm\right)$$
$$d_3 - \lambda_{RF}/2 = -0.629\%\left(0.354mm\right)$$

all of which a-re within 1% (0.562mm) of half wavelength at RF. The difference of the lengths between l_i and l_c due to the proximity is

$$l_1 - l_c = 0.0044\%\,(0.132mm)$$
$$l_2 - l_c = 0.0395\%\,(1.186mm)$$
$$l_3 - l_c = 0.0395\%\,(1.186mm)$$
$$l_4 - l_c = 0.0044\%\,(0.132mm)$$

while these errors were just ignored when all the arriving waves were supposed to be plane waves. The simulation results including only one error (either of the inaccurate element interval, the phase difference, or the propagation loss) are shown in Fig. 3-15. The behaviors when including the phase difference or the error due to the propagation loss is completely irrespective to the angle θ_r, which means that these two errors hardly affect to the estimation error. However, due to the inaccurate element interval, the estimation error arises around θ_r = ±90 degree. An ideal mode vector of liner array for the MUSIC algorithm is given by

$$a(\theta) = \begin{bmatrix} 1, \exp\left(-j\dfrac{2\pi}{\lambda_{RF}} d_1 \sin\theta_r\right), \\ \exp\left(-j\dfrac{2\pi}{\lambda_{RF}} \left(d_1 + d_2\right) \sin\theta_r\right), \\ \exp\left(-j\dfrac{2\pi}{\lambda_{RF}} \left(d_1 + d_2 + d_3\right) \sin\theta_r\right) \end{bmatrix} \tag{3.6}$$

From Equation (3.6), a mode vector varies according to d_n when the angle θ_r gets close to ±90 degree. Therefore, the inaccurate element interval affects the estimation error around θ_r = ±90 degree. The estimation error also would be occurred by the mutual coupling between elements, because general DOA algorithms do not mention to the mutual coupling between elements. In order to estimate the DOA more accurately, we require a novel algorithm which can consider the mode vector including the inaccurate element interval and the mutual coupling.

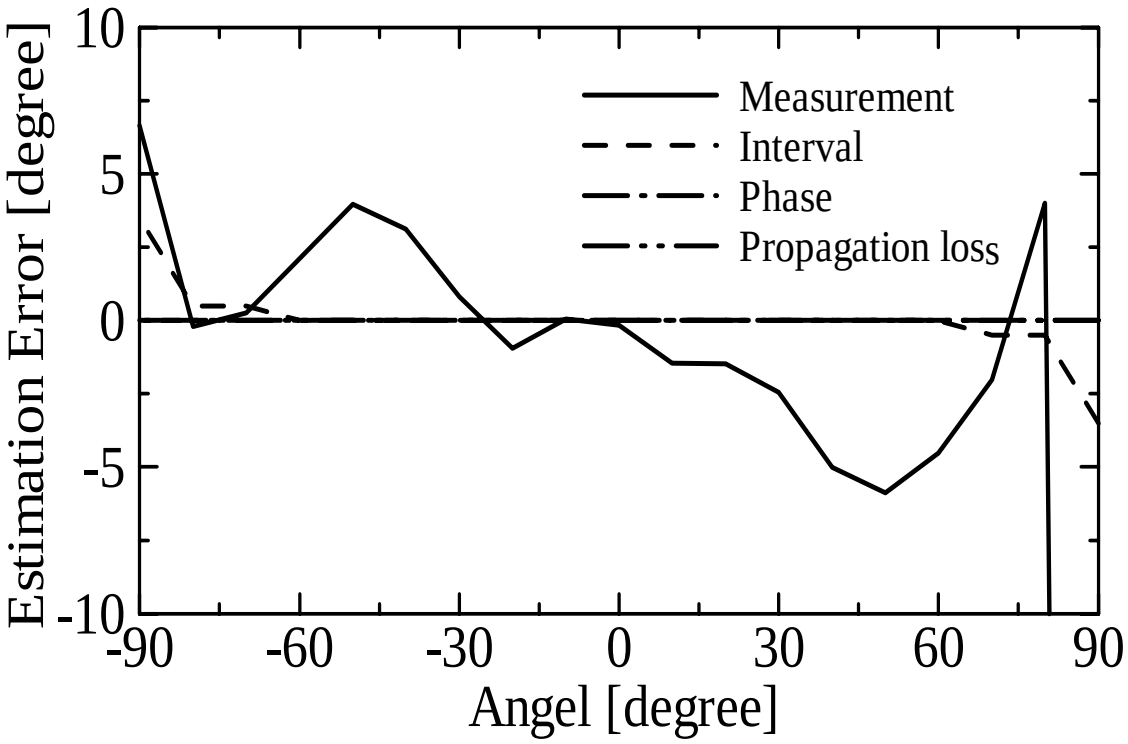

Fig. 3-15: Estimation error in case of 1 transmission source (by experiments)

3.2.4. Doa Estimation in indoor environment

We demonstrate DOA estimation by using proposed receiver in indoor environment at 2.6 GHz. Esprit method [13] which can clearly classify the propagation path rather than MUSIC spectrum is used for estimation algorithm, because we have to find the propagation path in indoor environment for high speed wireless communications. Fig. 3-16 shows indoor measurement environment surrounded by concrete walls and glass door. Proposed DBF receiver (Fig. 3-2, specification of the system is same as Table.2-3) is fixed an asterisk point. When transmission source is arranged in two places of A point and B point, propagation path is estimated by using proposed DBF receiver. Fig. 3-17 and Fig. 3-18 shows estimate result in A point and B point. In case of line of sight (A point), and direct wave is estimated by direction of transmission source, and reflection wave by a concrete wall of a side is estimated. In case of no line of sight (B point), diffraction wave and reflection wave are estimated. It is mostly in agreement with the arrival direction which can estimate in consideration of the propagation path. Compared with the case of using 4 elements and the case of using 7 elements, we can be estimated only to 2 waves in the case of using 4 elements, and estimated precision is generally low. On the other hand, estimated precision rises in the case of using 7 elements because it can be estimated to more than 4 waves. Therefore, since reflection by a glass door is not observed in the case of using 4 elements, an estimated result shows that the reflection of a concrete wall is stronger than that of glass door.

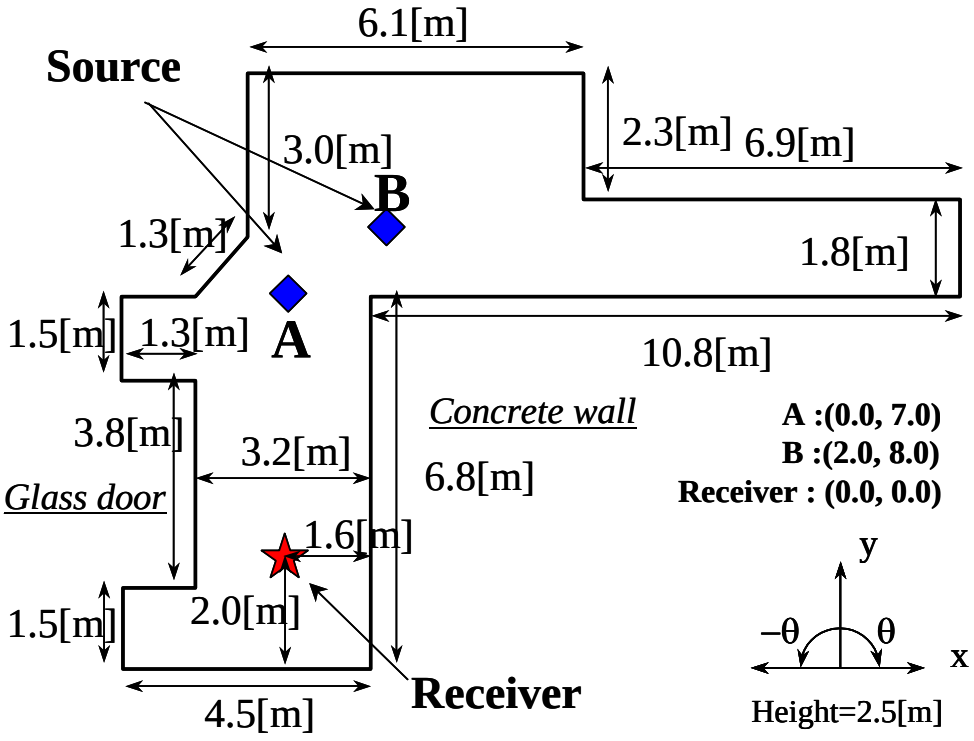

Fig. 3-16: Indoor environment

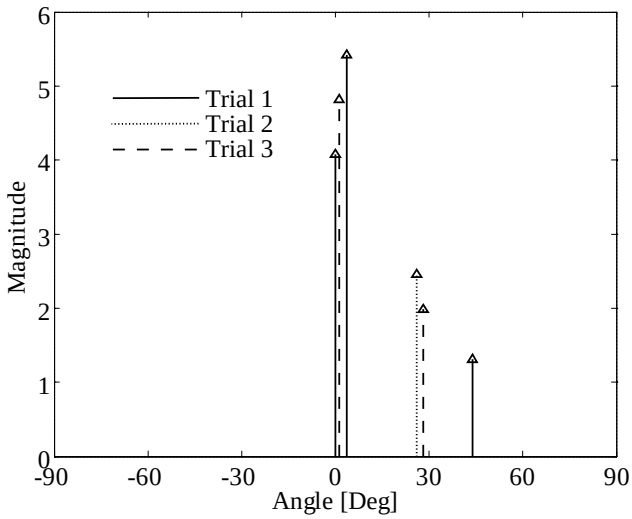

(a) By using 4 elements

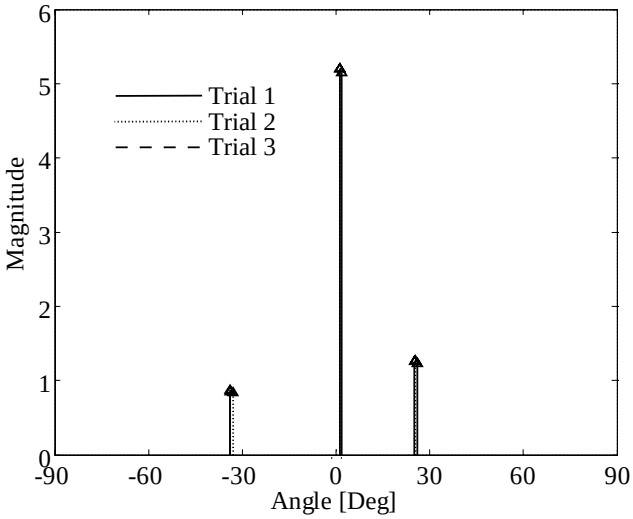

(b) By using 7 elements

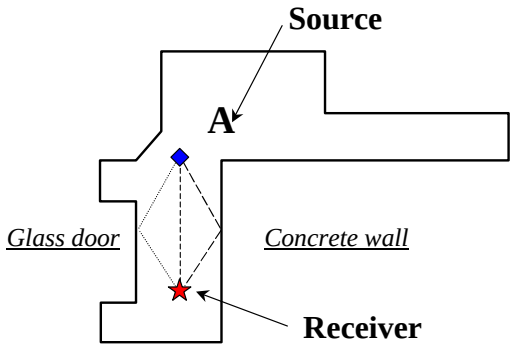

(c) Environment of A point

Fig. 3-17: Doa estimation at A point

Position of receiver is (0.0 [m], 0.0 [m]), Source (A) is (0.0 [m], 7.0 [m])

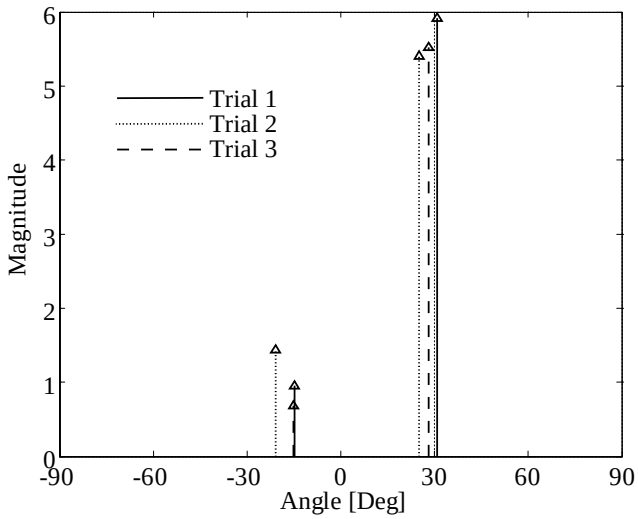

(a) By using 4 elements

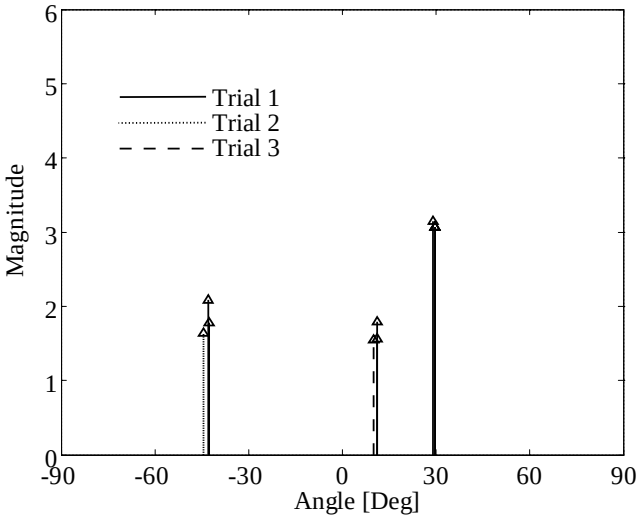

(b) By using 7 elements

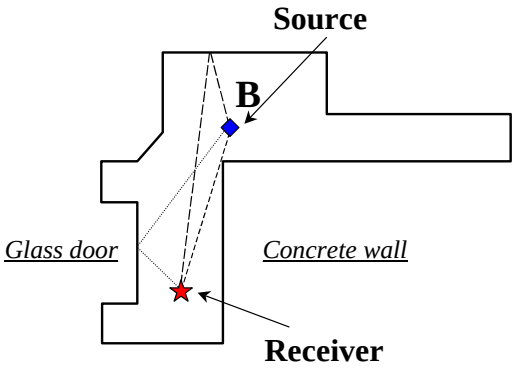

(c) Environment of B point

Fig. 3-18: Doa estimation at B point

Position of receiver is (0.0 [m], 0.0 [m]), Source (B) is (2.0 [m], 8.0 [m])

3.2.5. Beamforming results

In this section, the proposed receiver's ability is evaluated through function as a digital beam former inside a radio anechoic chamber. The construction of the experimental environment and the measurement setup are shown in Fig. 3-5. A signal of continuous wave (CW) from a signal generator is transmitted from a sleeve antenna (gain = 2.15[dBi]) through a high power amplifier. This transmitting antenna is installed 4 m far from the center of the receiving array antenna. Transmitting power is regulated it to apply to dynamic range of the proposed receiver (shown in Fig. 3-3). The CW signals received from the sleeve array are converted to IF signals (baseband) by the proposed receiver. The IF signals are sampled simultaneously by the A/D converter on the PC. The beam forming patterns are obtained by baseband data collected from each antenna element using off-line processing. Measured antenna patterns of each array element calculated based on IF outputs using 4 elements and 7 elements with rotation shown in Fig. 3-19 and Fig. 3-20, respectively. The measurement is used 12-bit A/D converter with an accuracy of about 0.01dB (±0.01[V], 2Vpp). We can find the effects of mutual coupling. The radiation patterns of 4 elements have a ripple in gain around 4 dB between ±45°, and that of 7 elements have also a ripple.

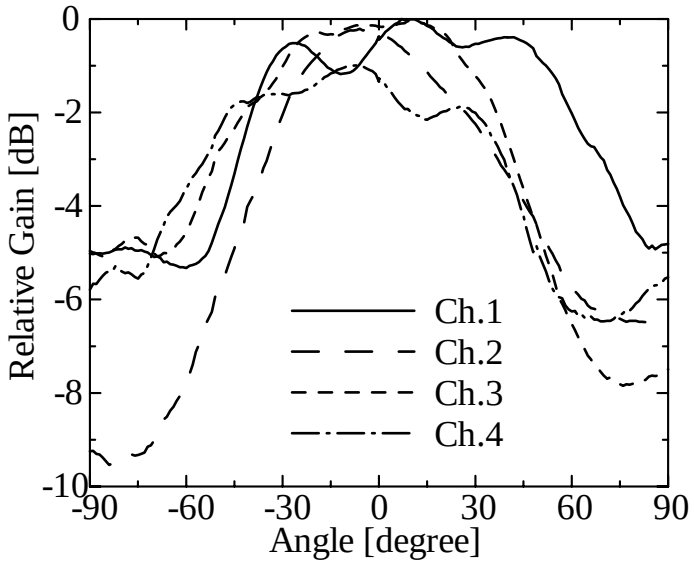

Fig. 3-19: Computed element pattern at IF using 4 elements

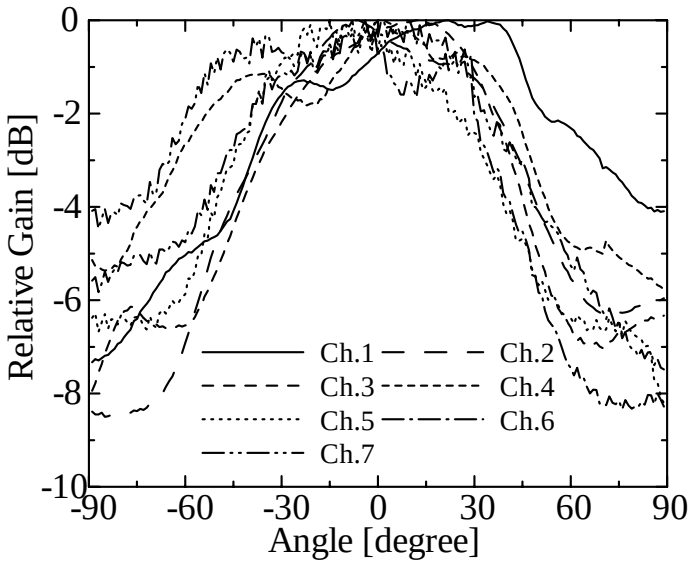

Fig. 3-20: Computed element pattern at IF using 7 elements with rotation

Beamforming is using an antenna array with variable amplitude and phase control of each antenna element [14] in conjunction with an adaptive control algorithm, which synthesizes beam direction. In this approach, the beam of the array may not only be directed to maximize the reception of the desired signal, but also can be tailored to suppress undesired interference signals. Beamforming is the vector addition of individual measured element radiation patterns by using IF data. A unity complex weight apply to any elements changes the magnitude and phase of that element's radiation pattern at every angle [15].

The synthesized beam pattern using 4 elements with main beam directed towards 30, 0 and –40° is shown in Fig. 3-19. In case of towards 0° direction, the beam has a side lobe at –11.3 dB relative to main beam and symmetrical nulls at ±30°. As the result, the synthesized beam forming pattern using 4 element can realize that side lobe level is below –10 dB and half power beam width is about 25° and scanning range is limited from ±45°.

The beam forming pattern is obtained by calculation of the pattern from an array of 7 elements with the rotation by using 4 elements. The beam pattern using 7 elements with main beam directed towards 30, 0 and –40° is shown in Fig. 3-22. In case of towards -40° direction, the beam has a first side lobe at –12.8 dB relative to main beam and nulls at –63°, –18°, -2°, 15°, 33°, and 55°. It can also realize that side lobe level is below –10 dB and the half power beam width is about 15° and scanning range is limited from ±65°. Fig. 3-23 shows beamforming error by using 4 elements and 7 elements. It is found from the result that it is an about equal error when 4 elements and 7 elements are used.

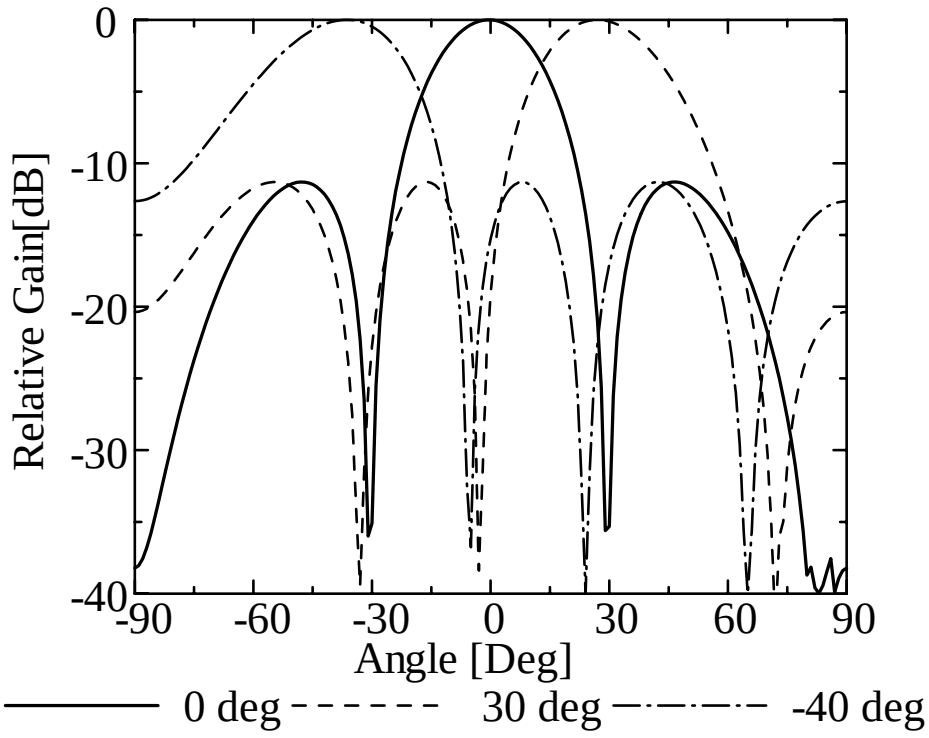

Fig. 3-21: Beam forming by using 4 elements

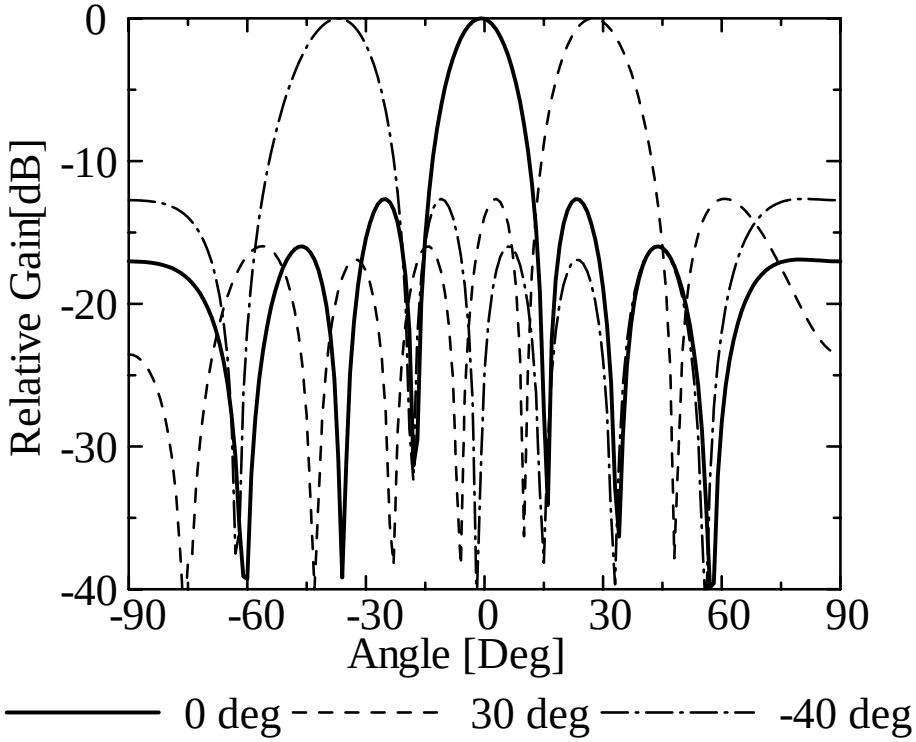

Fig. 3-22: Beam forming by using 7 elements

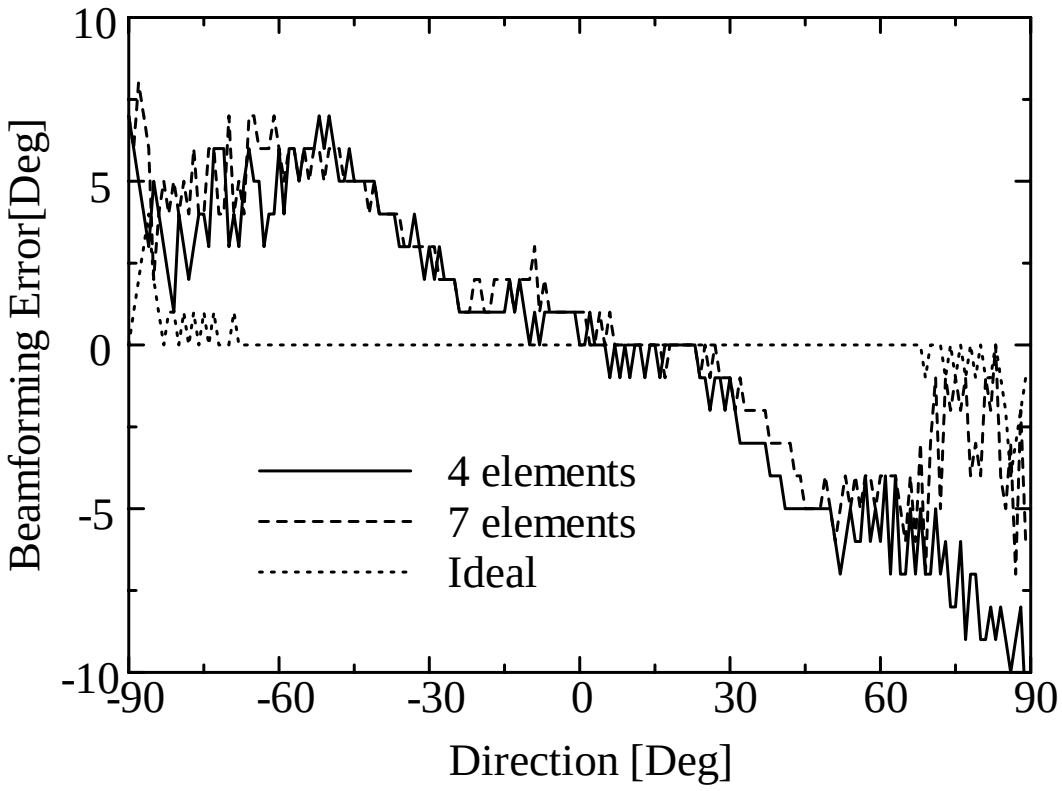

Fig. 3-23: Beamforming error by using 4 elements and 7 elements

3.2.6. Summary

This section proposed a 2.6GHz low cost DBF array antenna system and reported its evaluation based on our experimental results. The proposed system was partially constructed by digital devices for the simplification of hardware, and employs some techniques for the resolution improvement. The system was evaluated through the DOA estimation by the MUSIC algorithm inside a radio anechoic chamber. As a result, we found that the proposed system estimates the DOA with the highest accuracy at which MUSIC algorithm could perform. Moreover, this section discussed on the estimation errors. We found that the estimation error was particularly affected from the inaccurate element interval. We also described estimation by the Esprit method in indoor environment.

We also demonstrated calculating beam forming pattern inside a radio anechoic chamber. As a result, this proposed system could form desired pattern by a limited range of about ± 60 degrees direction, additionally estimates the propagation path in indoor environment.

3.3. Calibration method for DBF

3.3.1. Introduction

For the DBF array antennas, phase and amplitude characteristics of transceiver decide transceiver's ability. The DBF configuration requires the transceivers to be connected to all branches, and the individual characteristics (phase and amplitude) of the transceivers change the beam and null direction in the radiation pattern. Therefore, a calibration is required to compensate for the difference in the transceiver [16]. In order to improve precision of DOA estimation and beam forming, a calibration of phase and amplitude is necessary, in consideration of various error factors, such as un-uniformity of the RF circuit element characteristic (passive elements, such as antennas and active elements, such as amplifiers) or array branch element space error, etc.. In this section, we consider calibration method and circuit for DBF array antenna to reduce an error caused by characteristics among the branches. This calibration circuit is composed two modules: one is phase and amplitude tuning circuit; the other is reference signal generator.

3.3.2. Phase and amplitude tuning

In case of IF frequency (center frequency of data rate) is comparatively high for carrier frequency, phase rotations occur by phase un-uniformity among array branches, the phase information in a data symbol interfere with contiguity symbols, and the information on data may be missing. Therefore, before sampling IF signal with A/D converter, the analog phase tuning among array branches is needed.

Fig. 3-24 shows that simulation result, which is beamforming error versus the number of branches including 30° phase random unbalance among array branches. If the number of branches increase, beamforming error is decreased. Fig. 3-25 also shows that simulation result, which is beamforming error versus direction of transmitter including 10°, 20°, 30°, 40° phase random unbalance among array branches by using 4 array branches. The beamforming error rises rapidly in the scanning range of ± 60° or more. The beamforming error becomes large so that phase unbalance is large. Therefore, in order to extend the beam scanning range, strict phase tuning is needed. Fig. 3-26 shows beamforming error versus phase tuning error between ±60° scanning range using 360 times, 180 times and 4 times over sampling with A/D converter. In case of ±60° scanning range and 360 times over sampling, in order to reduce the beamforming error in less than 1 degree, the strict phase tuning within the limits of 6 degree is needed. Another case of 4 times over sampling, we need within 2 degree correctness.

Moreover, about amplitude information, in order to carry out the maximum effective use of the maximum dynamic range of A/D converter, the amplitude tuning between array branches is also needed. Let us consider dynamic range of analog receiver from the viewpoint of microwave circuit. In microwave circuit, even when there is no input signal, a small output voltage can be measured. We refer to this small out put power as the noise power. Equation (3.7) shows noise power N_0 of receiver depends on the bandwidth and not a given center frequency.

$$N_0 = FGkTB \tag{3.7}$$

Where F is noise figure of receiver, T is the noise temperature and k is Boltzmann's constant. Therefore, we can represent dynamic range of analog transceiver (DR_{AR}) in an equation as follows.

$$DR_{AR} = P_{\max} - P_{\min} \tag{3.8}$$

$$P_{\max} = P_{1dB} \tag{3.9}$$

$$P_{\min} = N_0 + D_{\min} \tag{3.10}$$

Where $P_{\max}$, $P_{\min}$ denotes maximum and minimum input power, P_{1dB} denotes 1-dB gain compression point of transceiver, and $D_{\min}$ is minimum detected level. The dynamic range of analog transceiver depends on noise power and detected level.

On the other hand, the dynamic range of A/D converter ($DR_{A/D}$) can be represent as follows:

$$DR_{A/D} = 6.02N + 1.76dB - \alpha + 10\log_{10}\left(f_S \big/ f_B \right) \tag{3.11}$$

N is the number of bit in the A/D converter, α is the peak to root mean square (rms) radio, f_S is the sampling frequency, f_B is bandwidth of IF [17].

Let us consider dynamic range of digital receiver with analog receiver and A/D converter. Since phase distortion occurs when $P_{\max}$ is larger than P_{1dB}, $P_{\max}$ must be less than P_{1dB}. Equation (3.12) shows the minimum detected level $D_{\min}$ of digital receiver depends on A/D converter.

$$D_{\min} = P_{\max} + G_{AR} - DR_{A/D} \tag{3.12}$$

Where G_{AR} is gain of receiver. Therefore, we can represent dynamic range of analog transceiver

(DR_{DR}) in an equation as follows.

$$DR_{DR} = DR_{A/D} - N_0 - G_{AR} \qquad (3.13)$$

The dynamic range of digital receiver depends on that of A/D converter and gain of receiver (G_{AR}). Hence, in order to carry out the maximum effective use of the maximum dynamic range of digital receiver, it is necessary to tune the amplitude (G_{AR}) between array branches. We also need to implement auto gain control (A.G.C.) each for digital transceiver.

Fig. 3-27 shows that simulation result, which is beamforming error versus direction of transmitter including maximum amplitude unbalance among array branches by using 4 array branches in consideration of the dynamic range. In this result, if the dynamic range is taken into consideration even if there is unbalance of amplitude among array branches, the beamforming error is stored in ±1°.

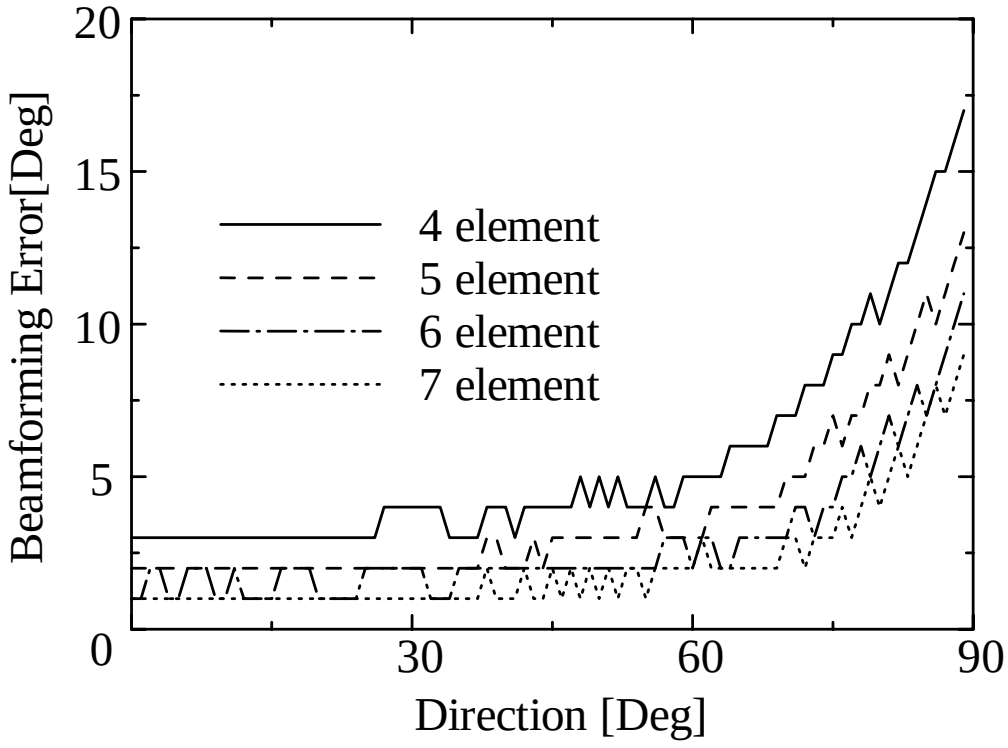

Fig. 3-24: Beamforming versus the number of branch error with 30° phase unbalance
12 bit 4 times over sampling

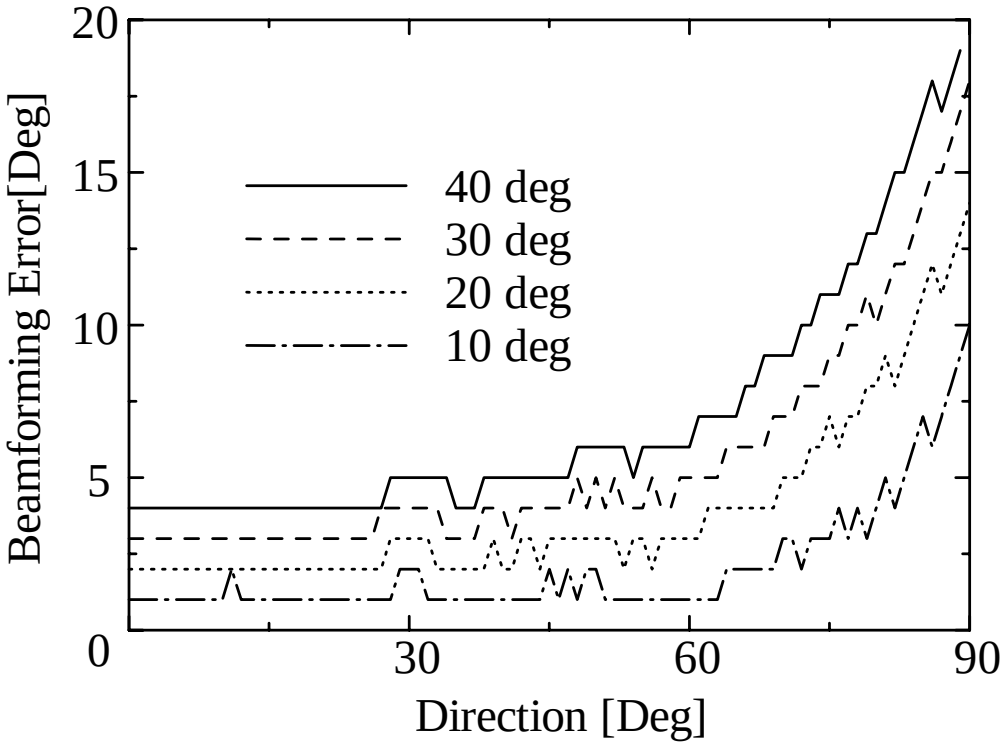

Fig. 3-25: Beamforming error with 10°, 20°, 30°, 40° phase unbalance

The number of branch is 4. 12 bit 4 times over sampling

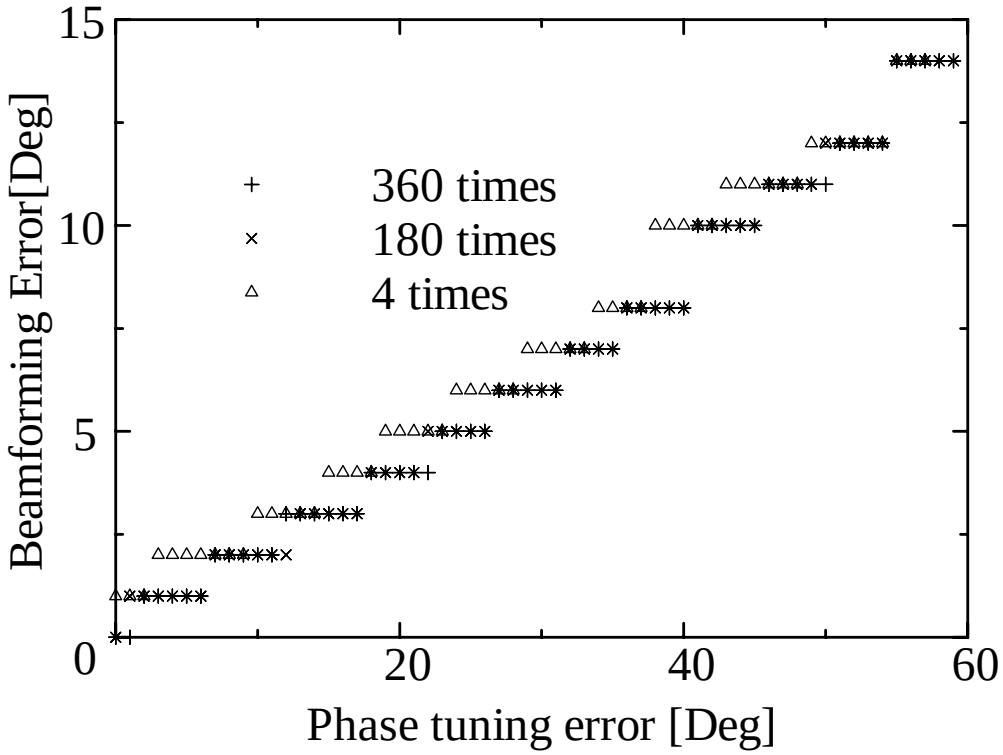

Fig. 3-26: Beamforming error versus phase tuning error in case of ±60° scanning range.

The number of branch is 4. 12 bit 360, 180 and 4 times over sampling

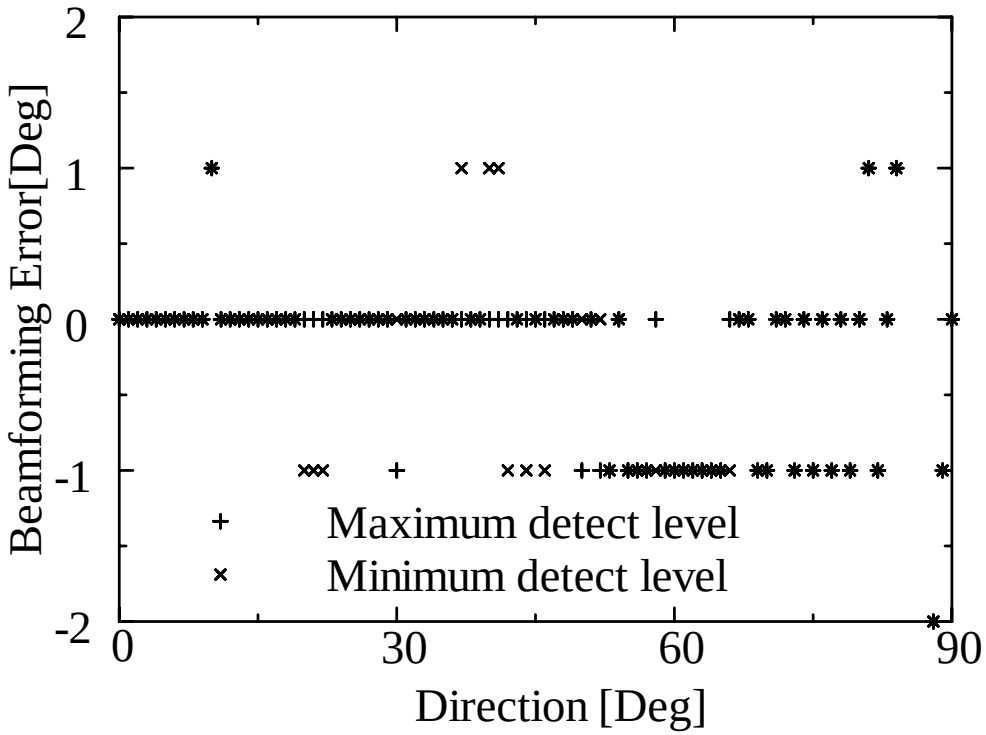

Fig. 3-27: Beamforming error versus amplitude tuning error

The number of branch is 4. 12 bit 360times and 4 times over sampling

Fig. 3-28 shows two type of tuning circuit, which are different in a method of phase tuning. One is phase tuning at IF part (a), another is at LO part (b). When broadband signal is used by using (a), phase tuning cannot be done by the same quantity over all bands. Phase tuning in the case of (b) is calibrated by changing the phase of the local signal inputted into the mixer of each array branches elements. The phase shifter of this case is necessary to operate only on single local frequency and easy to design.

Phase and amplitude are calibrated by using the circuit which can be controlled in the voltage. We needs to table-ize the amount of phase tuning (P_n) and the amount of amplitude tuning (G_n) of each array branches by control voltage (V_{P_n} and V_{G_n}) like a formula (3.14) and (3.15). Although the accuracy of a table depends on precision of D/A converter outputting the control voltage, it is sufficient if suitable tuning circuits are chosen, taking a dynamic range and phase unbalance into consideration.

$$P_n(V_{P_n}) = A_{p_n}(V_{P_n})e^{j(\phi p_n(V_{P_n}))} \qquad (3.14)$$

$$G_n(V_{G_n}) = A_{G_n}(V_{G_n})e^{j(\phi G_n(V_{G_n}))} \qquad (3.15)$$

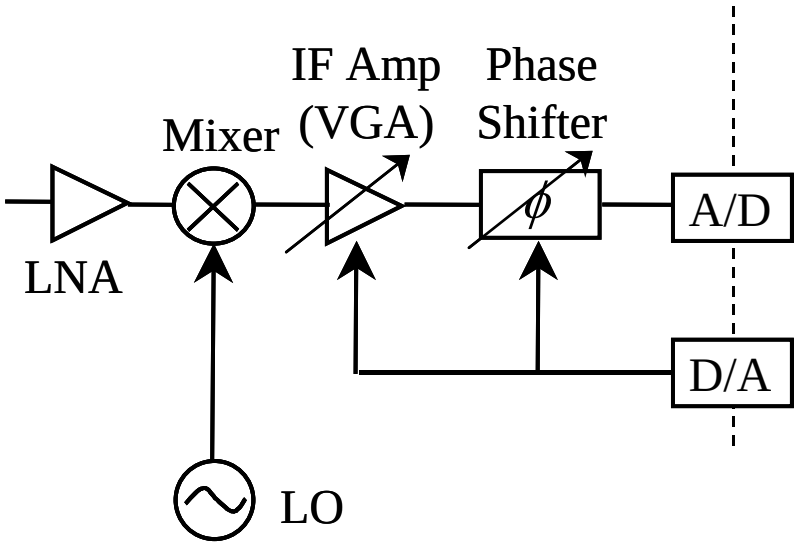

(a) Phase and amplitude tuning at IF part

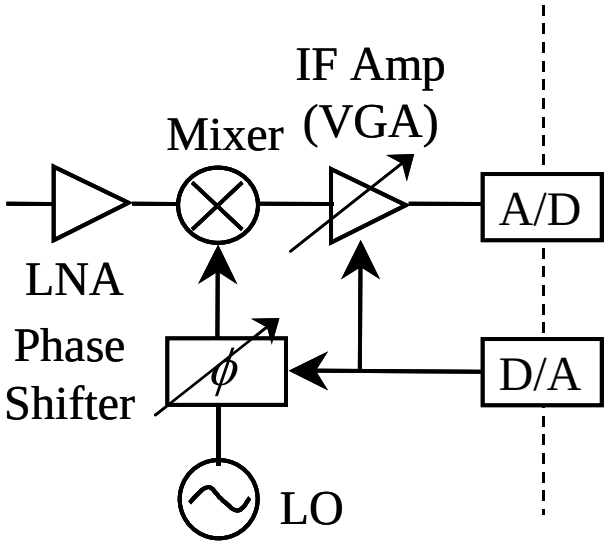

(b) Phase tuning at LO part and amplitude tuning at IF part

Fig. 3-28: Phase and amplitude tuning circuit

3.3.3. Reference signal generator

3.3.3.1. Procedure of calibration

A reference signal generator for calibration is conventionally arranged at the distant place of a receiving antenna, a plane wave is assumed, and phase and amplitude among branches are calibrated. In this section, the reference signal generator is arranged in an around array antennas shown in Fig. 3-29. One part of LO signal is branched and mixed with IF regenerated signal (CW) to generate the reference signal. This reference signal is same frequency as a received signal and transmitted from the reference antenna. The calibration is used reference signal generator with the following procedure.

(1) The reference signal generator mix one part of branched local signal ($A_{LO}e^{j(\omega_{LO}t+\phi_{LO})}$) with IF regenerated signal ($A_{IF}e^{j(\omega_{IF}t+\phi_{IF})}$) and generate a reference signal ($A_{re}e^{j(\omega_{re}t+\phi_{re})}$) same as carrier frequency.

$$A_{re}e^{j(\omega_{re}t+\phi_{re})} = A_{LO}e^{j(\omega_{LO}t+\phi_{LO})} \times A_{IF}e^{j(\omega_{IF}t+\phi_{IF})} \tag{3.16}$$

(2) The reference signal ($A_{re}e^{j(\omega_{re}t+\phi_{re})}$) is transmitted with array arrangement from the reference antenna where a relative position is known, and received with each element of array antenna ($A_{E_n}e^{j(\omega_{E_n}t+\phi_{E_n})}$).

$$A_{E_n}e^{j(\omega_{E_n}t+\phi_{E_n})} = A_{re}A_{M_n}e^{j(\omega_{re}t+\phi_{re}+\phi_{M_n})} \tag{3.17}$$

In addition, as shown in Fig. 3-30, whenever we place the reference antenna to the fixed place, the relative position of reference antenna and array antennas are constant and known. When d_0 denotes distance of between reference element and center of array center, d_{M_n} denotes distance of between reference element and each array element; we can derive phase difference ϕ_{M_n} and amplitude difference A_{M_n} among branches from relative distance d_0 and transmission formula. ϕ_{M_n} and A_{M_n} can be written in forms:

$$\phi_{M_n} = \frac{2\pi\left|d_{M_n} - d_0\right|}{\lambda_{RF}} \tag{3.18}$$

$$A_{M_n} = \frac{\lambda_{RF}}{2\pi\left|d_{M_n}\right|} \tag{3.19}$$

(3) When the reference signal is converted IF band and sampled, it becomes (3.20), and gets $A_n e^{j\phi_n}$ as the calibration data of each branches. $A_{b_n} e^{j\phi_{b_n}}$ denotes the characteristic of each branch including the individual difference of an antenna, an amplifier, a frequency conversion. $A_{b_n}{}' e^{j\phi_{b_n}'}$ denotes a characteristic of each branch which included an individual difference of local signal. Based on (3.18) and (3.19), phase and amplitude are tuned and calibrated using the circuit which was table-ized like (3.14) and (3.15) with voltage control.

$$\begin{aligned} & A_n e^{j(\omega t+\phi_n)} \\ & = A_{LO_n} A_{E_n} A_{b_n} e^{j\{(\omega_{LO_n}-\omega_{E_n})t+\phi_{LO_n}+\phi_{E_n}+\phi_{b_n}\}} \\ & = A_{M_n} A_{b_n}{}' e^{j(\omega_{IF}t+\phi_{M_n}+\phi_{b_n}')} \end{aligned} \qquad (3.20)$$

By using above mentions procedure, phase and amplitude difference among array branches can be calibrated. As for final fine tuning of the temperature characteristic of branch elements, the digital calibration included in adaptive algorithm has necessity. Therefore, it is necessary to use both analog calibration and digital calibration.

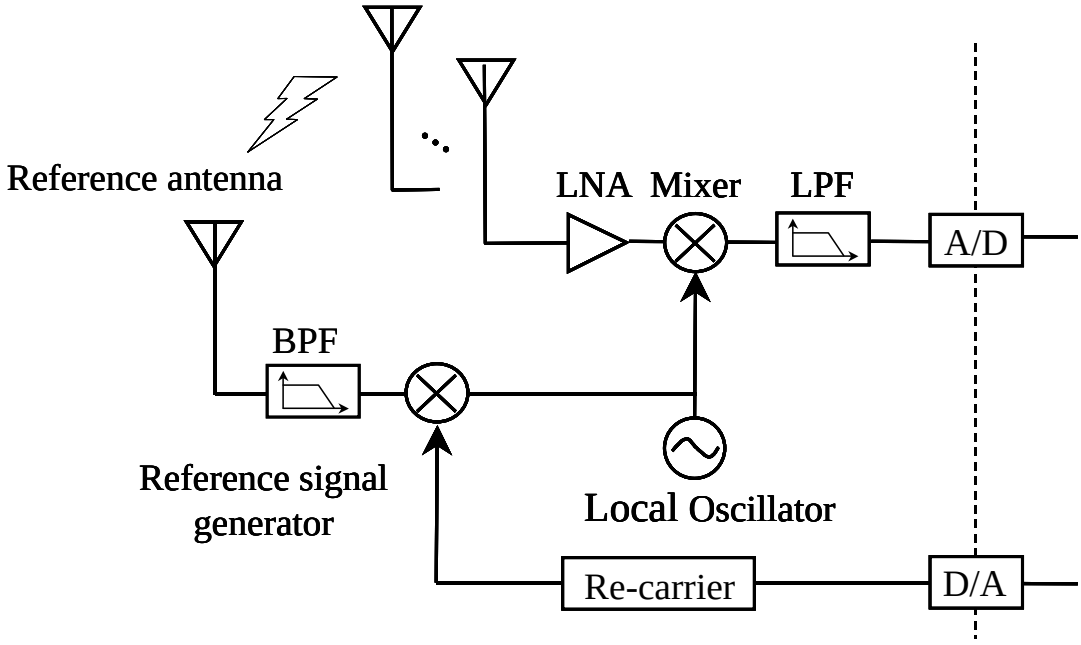

Fig. 3-29: Reference signal generator

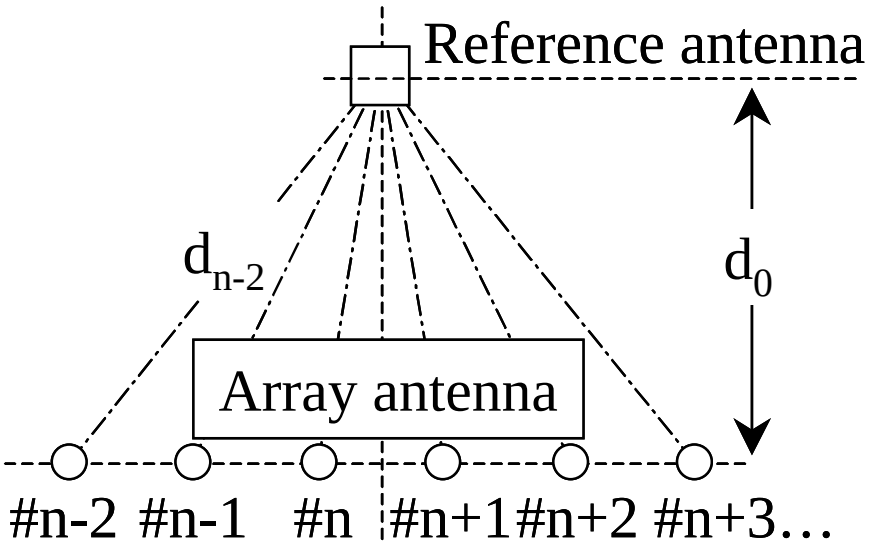

Fig. 3-30: Position of reference antenna and receiving array antenna

3.3.3.2. Position of Reference antenna

Let us consider the position of the reference antenna by using 8.45 GHz receiver. The construction of measurement is shown in Fig. 3-31, the measurement setup is shown in Table. 3-2. This setup is triple super heterodyne receiver included reference signal generator. The reference antenna is arranged at the position where phase difference among branches is the smallest. As shown in Fig. 3-30, in the case of the same plane between reference antenna and array antenna, via the center of array arrangement, the reference antenna is arranged plumb for direction of array arrangement.

In the case of six array antennas (as shown in Fig. 3-30), when changing d_0 (distance of reference antenna and array antenna), measurement of phase difference and an amplitude ratio between #n+1 and #n+2 or #n+1 and #n+3 are shown in Fig. 3-32 and Fig. 3-33. In addition, the amplitude ratio is normalized with the #n+2 element amplitude value case of $d_0 = 1\lambda_{RF}$. Therefore, in case of the reference antenna is arranged near the array center (less than three waves length), the ideal phase difference and amplitude ratio which can be derived from the path difference shown in the formula (3.18) or the propagation formula (3.19) can be mostly applied, and we can calibrate among array branches. However, when the reference antenna is arranged by 10 or less wavelength from three, phase difference can not wave length be derived from a course difference. Therefore in

this case, the calibration is difficult. In case of more than 10 wave length, it becomes similar when we arranged a reference antenna in a distant place.

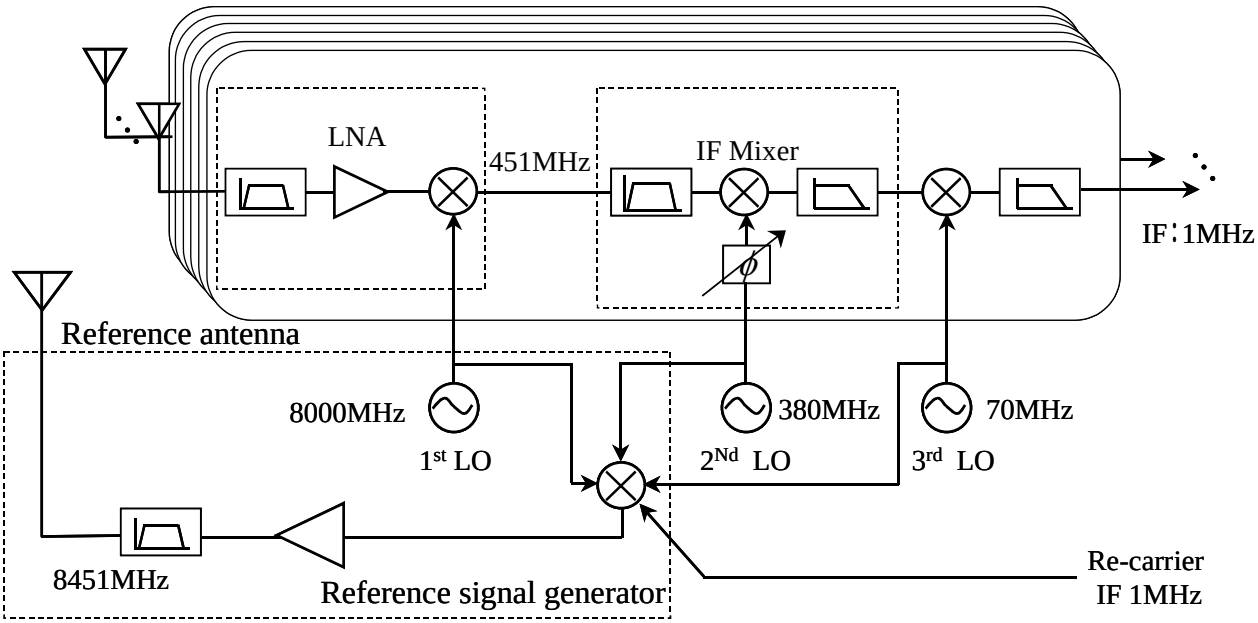

Fig. 3-31: Black diagram of the DBF receiver at 8.45 GHz

Table. 3-2: Measurement setup for calibration

RF (Measurement Frequency)	8.45GHz
IF	1st 450MHz, 2nd 70MHz, 3rd 1MHz
Receiving antenna	Sleeve antenna
The number of array element	6 linear array**
Receiver Gain	+40dB
Distance between transmit and receiver	3m
A/D converter	12bit, 5MS/s
Reference antenna	Sleeve antenna

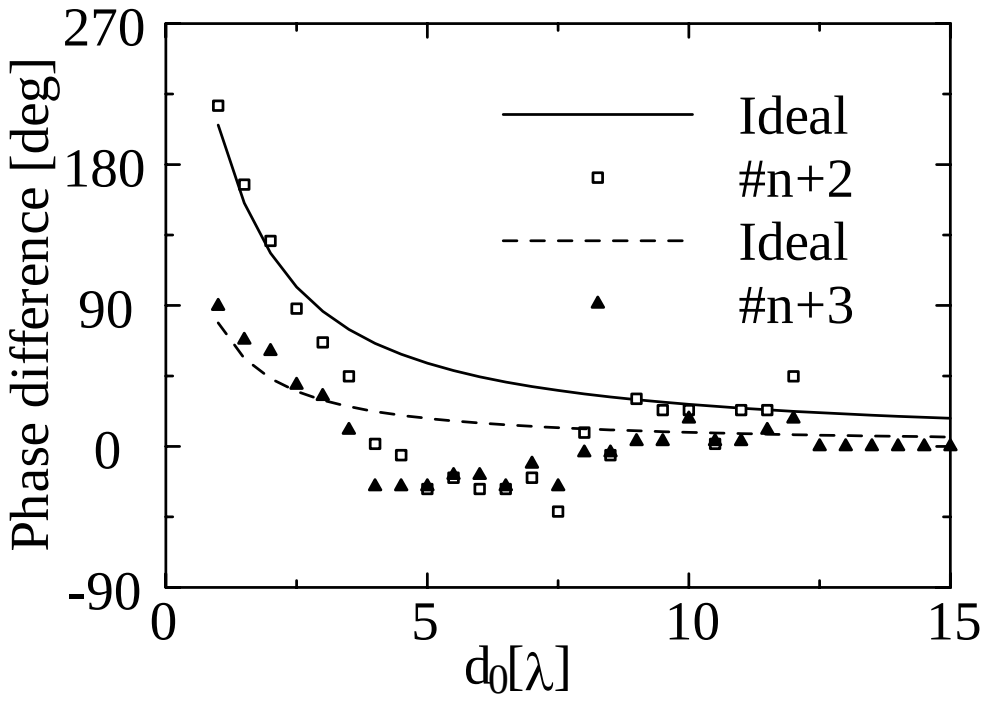

Fig. 3-32: Phase versus position of reference antenna and receiving array antenna

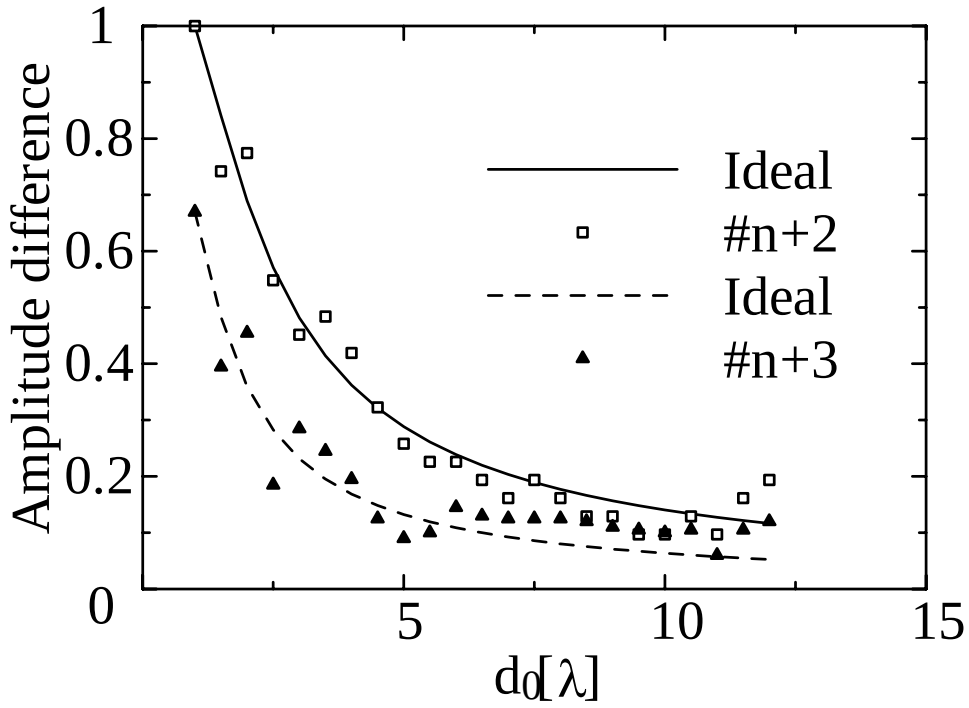

Fig. 3-33: Amplitude versus position of reference antenna and receiving array antenna

3.4. Active antenna Receivers for Digital Beamforming

3.4.1. Introduction

In micro-cell or ad hoc network of next generation high speed wireless communication, antennas of base station and terminal are required multi function, low cost, miniaturization. Research and development of small DBF system is demanded. The small direct conversion DBF receiver, which used the active integrated antenna was reported [18]. The active integrated antenna is designed to form the antenna as a passive element and an active circuit on the same substrate and can reduce transmission loss. Because of the unification passive elements (antennas) and active elements (amplifiers etc.), the feeding cable is unnecessary, can shorten an feeding transmission line to the extreme, and has the advantage which can reduce the phase and amplitude difference among array branch elements. An active integrated antenna has very advantageous for DBF which performance depends on phase and an amplitude characteristic between array branch elements. Furthermore, we can achieve miniaturization of DBF and restraint of an individual difference of a characteristic among array branch elements, by using technology that can reduce active elements such as direct conversion or Low IF system. In this section, we demonstrate near zero IF receiver with calibration circuit for DBF at 8.45 GHz. We describe active patch antennas with amplifier and near zero IF mixer for this proposed receivers.

3.4.2. Configuration of Receiver

Fig. 3-34 and Table. 3-3 show block diagram and specification of 8.45 GHz active antenna DBF receiver with calibration circuit. A RF signal received from receiving array antennas (the distance of each antenna is 8.45 GHz half wavelength) pass through LNAs, gate mixer and A/D converter, are converted IF signals excluded DC. This digital IF signals detect using digital down conversion technique (DDC) on PC [19]. Common receivers divide the received signal into I and Q signals by using a quadrature hybrid, generally implemented by analog circuits, in order to obtain phase information. However, in this case, it is difficult to make the orthogonal detection precisely, and the phase error causes beamforming error. To simplify the hardware construction, this receiver utilizes DDC, which can be implemented as a finite impulse response (FIR) digital filter, instead of the analog orthogonal detector. Another advantages can reduce by half the number of A/D convector. Moreover, since the signal sampled with A/D convector is an IF signal which does not contain a DC, it is not necessary to take DC offset noise into consideration like a direct conversion system.

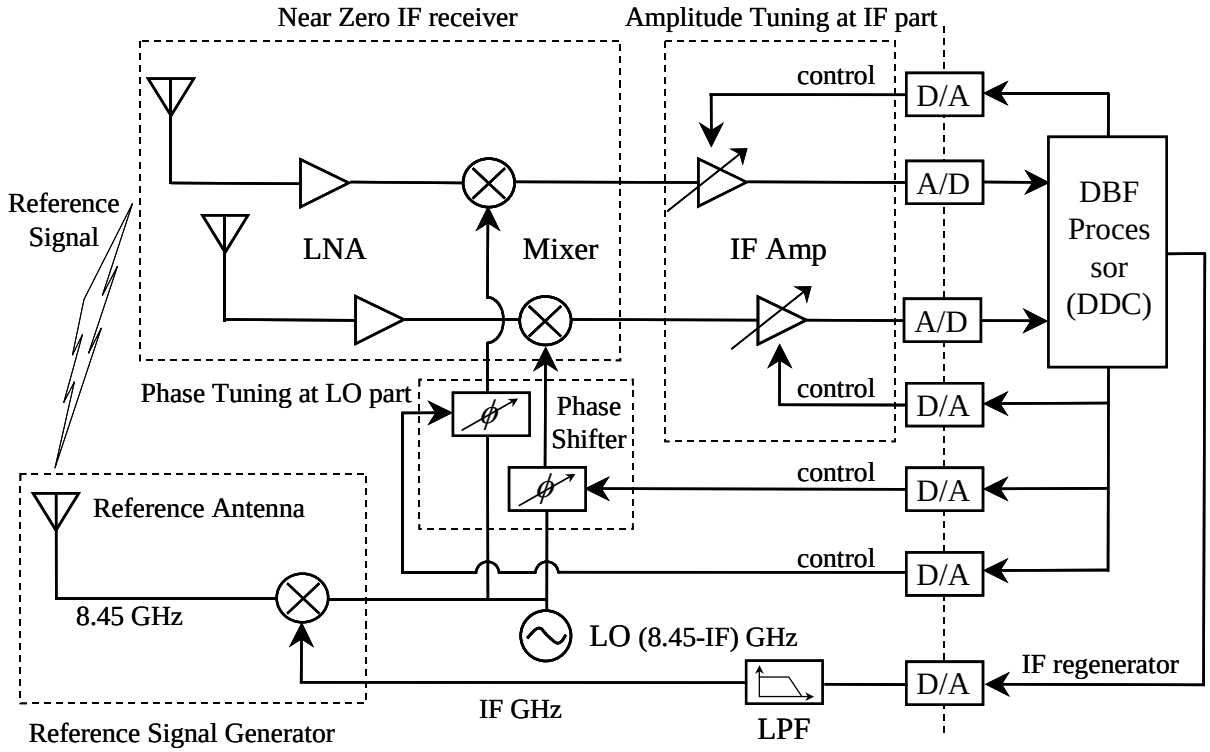

Fig. 3-34: Block diagram of active antenna receiver DBF at 8.45GHz

Table. 3-3: Specification of active antenna receiver DBF at 8.45GHz

IF center frequency	1st 10MHz
IF output	±2.0V (4Vp-p)
A/D resolution	12bit
A/D Sampling frequency	40MHz
Gain	20dB(±3dB)
Linear Dynamic range	50dB(-60～-10dBm)
Tuning Voltage	DC 0～5V
Amplifier control	±5dB (IF Part)
Phase control	±45 (LO Part)

3.4.3. Active patch antennas with amplifier

The active integrated patch antenna with amplifier is used for the receiving antenna of proposal system. Although a patch antenna is widely used as flat small antenna, matching circuit or offset feeding are necessary to use in 50 Ω systems, because input impedance of end part of patch is very high. However, if an input impedance of amplifier used for after step of patch antenna is high, we can directly connect by high impedance. Therefore, a feeding transmission line can be shortened, and phase and amplitude difference between array antenna elements can be reduced. Generally, since the input impedance of FET amplifier of source grounding is high, it can be directly connected with a patch antenna. Fig. 3-35 shows configuration of active patch antenna. On a Teflon dielectric substrate (ε_r=2.6, Thickness = 0.8 mm), HJ FET (NE3210S10, NF = 0.35 dB, Ga = 13.5 dB @f = 12 GHz, Lg = 0.20 μm, Wg = 160 μm) is arranged as a low noise amplifier. The patch antenna (length is $\lambda_{RF}/2$) through the microstrip line that is 0.4 mm is connected to the gate of FET. DC bias (Vds = 2.0 V, Vgs=-0.4 V) is applied using 1/4 wave of open radial stub. Fig. 3-36 shows input characteristic of active patch antenna. This calculation is used Microwave Office [20]. The bandwidth of this active antenna is almost same as a conventional patch antenna. Fig. 3-37 and Fig. 3-38 shows E-plane and H-plane radiation pattern of active patch antenna. It is normalized by a gain of the maximum direction of a patch antenna using offset feeding in 50 Ω microstrip line. About 12 dB is amplified compared with a conventional patch antenna, and it's characteristic is sufficient what M.S.G. of HJFET is about 16 dB. However, because of the radiation from radial stub of amplifier etc., a cross-polarization level is high in E-plane and H-plane, and the radiation pattern is distorted. It is required although a shield is used in order to reduce this back robe.

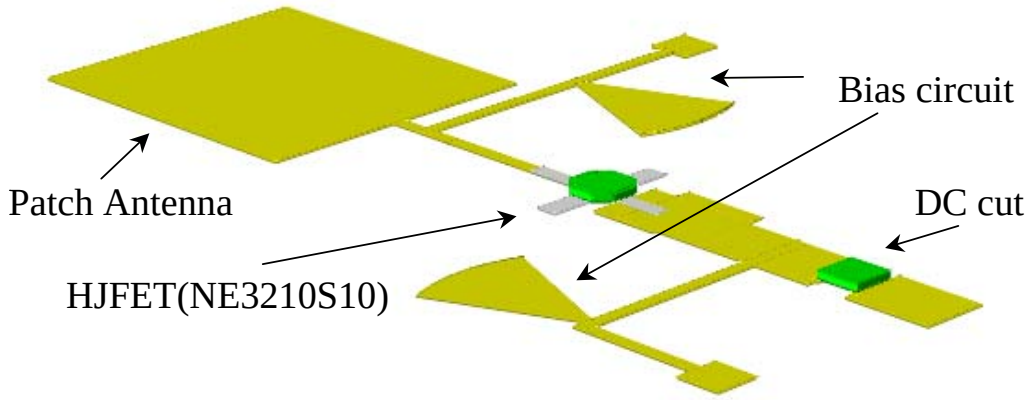

Fig. 3-35: Configuration of active patch antenna

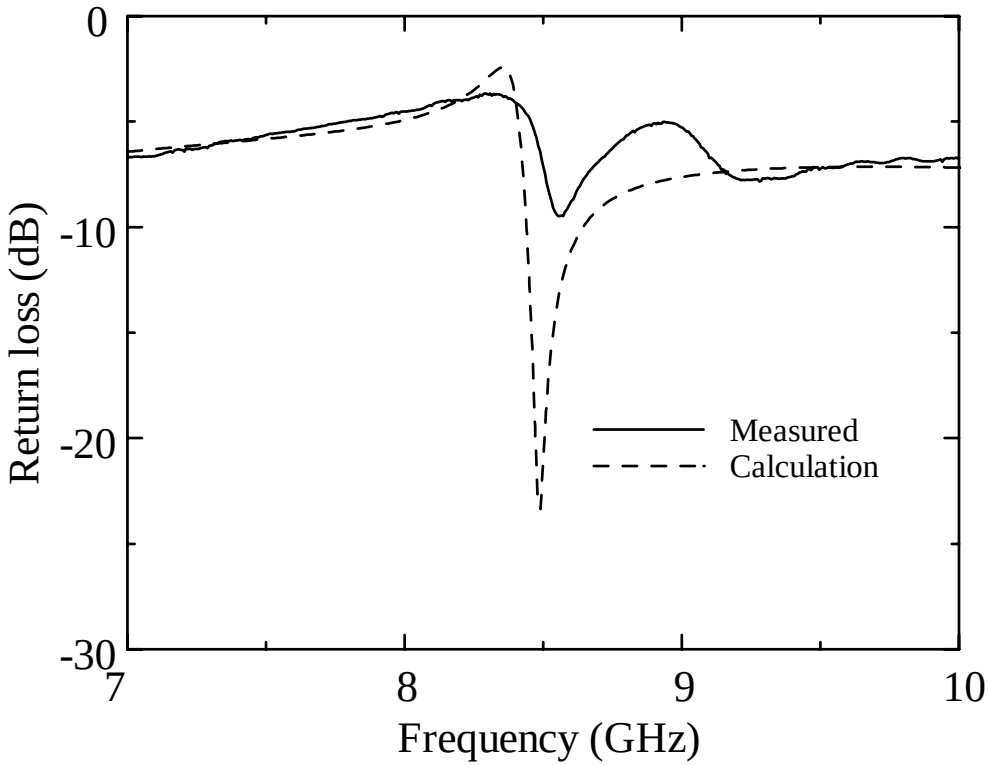

Fig. 3-36: Return loss of active patch antenna

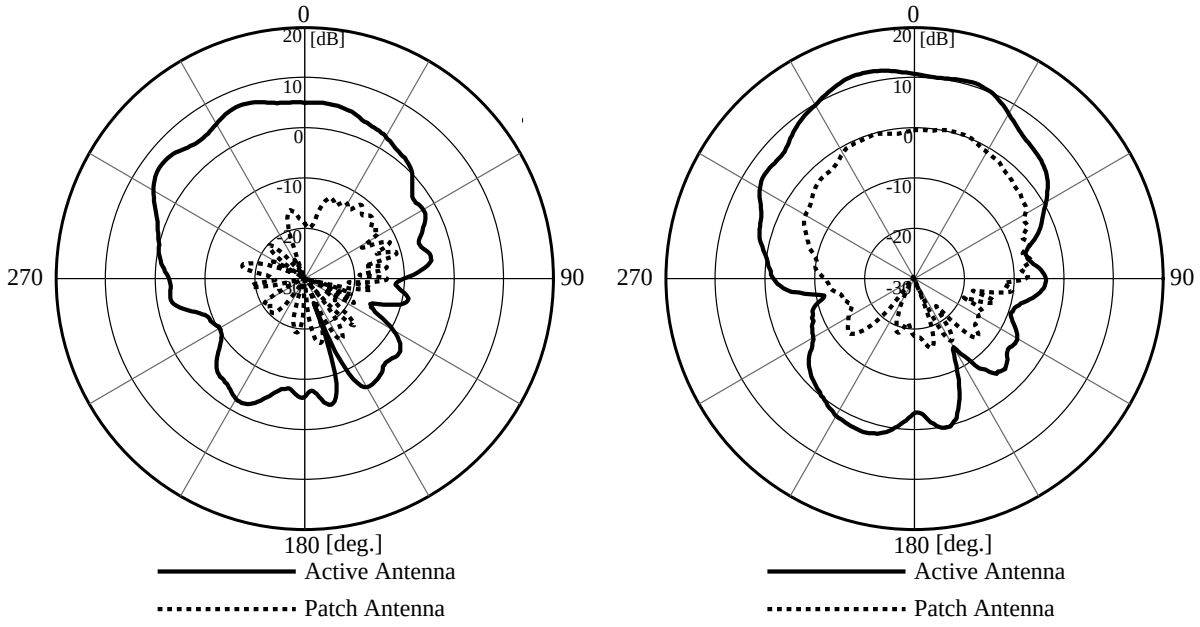

(a) Co- polarization (b) Cross- polarization

Fig. 3-37: E-plane radiation pattern of active patch antenna

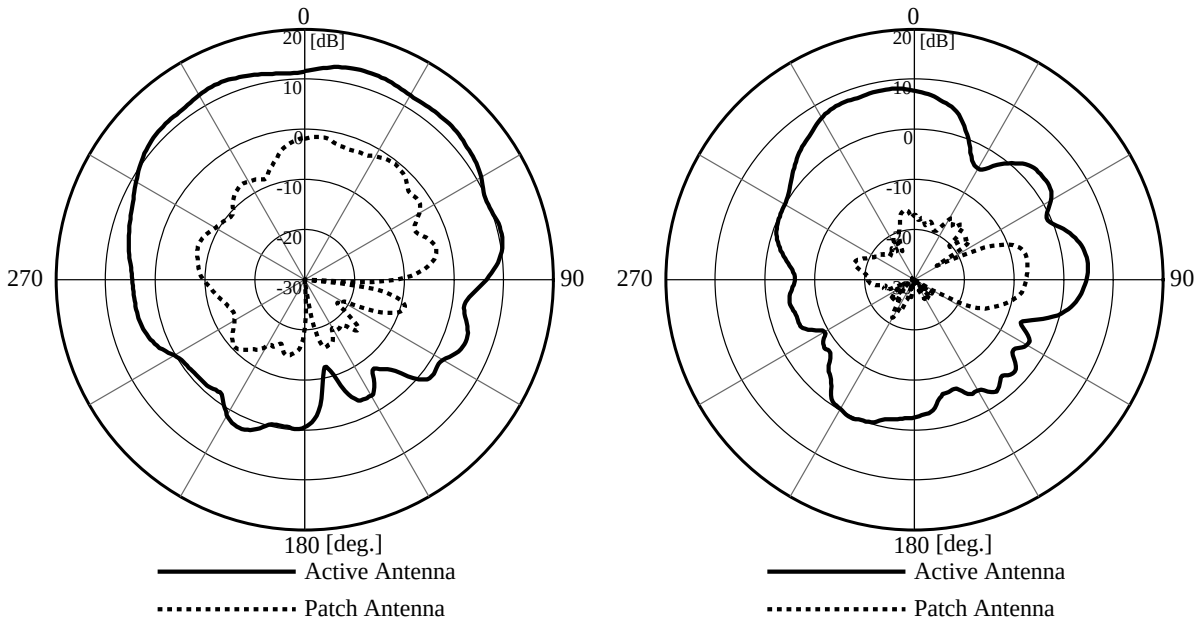

(a) Co- polarization (b) Cross- polarization

Fig. 3-38: H-plane radiation pattern of active patch antenna

3.4.4. Near zero IF Mixer

In this section, we describe near zero IF mixer. Fig. 3-39 shows the FET gate mixer constructed on 0.8 mm thick Teflon substrate (εr=2.6, thickness of copper = 18mm). The FET is used NEC NE3210S10 HJFETs. Because the frequency of RF and LO is almost same on this near zero IF receiver, this gate mixer has two advantages. One is that input-matching circuit can be simplified. The other is that power divider can be use. The LO signal (8.44GHz) and RF signal (8.45GHz) is applied to the gate of FET using the Wilkinson power divider by using microstrip line. In case of this mixer, the isolation between LO and RF is depended on divider, however, the divider isolation of more than –30 dB is sufficient for this application. The IF signal is extracted from drain by using low pass filter with microstrip line. IF versus RF power and conversion gain versus LO power is shown in Fig. 3-40 (a) and (b), respectively. The conversion gain of about 5 dB is achieved for a LO input power of +3 dBm. LO leak is less than –50dB. Second harmonic is less than –65dB.

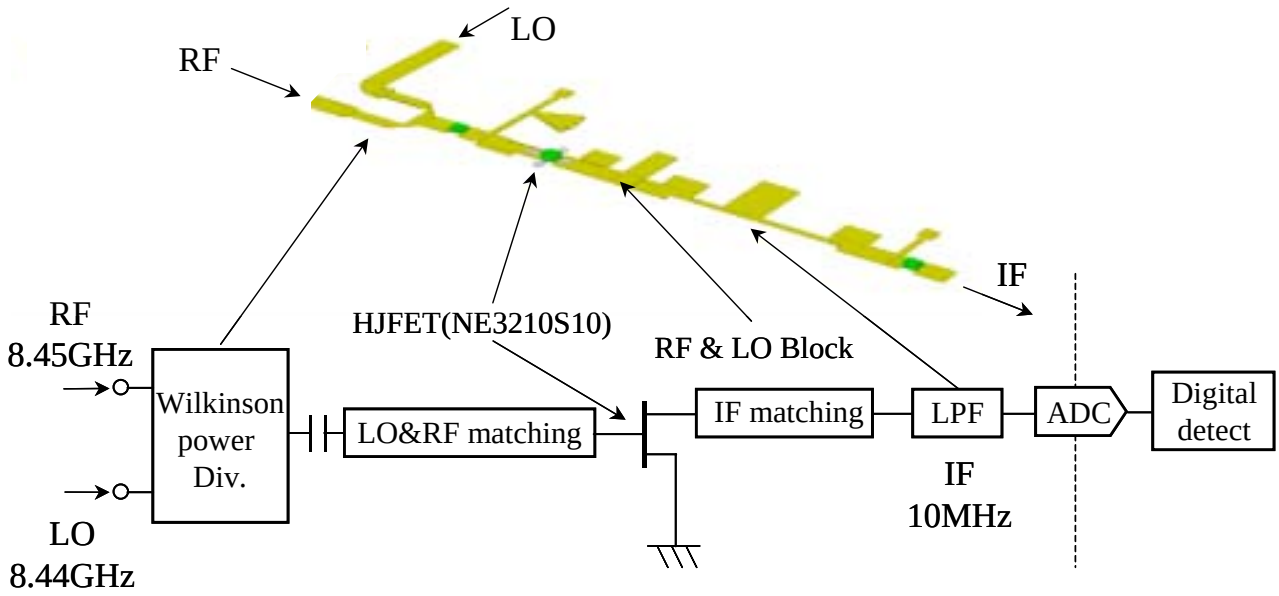

Fig. 3-39: Schematic of FET mixer for near zero IF receiver

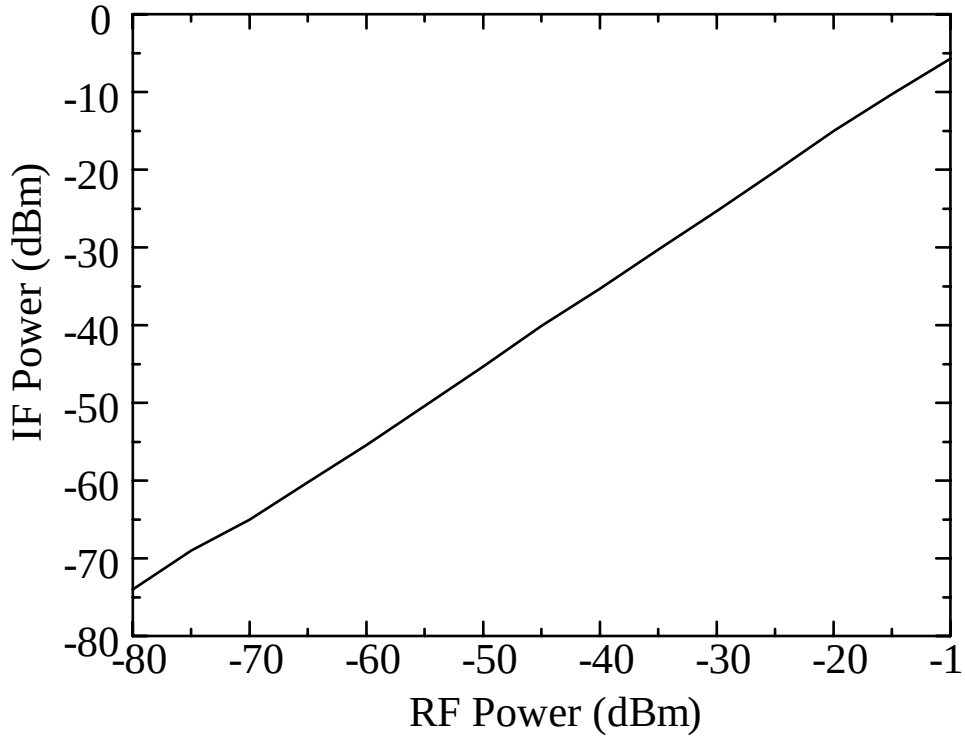

(a) IF versus. RF power at LO power = 0dBm

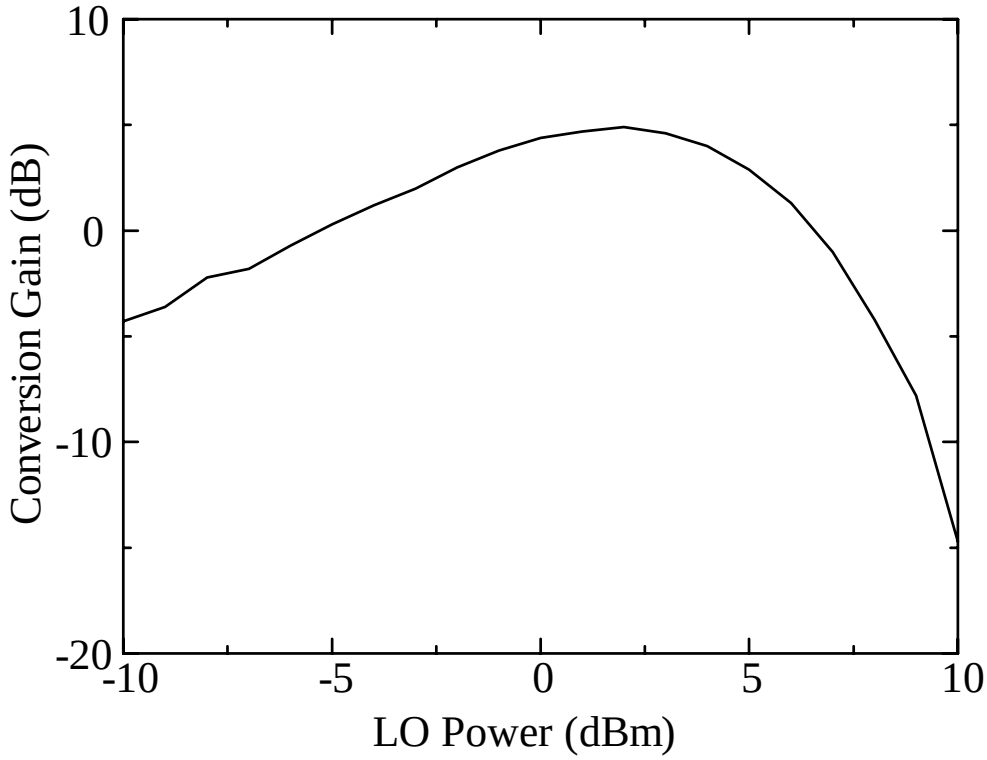

(b) Conversion. gain versus. LO power at RF power= -30dBm

Fig. 3-40: Performance of mixer

DC bias (Vds = 2.0 V, Vgs=-0.4 V)

3.4.5. Beamforming Results

Proposed near zero IF receiver's ability is evaluated through function as a digital beam former inside a radio anechoic chamber. The measurement setup is shown in Fig. 3-42. The signal of continuous wave (CW) from a signal generator is transmitted from a sleeve antenna through a high power amplifier. This transmitting antenna is installed 2 m far from the center of the receiving array antenna. Two proposed near zero IF receivers are arrayed in the half wavelength interval and connected active patch antenna. The CW signals received from the active patch array are converted to IF signals by the proposed receiver. The IF signals are sampled simultaneously by the A/D converter on the PC. Moreover, the proposed calibration method revises phase and amplitude unbalance among branches. The beam forming patterns are obtained by baseband data collected from each antenna element using off-line processing. Fig. 3-43 show the synthesized beam pattern with main beam directed towards ±30° (transmitting antenna is installed in these directions from the center of the receiving array antenna). In this result, the digital beam forming can be realize that side lobe level is below –5 dB and the half power beam width is about 70°, in case of scanning range is limited ±30° by using this proposed receiver. Fig. 3-44 shows beamforming error versus

direction of transmitter. The ability of receiver is almost same that of common receivers using isotopic antenna. It is sufficient for this high speed wireless communication application.

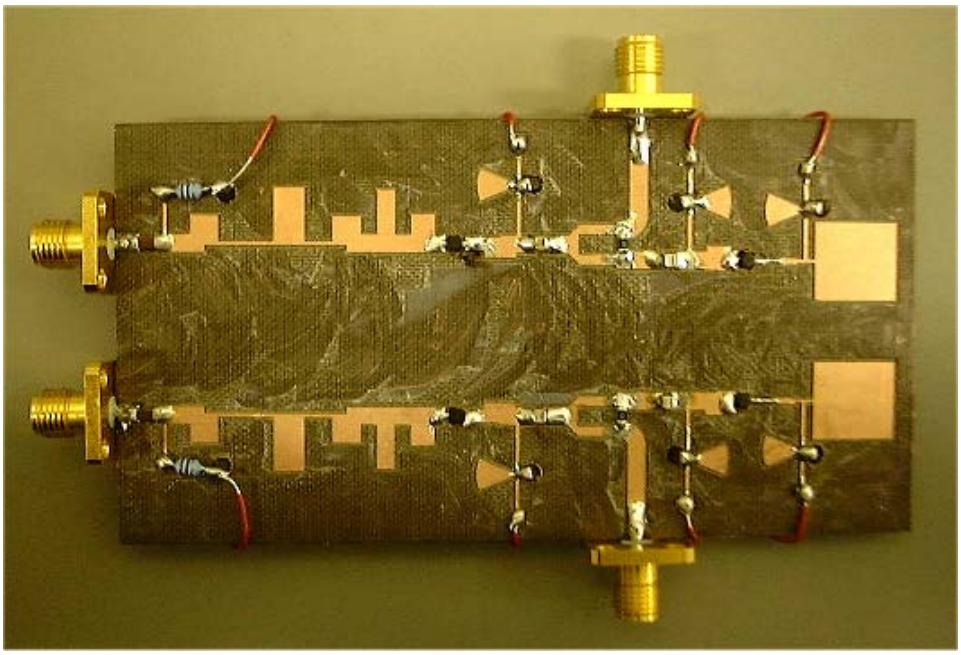

Fig. 3-41: 2 element proposed receiver

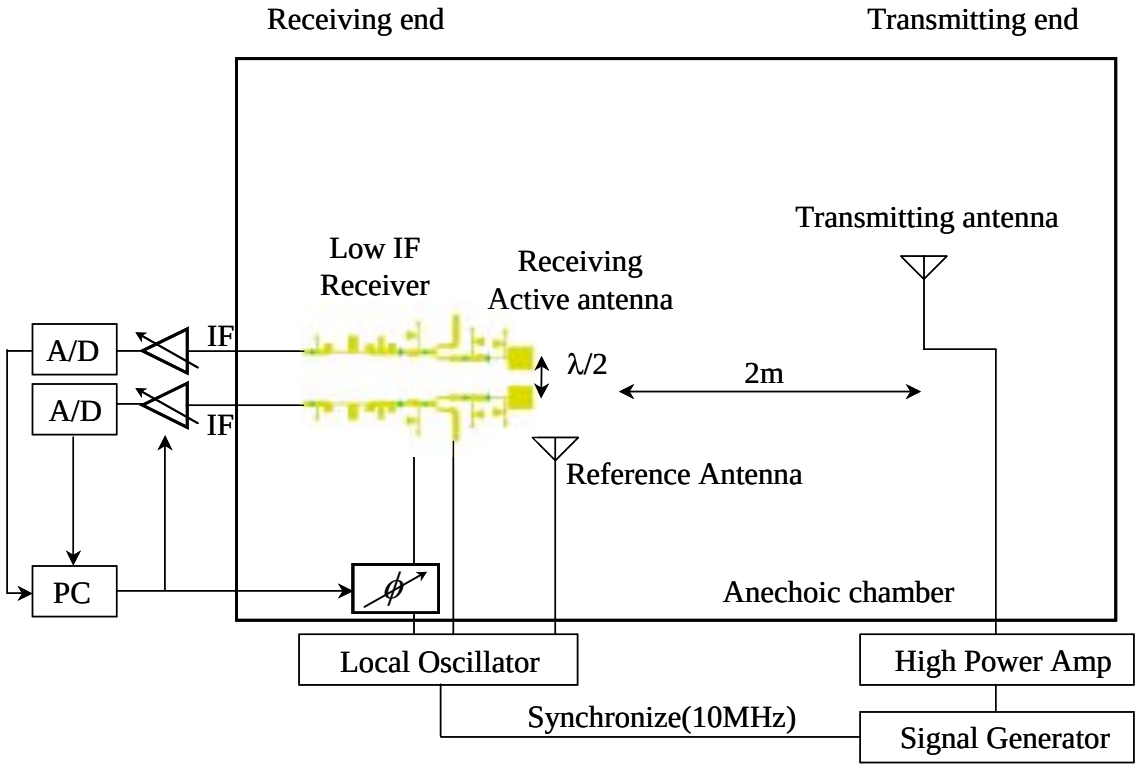

Fig. 3-42: Measurement setup for digital beamforming

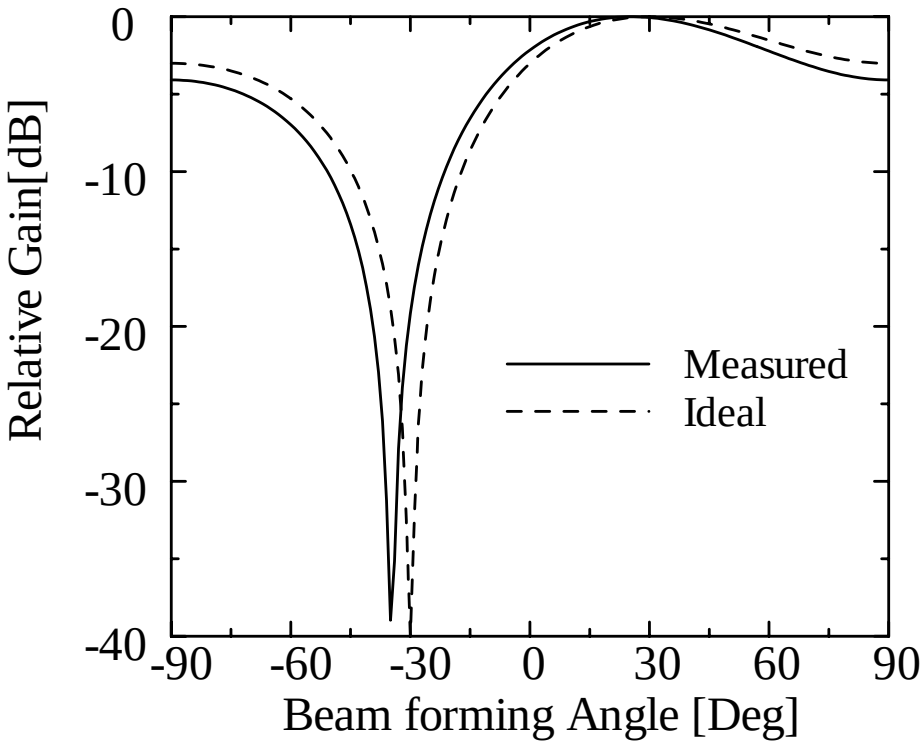

(a) Towards +30° direction

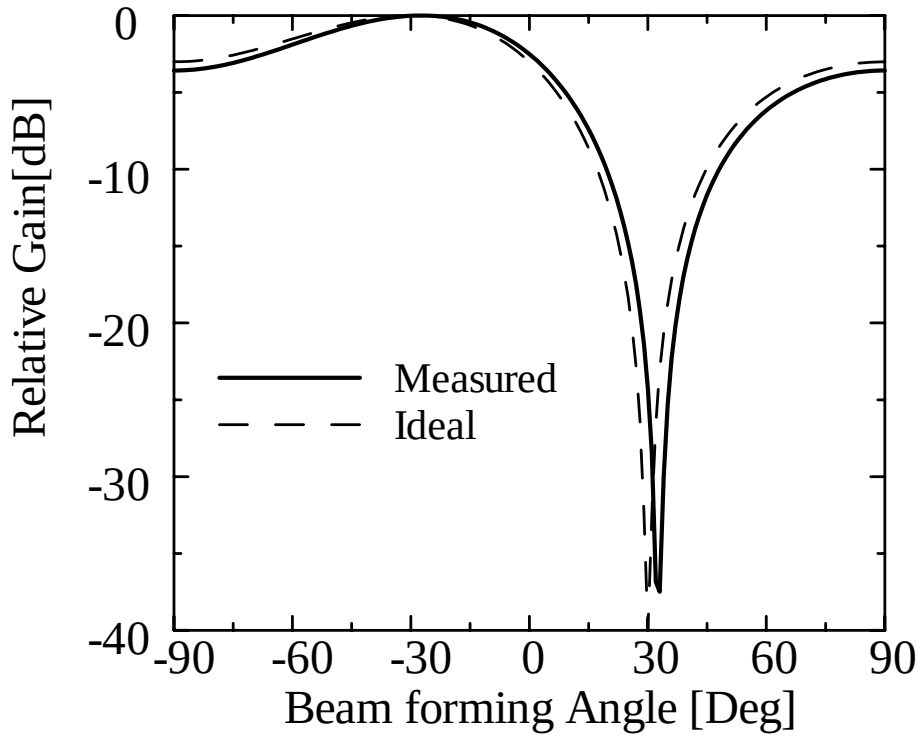

(b) Towards -30° direction

Fig. 3-43: Beamforming result

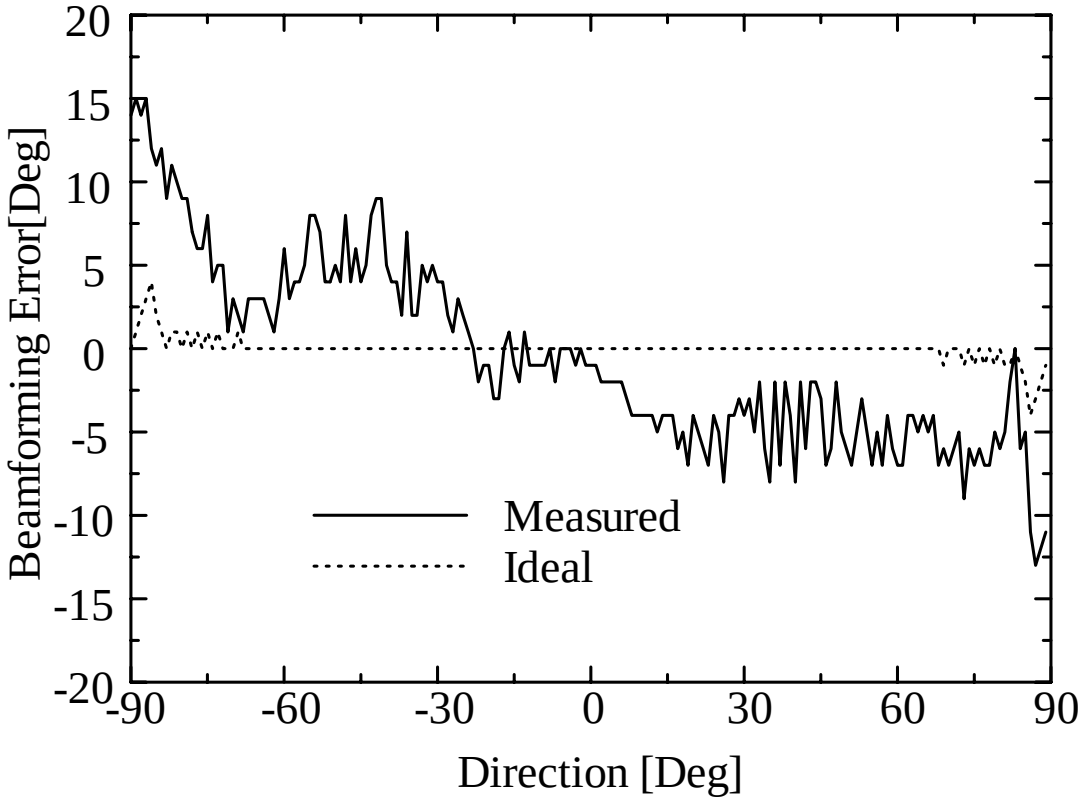

Fig. 3-44: Beamforming error using proposed receiver

3.4.6. Summary

We proposed near zero IF receiver with calibration circuit for DBF at 8.45 GHz. This mixer's conversion gain was about 5 dB. We also examined this proposed receiver's ability to function as a digital beam former. In this result, the digital beam forming could be realize that side lobe level was below –5 dB and the half power beam width was about 70°, in case of scanning range is limited ±20° by using this proposed receiver. The ability of this receiver is almost same that of common receivers using isotopic antenna. It is sufficient for this high-speed wireless communication application.

References

[8] T. Tanaka, R. Miura, and Y. Karasawa, "Implementation of a Digital Signal Processor in a DBF Self-Beam Steering Array Antenna", IEICE Trans. Communication, vol.E80-B, no.1, pp.166-175, Jan 1997.

[9] S.W. Ellingson, H.J. Kim, and K.S. Ayotte, "Low-Cost Adaptive Arrays for Analysis of Wireless Systems", IEEE AP-S International Symposium Digest, pp.1100-1103, Jul 1999.

[10] R.O. Schmidt, “Multiple Emitter Location and Signal Parameter Estimation”, IEEE Trans. Antennas and Propagation, vol.34, no.3, pp.276-280, Mar. 1986.

[11] A. Antoniou, “Digital Filters”, McGraw-Hill, NJ, 1993.

[12] T.J.Shan, M.Wax, and T.Kailath, “On spatial smoothing for directions of arrival estimation of coherent signals”, IEEE Trans. Acoustics, Speech and Signal Processing, vol.33, no.4, pp.806-811, Apr 1985.

[13] R.Roy and T.Kaikath, “ESPRIT-Estimation of Signal Parameters via Rotational Invariance Techniques”, IEEE Trans. Acoustics, Speech and Signal Processing, vol.37, no.6, pp.984-995, July 1989.

[14] P.N. Fletcher and P. Darwood, “Beamforming for circular and semicircular array antennas for low-cost wireless LAN data communications systems”, IEE Proceedings Microwaves, Antennas and Propagation, vol.145, no.2, p.153-158, Apr 1998.

[15] P.N. Fletcher and M. Dean, “Deviation of orthogonal beams and their application to beamforming in small phased arrays”, IEE Proceedings Microwaves, Antennas and Propagation, vol.143, no.4, p.304-308, Aug 1996.

[16] K.Nishimori, K.Cho, Y.Takatori, and T.Hori, “Automatic calibration method of adaptive array for FDD systems”, IEEE AP-S International Symposium Digest, pp.910-913, Jul 2000.

[17] John Khoury and Hai Tao, “Data Converters for Communication Systems”, IEEE Communication Magazine, Vol.36, pp113-117, Oct 1998.

[18]Seong-Sik Jeon, Yuanxun Wang, Yongxi Qian, Bijan Houshmand and Tatsuo Itoh, “Active Quasi-Yagi Antenna Direct Conversion Receiver Array With Digital Beamforming”, IEEE AP-S International Symposium Digest, pp.1268-1271, July 2000.

[19] M. Löhning, T. Hentschel, and G. P. Fettweis. “Digital Down Conversion in Software Radio Terminals”, 2000 EUSIPCO, volume 3, pp1517-1520, Sep 2000.

[20] Applied Wave Research, inc, www.mwoffice.com

4. Active antenna

4.1. Introduction

The active antenna has drawn attention as a high efficiency antenna for microwaves and millimeter waves [21]. The active antenna has an architecture designed to improve the antenna characteristic by combining an active device in a part of a passive element. Among active antennas, the active integrated antenna is designed to form the antenna as a passive element and an active circuit on the same substrate and (1) is small and light-weight, (2) can make the effective length of the antenna smaller, (3) can make the bandwidth large, and (4) can reduce noise and transmission loss. As the circuit for an active integrated antenna, amplifiers [22], mixers [23], oscillators [24], and so forth can be considered. Of these, an active antenna combining the oscillator using a Gunn diode or an FET is particularly important and has been extensively studied since the feed loss, an important factor at millimeter wave frequencies, is small [25, 26, 27, 28, 29]. As the radiating element, the microstrip antenna and the slot antenna are used. These antennas not only function as the load to the oscillator but also determine the oscillation frequency based on the antenna and the length of the transmission line. Hence, an active antenna combining an oscillator with an arbitrary frequency can be designed by means of the antenna parameters.

In general, the Q of the oscillator is degraded in an active antenna combining the oscillator, since the Q of the antenna connected to the active device is low. Therefore, if the active antenna is used alone, improvement of the stability of the oscillation frequency and the radiation pattern cannot be expected. In regard to the active antenna combined with an oscillator, the output power of the semiconductor device is relatively small. There are techniques to construct an array to carry out quasi-optical power combining. Studies have been conducted on the locking techniques important in the power combining [24, 25, 29]. In practice, however, the study of the oscillator stability affecting the transmission efficiency is limited to that of the array to enhance the power coupling stability by means of a dielectric resonator [29]. No discussion is carried out on the stability of the single active antenna. In this chapter, an active antenna is proposed in which a half-wave dipole parasitic resonator is placed on the GaAs FET oscillator using a coplanar waveguide with a ground plane [26-28]. An experimental investigation is carried out on enhancement of the stability of the oscillation frequency and improvement of the radiation pattern.

4.2. Antenna Configuration

The configuration of the active antenna is shown in Fig. 4-1. A GaAs FET (HEMT FHX35LG by Fujitsu) is placed as an active device on a dialectic substrate with a relative permittivity of 2.6 and a thickness of 1.6 mm. To its gate and drain are attached loads consisting of open-ended coplanar waveguide having a characteristic impedance of 50 Ω (s = 0.2 mm, w = 4.0 mm) and lengths of Lg and Ld. An optimized short-circuited 50 Ω coplanar waveguide with a length of Ls is connected to the source in order to increase the reflection coefficient and the unstable region for oscillation [30]. If this waveguide is not connected, the oscillation is found to become unstable. On the backside of the substrate, a copper ground plane is kept to suppress the radiation into the backward direction of the substrate. Further, from the backside of the substrate, a DC bias (Vds = 1.0 to 3.0 V) is connected to the • points on the front surface shown in Fig. 4-1 via the through holes (ϕ = 1.0 mm) so that the bias is directly applied between the drain and the source of the GaAs FET without using a DC cut, no bias is applied between the gate and the source (Vgs = 0 V) and hence the bias is a single bias with a simple configuration. The bias circuit is not complicated even if an array is formed.

The equivalent circuit of this oscillator is shown in Fig. 4-2. It is considered that a π-type feedback circuit is connected to the grounded-source FET. In general, the antenna is connected as a matched load on the gate side in the conventional FET oscillator-type active antenna discussed in [27]. In this section, the oscillation condition is satisfied by connecting only a short-circuited coplanar waveguide to the matched load. Since the parameters on the oscillation frequency are not clearly given in [6-8], basic data are measured. As shown in Fig. 4-3, the oscillation frequency can be adjusted by the length Lg of the load to the gate. If this length is about one-fourth of the wavelength at the oscillation frequency; a series resonance is forced and the oscillation frequency is almost determined. From the viewpoint of the equivalent circuit in Fig. 4-2, it is found that the reactance component connected to the gate determines the oscillation frequency.

Next, as shown in Fig. 4-4, the oscillation frequency also changes depending on the length Ld of the drain load. In comparison with Fig. 4-3, it is found that the change of the oscillation frequency is less than the case where the length Lg of the load to the gate is varied. In this configuration, this parameter does not provide a function to act as an oscillator but rather varies the oscillation condition. As shown in Fig. 4-5, the oscillation function changes with the bias voltage. As the bias voltage is increased to the value close to the maximum voltage of the GaAs FET, the oscillation frequency becomes higher while no oscillation is observed if the bias is decreased to less than 0.3 V.

Also, since similar variations are observed if the semiconductor device is replaced with another (2SK571 by NEC), the change of the oscillation frequency is found to be strongly dependent on the device. On the other hand, the oscillation level changes very little even if the bias voltage is varied. Since the coplanar waveguide with a ground plane is used, a TEM mode can be excited in the substrate and the oscillation condition may be affected depending on the size of the substrate. When the length of L1 in Fig. 4-1 is increased or decreased by about one-fourth of the wavelength at the oscillation frequency, the change of the oscillation frequency is less than 1% and is negligible. Hence, in comparison to the cases in Fig. 4-3 and Fig. 4-4, the variations of the oscillation condition dependent on the substrate size are negligible. This is similar when the length of L2 is varied. The variations of the radiation pattern versus substrate size are discussed in Section 4.4. The oscillation spectrum is as shown in Fig. 4-6. When the oscillation frequency is 1.574 GHz, the range in which the SNR is less than 30 dB is about ±50kHz and is about 0.003% of the oscillation frequency. Hence, a high Q is obtained even as a single oscillator.

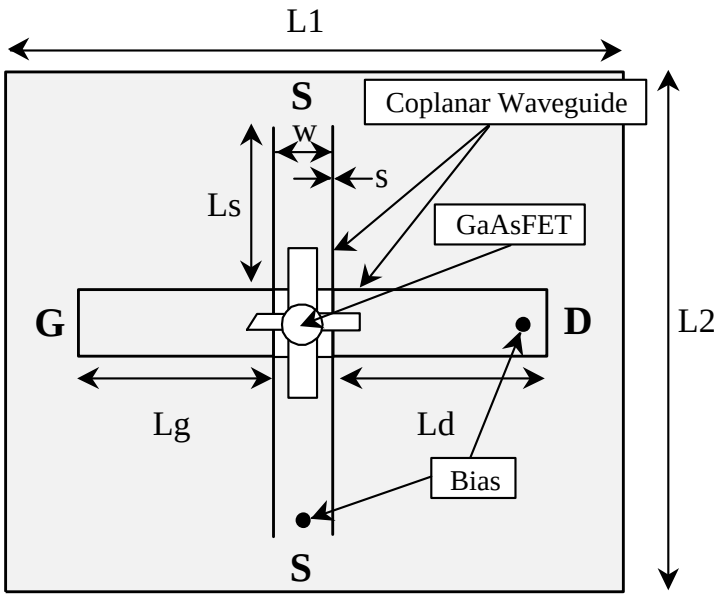

Fig. 4-1: Configuration of active antenna

Dielectric constant of substrate is 2.6, and its thickness is 1.5 mm

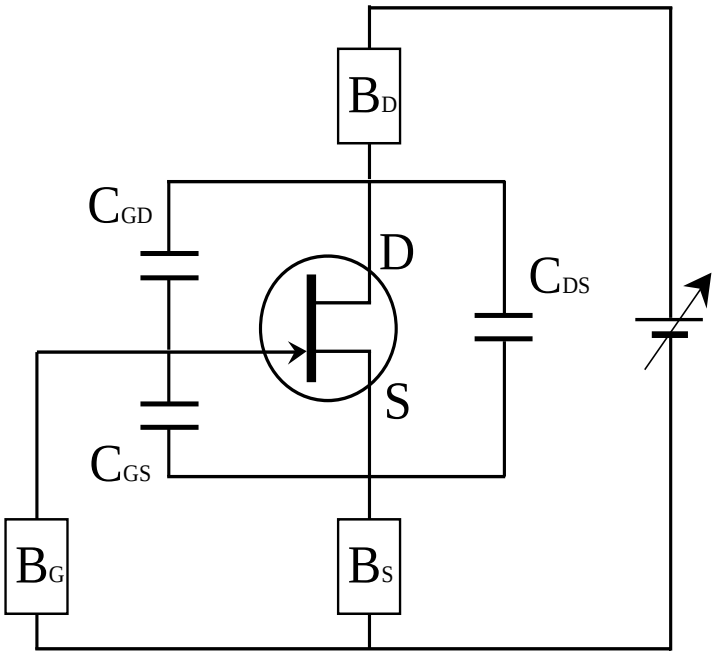

Fig. 4-2: An equivalent circuit of oscillator

Bx: reactance ingredient of load, Cx: stray capacitance

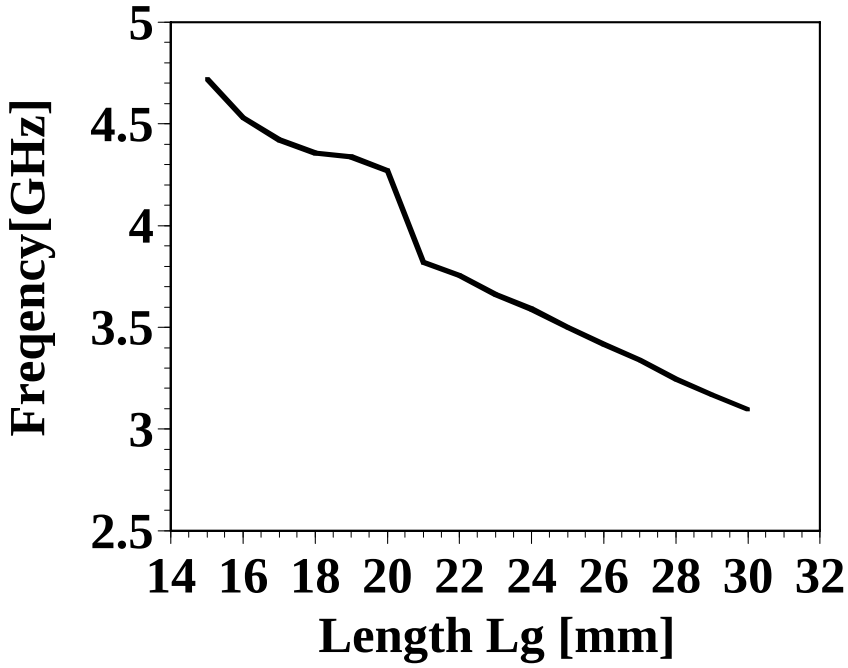

Fig. 4-3: Oscillation frequency versus Lg.

Ld = 30.0 mm, Ls = 20.6 mm, Vds = 3.0V

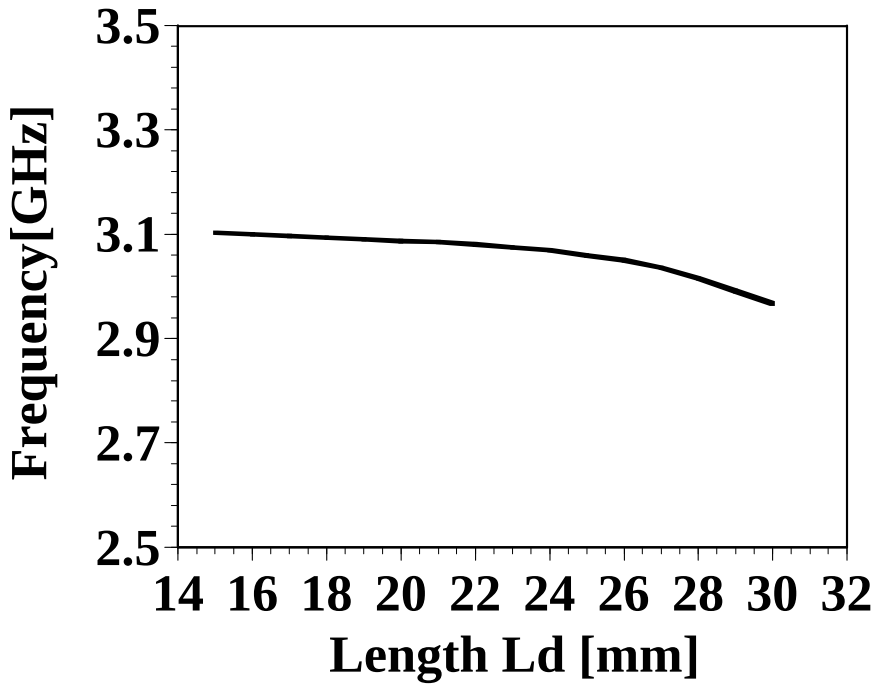

Fig. 4-4: Oscillation frequency versus Ld.

Lg = 15.0 mm, Ls = 20.6 mm, Vds = 3.0 V

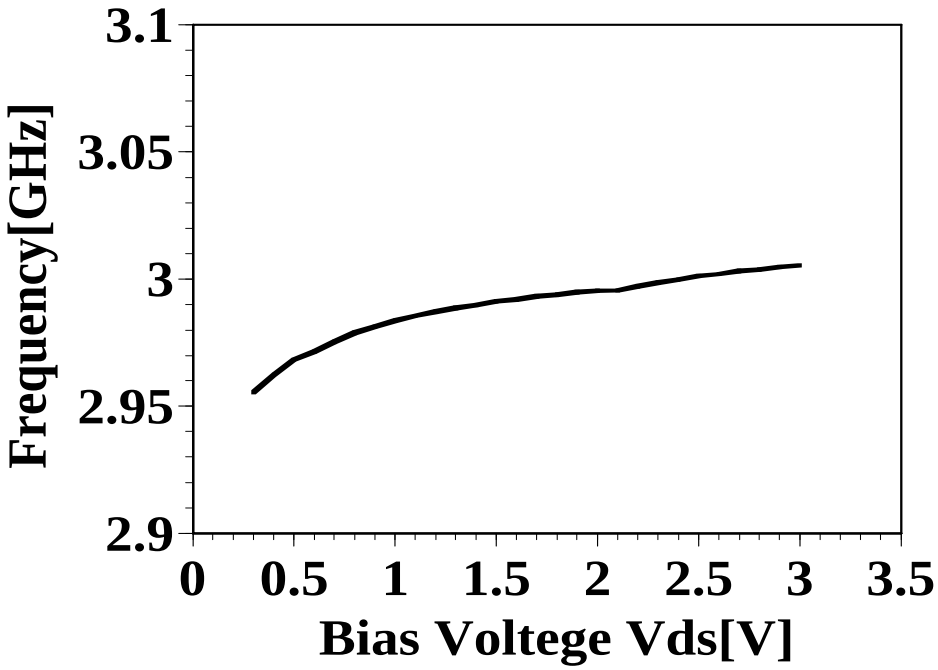

Fig. 4-5: Oscillation frequency versus bias voltage.

Lg = 15.0 mm, Ld = 15.0 mm Ls = 20.6 mm

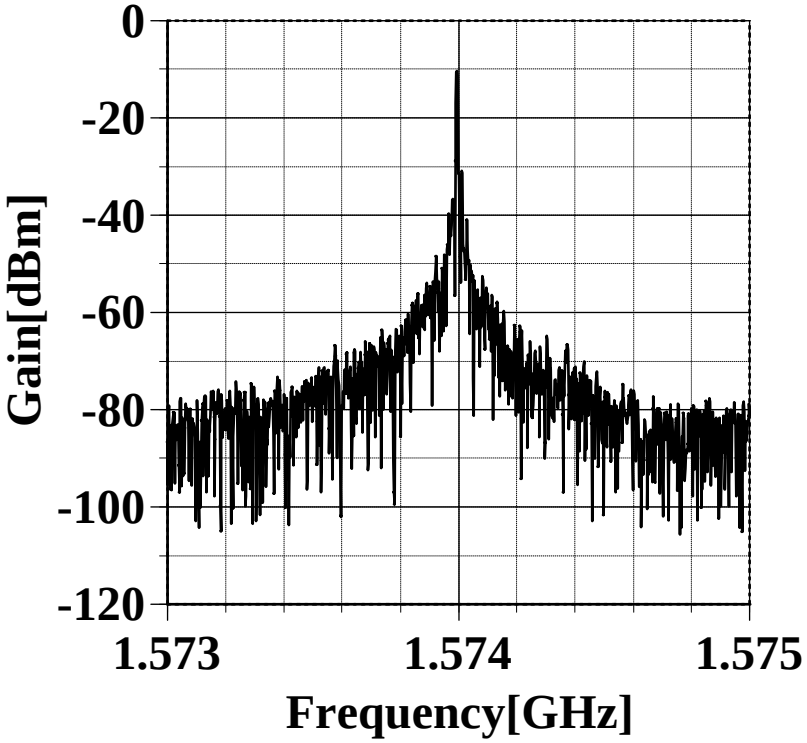

Fig. 4-6: Oscillation spectrum.

VBW = 20 MHz, REW = 10 MHz, Lg = 15.0 mm, Ls = 20.6 mm, Vds = 3.0 V

4.3. Active Antenna Using Parasitic Resonator

In this section, in order to improve the oscillation Q and the radiation pattern, an oscillator with a parasitic resonator is proposed in which a half-wave dipole parasitic resonator is placed between the gate and the drain of the oscillator. When a dipole is placed as a parasitic resonator, the gain may be improved if the dipole works as a director in a Yagi-Uda antenna. On the other hand, if a strip-type element with a narrow width is placed as a parasitic resonator, the gain is degraded and the radiation pattern is often destroyed. Further, if the parasitic element is a planar structure such as a patch antenna, the oscillation condition may be changed substantially depending on the positional relationship with the antenna. In this section, a wire dipole with a few parameters is used as the parasitic resonator. This dipole is fabricated with copper wire and is fixed on the oscillator by using an insulator with a relative permittivity close to 1.0 so that an effect on the oscillation is minimized. Fig. 4-8 shows the equivalent circuit including the parasitic resonator. It is considered that feedback exists by means of coupling to the loads connected to the gate and the drain.

Fig. 4-9 shows the variations of the oscillation frequency dependent on the length of the parasitic resonator and the distance from the oscillator. When the length of the parasitic resonator is made shorter than about one-half wavelength, the oscillation frequency increases to a certain extent. When the distance from the oscillator is decreased, the oscillation frequency becomes lower, whereas it approaches that without the parasitic resonator if the distance is increased. As shown in Fig. 4-8, the parasitic resonator changes the oscillation condition.

Fig. 4-10 shows the average of the oscillation level when the length of the resonator and its distance from the oscillator are varied. The oscillation level is measured from the reception by a dipole antenna placed horizontally at a distance of about 30 cm from the active antenna. It is found that the oscillation level does not change when the length and the distance are varied. It is also seen that the oscillation level increases somewhat (about 5 dB) over the value of the oscillator alone if the parasitic resonator is provided.

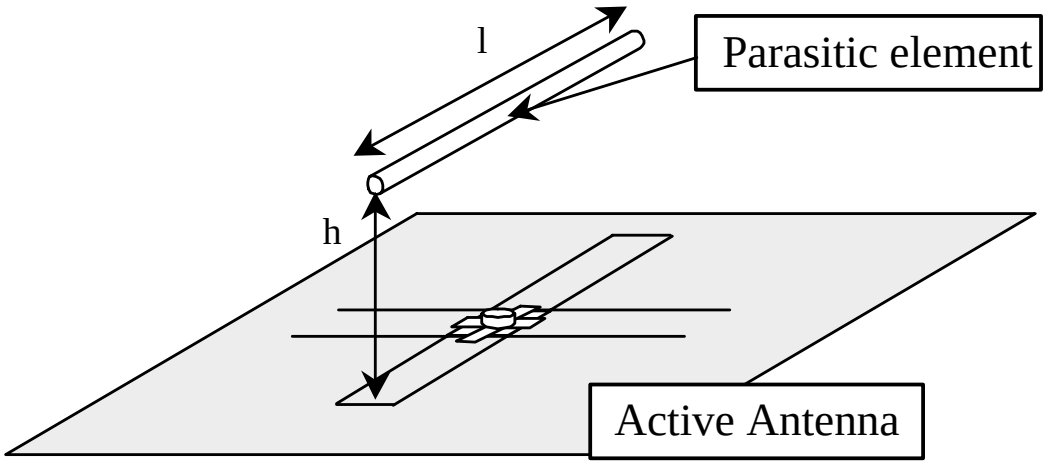

Fig. 4-7: Active antenna with parasitic element.

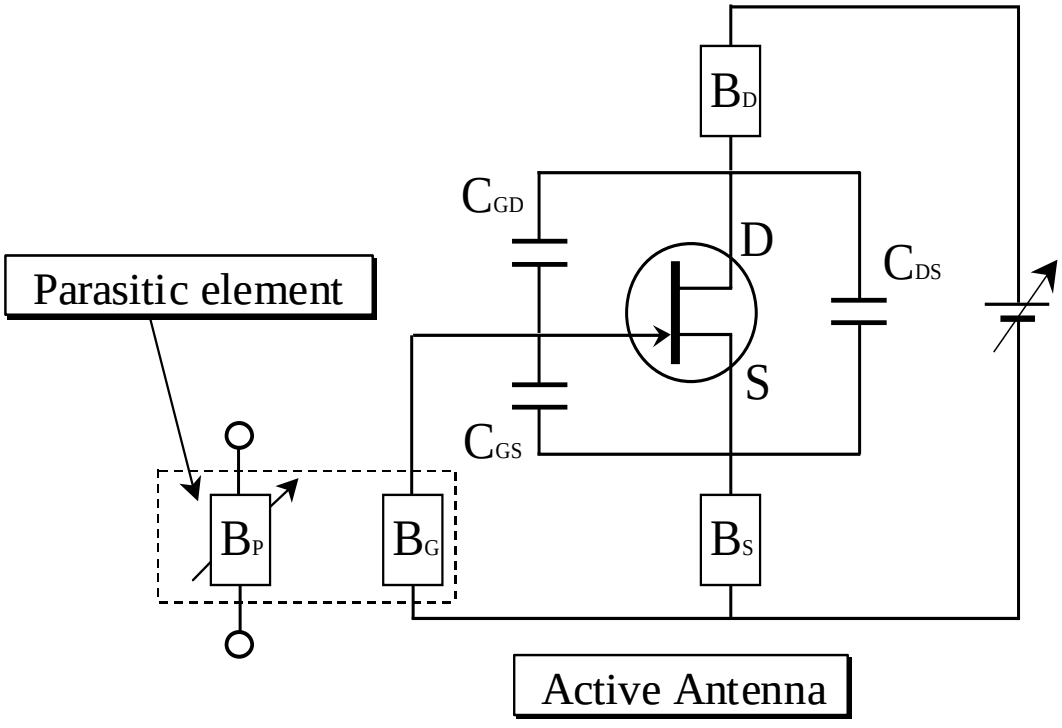

Fig. 4-8: An equivalent circuit of active antenna with parasitic element

Bp: reactance ingredient of parasitic element, Bx: reactance ingredient of load,

Cx: stray capacitance

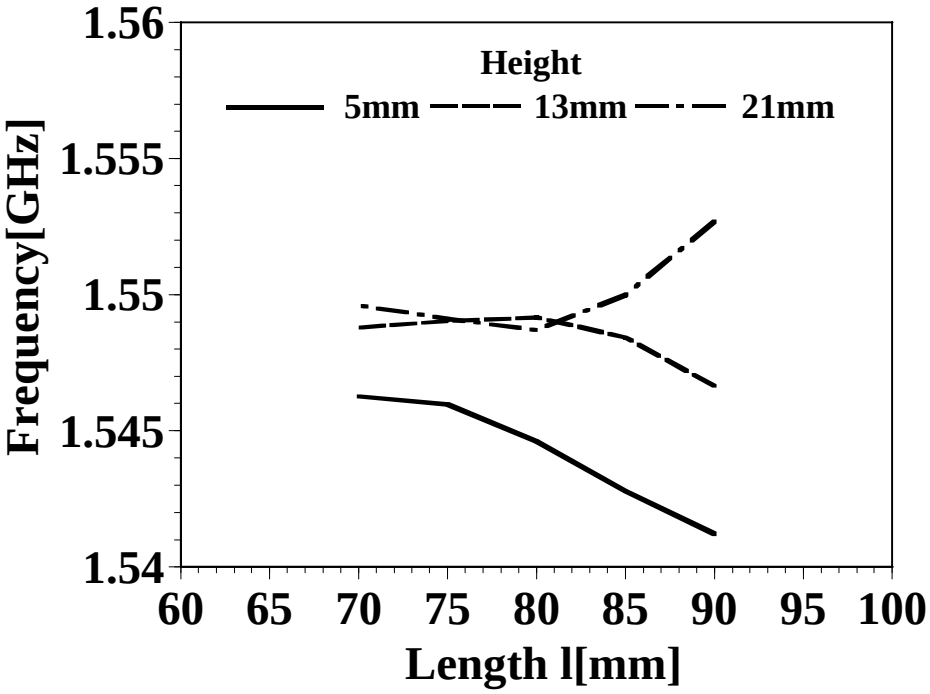

Fig. 4-9: Oscillation frequency versus parasitic element

Lg = Ld = 43.5 mm, Ls = 30.0 mm, Vds = 3.0 V

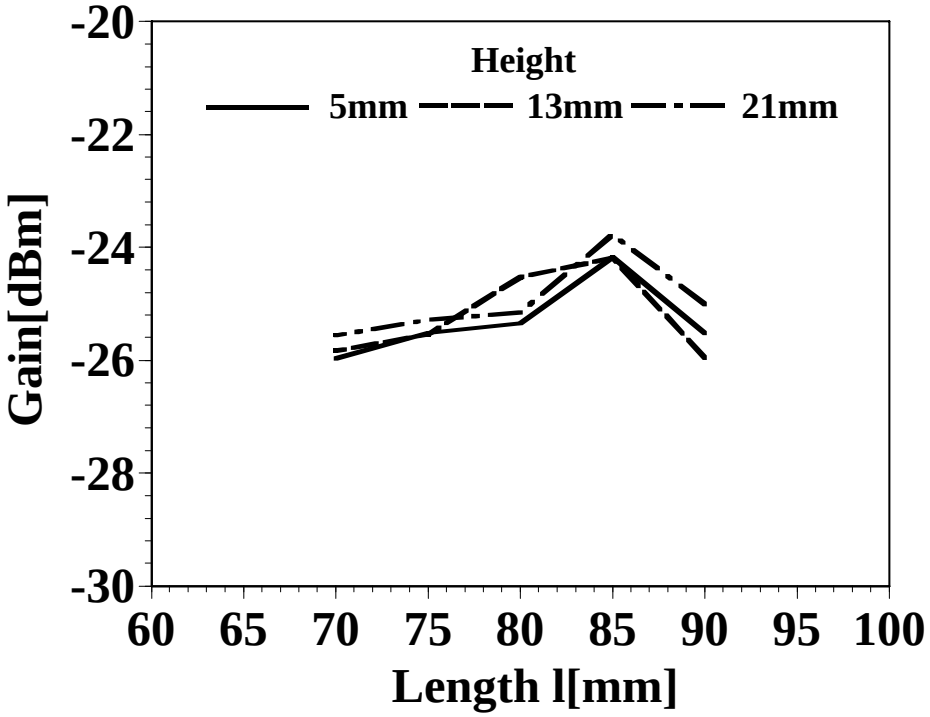

Fig. 4-10: Gain versus parasitic element

Lg = Ld = 43.5 mm, Ls = 30.0 mm, Vds = 3.0 V

4.4. Improvement of Radiation Pattern

Fig. 4-11 shows the effect of improvement of the radiation pattern by the parasitic resonator. It is clear from the experimental results in Fig. 3 that the radiation takes place from the 1/4 wavelength resonator loaded to the gate. In this case, the main electric field is parallel to the gate-to-drain. However, since the backside of the substrate is metalized, there arises a TEM mode that radiates from the edges of the substrate and is diffracted at the edges so that the radiation pattern in the normal direction is disturbed as shown in Fig. 4-11. This disturbance is alleviated by the parasitic element. Measurement is carried out with a receiving antenna (a dipole antenna with a nominal gain of 2 dBi) placed 30 cm away. From the measured result, the maximum received power in the front direction is -24.2 dBm. The E.1.R.P. is not derived, since the measurement of the antenna gain is difficult. In the case of a single element, the E-plane radiation pattern indicates strong radiation in the directions of 90° and 270°. Hence, it is considered that the electromagnetic wave is radiated more strongly in the gate-to-drain direction on the side rather than the surface of the dielectric substrate. Also, the H-plane radiation pattern shows strong radiation from the surface and the backside of the dielectric substrate. Next, when the parasitic element is provided, the radiation pattern is more focused toward the front direction than that for the single active antenna so that the F/B ratio is improved by about 5.5 dB This is caused by suppression of the parallel plate mode generated inside the dielectric substrate by means of the parasitic resonator. The parasitic radiator is coupled to the oscillator and acts as a director of the Yagi-Uda antenna. Therefore, the radiation to the side of the substrate is suppressed and is focused in the front direction.

In the active antenna using the coplanar waveguide with a ground plane, the parallel plate mode is generated so that the radiation pattern depends on the size of the substrate. Both L1 and L2 are increased and decreased by about one-quarter wavelength at the oscillation frequency. In both cases, the gain in the front direction is found to be improved by about 5 dB as in the results shown in Fig. 4-11.

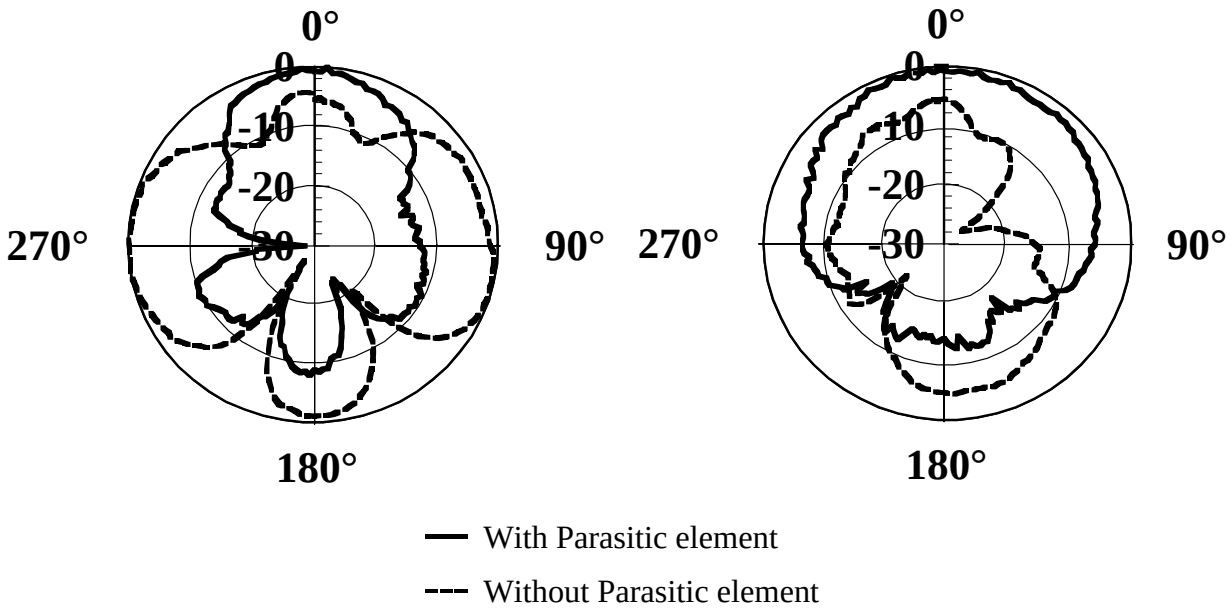

(a)E-plane (b)H-Plane

Fig. 4-11: Radiation pattern
Lg = Ld = 43.5 mm, Ls = 30.0 mm, L1=135.0 mm, L2=70.0 mm,
l=70.0 mm, h=10.0 mm, Vds = 3.0 V

4.5. Stability of Oscillation Frequency

This section considers the oscillation frequency stability of the active antenna. If the oscillation frequency stability is higher, the device becomes more tolerant to modulation so that it is more suitable for a high-capacity communication. Therefore, the requirements for the active antenna increase as the oscillation frequency stability becomes higher. In this section, the oscillation frequency stability is defined by Eq.(4.1). The frequency is measured for about 30 minutes to 1 hour under a particular measurement condition (such as a certain temperature, a time duration after a certain time from the start of oscillation). The frequency variations during this period (maximum frequency - minimum frequency) is divided by the average frequency. Its percentage is used as the oscillation frequency stability: S_t

$$S_t = \frac{f_{\max} - f_{\min}}{f_{avg}} \tag{4.1}$$

where S_t is the stability in the time duration t under a certain condition, $f_{\min}$ is the maximum frequency, $f_{\min}$ is the minimum frequency, and f_{avg} is the average frequency. This oscillation

frequency stability S_t indicates that the fluctuation of the oscillation becomes smaller and the oscillation becomes more stable as the numerical value becomes smaller.

In this section, the oscillation frequency stability is evaluated for the temperature variation, current and voltage (bias) variation, and time variation. The oscillation frequency stability of the active antenna is measured by the system shown in Fig. 4-12. In general, because semiconductor devices (GaAs FET in this chapter) are easily affected by temperature, measurements are carried out in a constant-temperature oven. A constant voltage power supply is used for biasing. The oscillation frequency is measured by a dipole antenna placed horizontally about 30 cm from the active antenna. The received electromagnetic wave is measured with a spectrum analyzer.

First, the temperature stability of the oscillation frequency between room temperature (15°C) and high temperatures is shown in Fig. 4-13. The variation of the stability of the oscillation frequency versus temperature is studied. As an overall tendency, the oscillation frequency increases as the temperature becomes higher and the stability becomes lower. The cause lies mainly in the semiconductor and the antenna configuration does not contribute to degradation of the stability. For improvement, it is necessary to replace the device with another having better characteristics. Under the usual operating conditions, namely, at a temperature around 20°C, the stability is somewhat higher than at other temperatures. The subsequent stability measurement is carried out at about 20°C.

Fig. 4-14 shows the variation of the stability of the oscillation frequency when the bias voltage is varied. It is confirmed that the stability improves as the bias voltage is increased. However, as in the case of the temperature dependence of the stability, the bias dependence of the stability is largely affected by the semiconductor device. A certain improvement is expected if the device is replaced. No improvement is expected by replacement of the antenna.

Next, the time variation of the oscillation frequency and the stability after oscillation is initiated by an application of a constant bias is measured within a constant temperature oven at 25°C with a constant bias of 3.0 V. In order to study differences in the stability dependent on the active antenna configuration, three structures are investigated. The first is the structure in Fig. 4-1 made of a single oscillator only. The second is a combination of the general active antenna and the planar antenna. As shown in Fig. 4-15, an oscillator with a two-layered configuration is used in which the patch antenna is connected to the active antenna with a short pin [27]. The length of the patch antenna is designed according to the oscillation frequency. An offset feed is used. The dielectric substrate has a relative permittivity of 2.6 and a thickness of 0.9 mm. The height of the patch antenna and the oscillator is 10mm. Another structure is the oscillator with a parasitic resonator shown in Fig. 4-7.

The length of the parasitic resonator is 70 mm while its height from the oscillator is 10 mm, which is the same as that in the oscillator with a patch antenna. The time variations of the oscillation frequency and the stability for the three structures are shown in Fig. 4-16 to 18. The stability is computed using Eq. (4.1) with a time interval of about 30 minutes.

Due to the effect of the semiconductor device, the stability is low immediately after the start of oscillation in all cases. However, the stability increases as time progresses. When the patch antenna is provided with a short pin, the stability is improved somewhat over the single oscillator. However, the stability is further improved when a parasitic resonator is placed over the case with a patch antenna.

Table. 4-1 shows the average stability and the Q in the steady state (more than 1000 minutes after start of oscillation), note that Q is obtained as a quotient of the resonant frequency divided by the frequency range of 3 dB lower than the maximum power. The stability is improved by about fivefold over the single oscillator if a parasitic resonator is used. Further, Q is increased by about 40%. The reason is that the parasitic resonator diverts the radiation into the direction normal to the dielectric substrate so that the dielectric loss of the propagation in the dielectric substrate is reduced. Also, when the patch antenna is placed as shown in Fig. 4-15, the stability is improved by about threefold while Q is not increased. This is because the dielectric loss in the oscillator is reduced while the dielectric loss in the patch antenna is increased so that Q is decreased. It is now confirmed that the oscillator Q is increased and the oscillation stability is improved if a parasitic resonator is placed without modifying the antenna. However, quantitative relationships of the dielectric loss, radiation loss, and conductor loss for each structure must be derived accurately by means of numerical calculations of the electromagnetic field distributions near the antenna.

When the parasitic resonator is placed closer to the antenna as shown in Fig. 4-19, the oscillation frequency is reduced. On the other hand, if the parasitic resonator is moved away from the antenna, the oscillation frequency approaches that of the oscillator alone and the stability is reduced. Further, it is found in Fig. 4-20 that the oscillation frequency is reduced if the length of the parasitic resonator is increased. The stability is not strongly dependent on the length of the parasitic resonator. However, if the length exceeds that of the load of the gate-to-drain, the stability approaches that of the oscillator alone. Thus, the parasitic resonator has been demonstrated to be related to the oscillation.

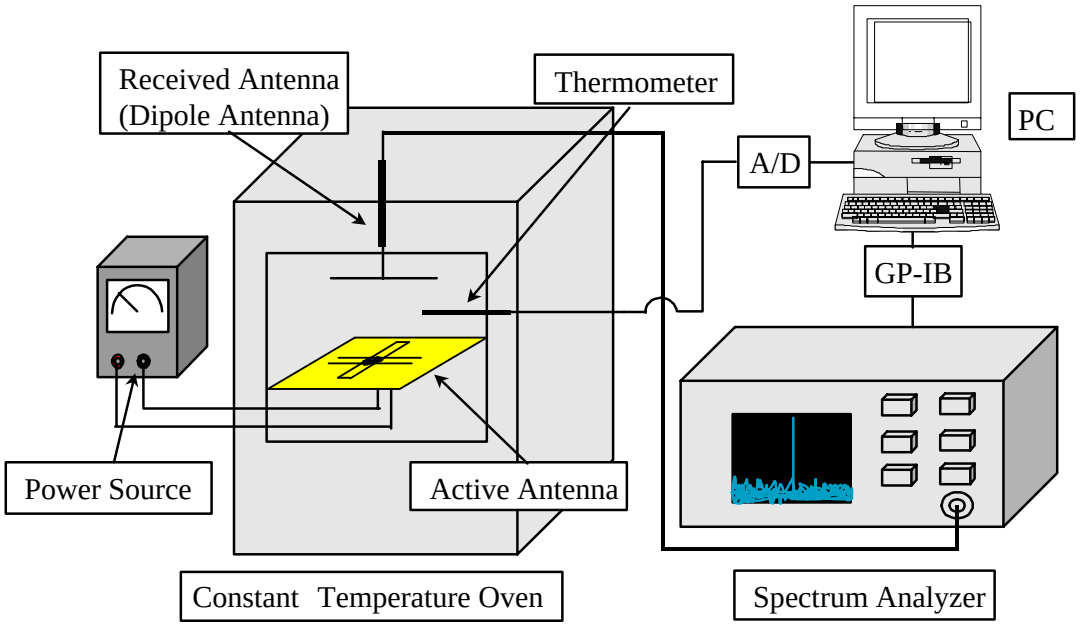

Fig. 4-12: Experimental set up for frequency stability measurement

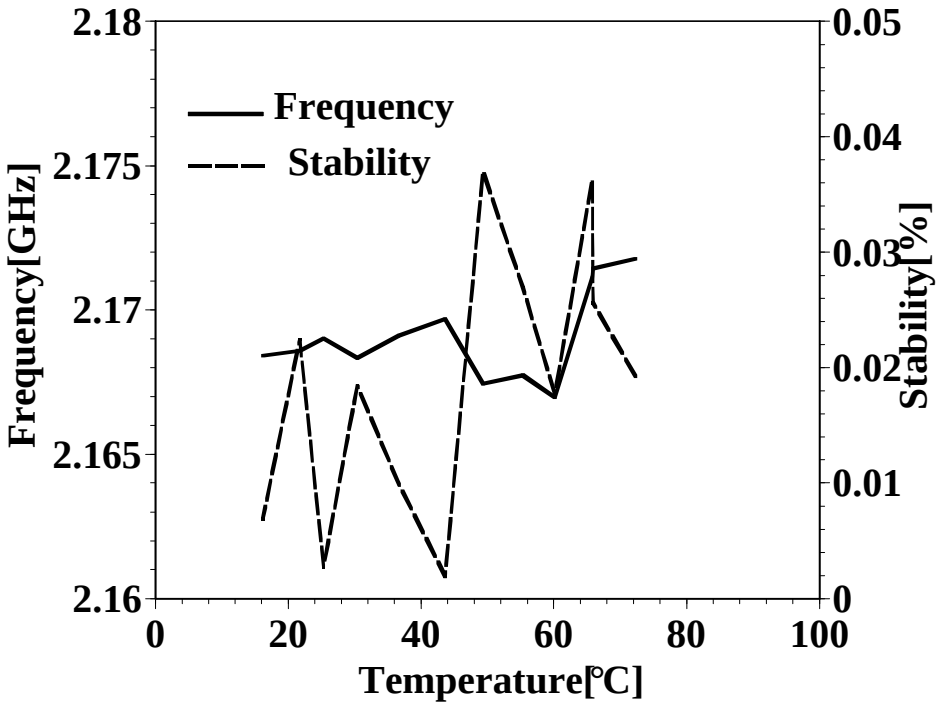

Fig. 4-13: Stability of oscillation versus temperature.

Lg = Ld = 43.5 mm, Ls = 30.0 mm, Vds = 3.0 V.

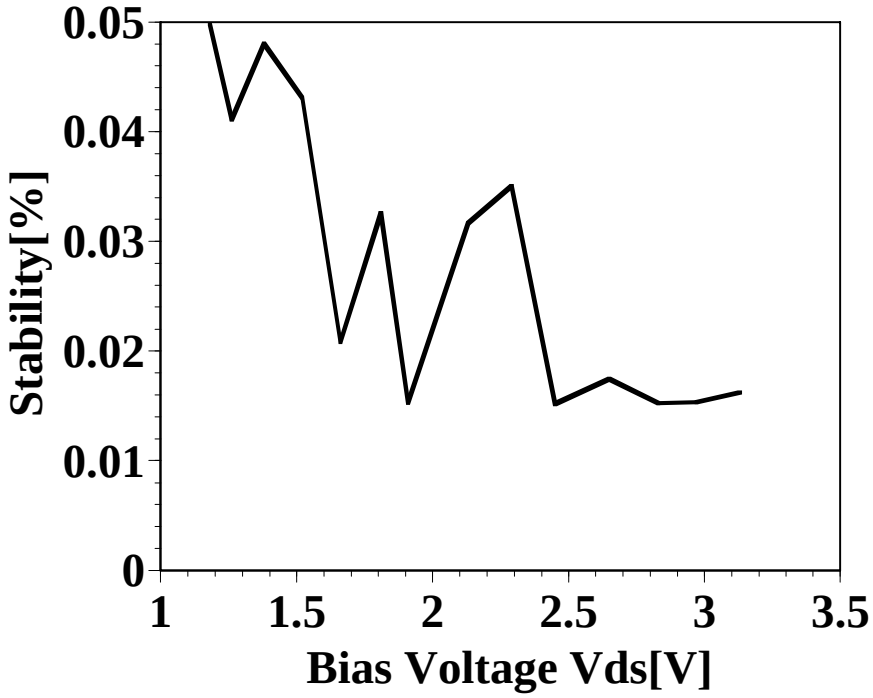

Fig. 4-14: Stability of oscillation versus bias voltage.
Lg=Ld=43.5mm, Ls=30.0mm, temperature=20°C.

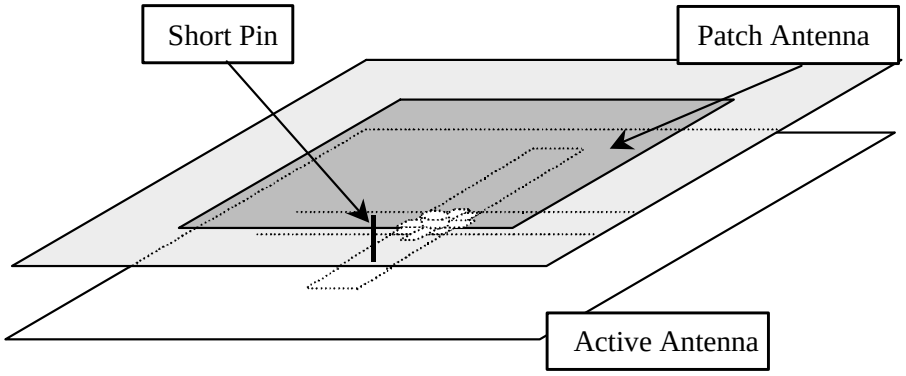

Fig. 4-15: Active antenna loaded with patch antenna

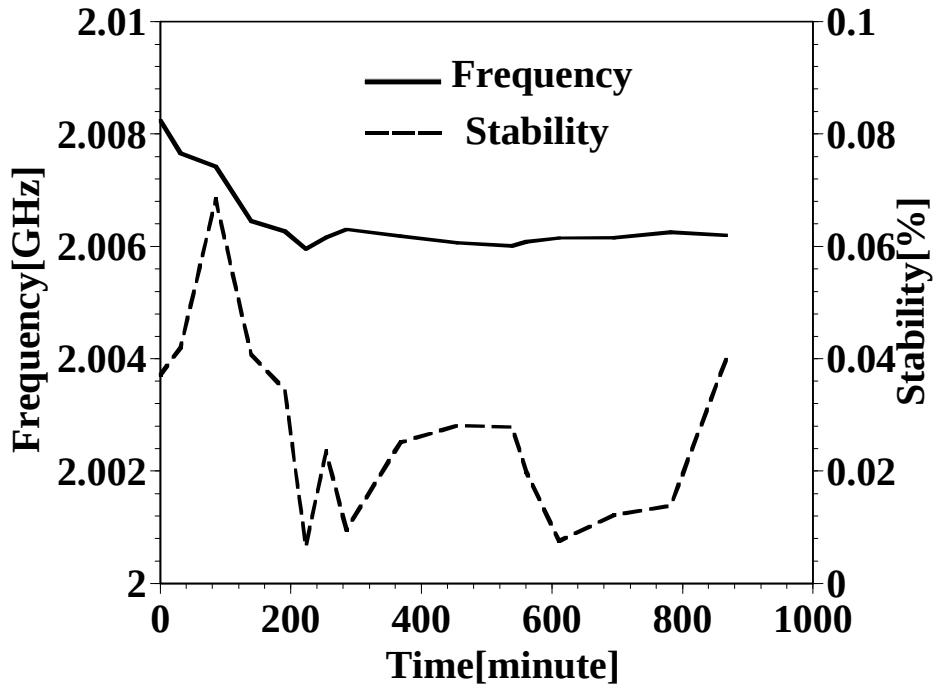

Fig. 4-16: Oscillation Stability as a function of measurement time (only oscillator).
Lg = Ld = 43.5 mm, Ls = 30.0 mm, Vds = 3.0 V, temperature = 20°C.

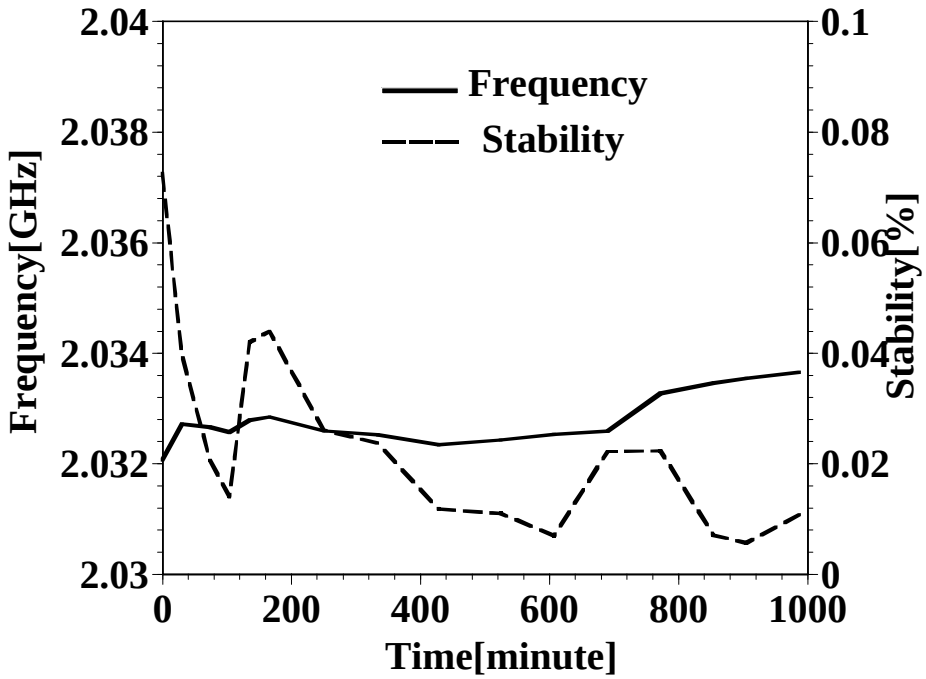

Fig. 4-17: Oscillation Stability as a function of measurement time (with patch antenna).
Lg = Ld = 43.5 mm, Ls = 30.0 mm, Vds = 3.0 V, temperature = 20°C.

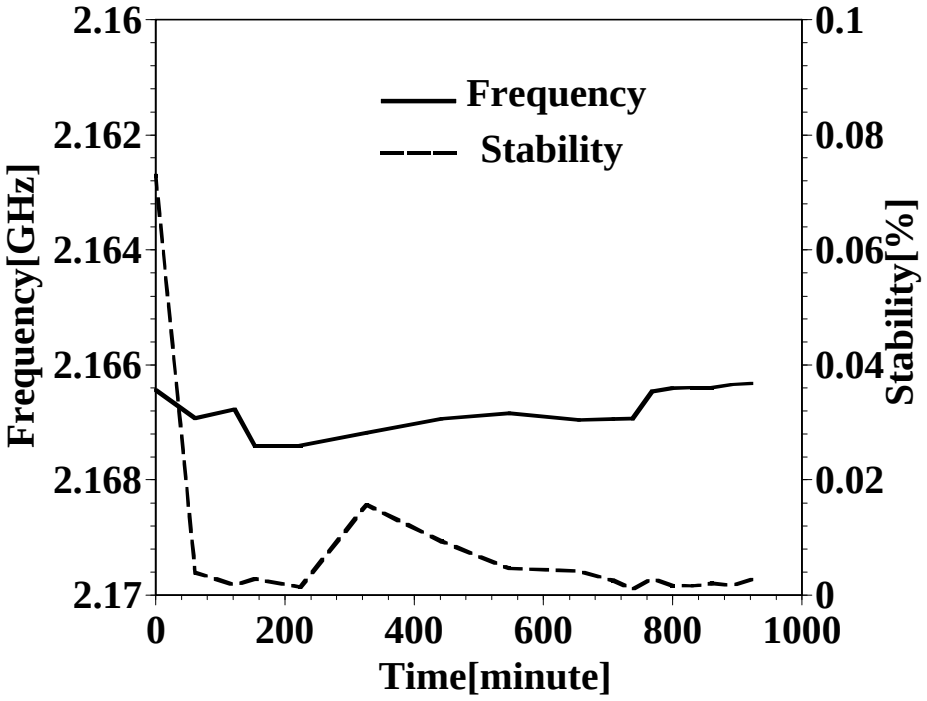

Fig. 4-18: Oscillation Stability as a function of measurement time (with parasitic element). Lg = Ld = 43.5 mm, Ls = 30.0 mm, Vds = 3.0 V, temperature = 20°C.

Table. 4-1: Oscillation stability and Q factor

	Oscillator only	With a patch antenna	Parasitic resonator
Stability (%)	0.05	0.03	0.01
Q [10^5]	4.91	4.82	6.97

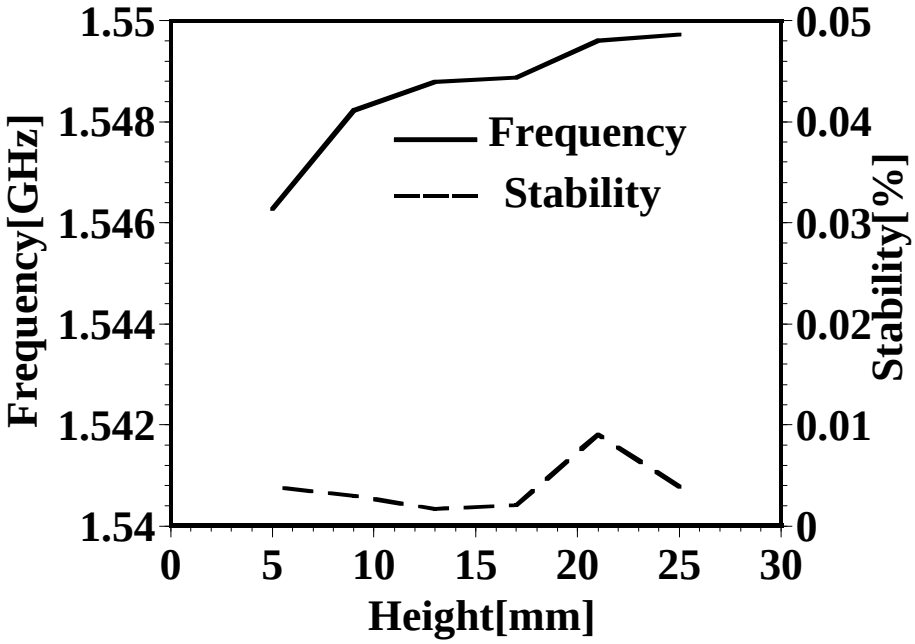

Fig. 4-19: Stability of oscillation versus height of parasitic element.

Lg = Ld = 43.5 mm, Ls = 30.0 mm, l = 70.0 mm, Vds = 3.0 V, temperature = 20°C.

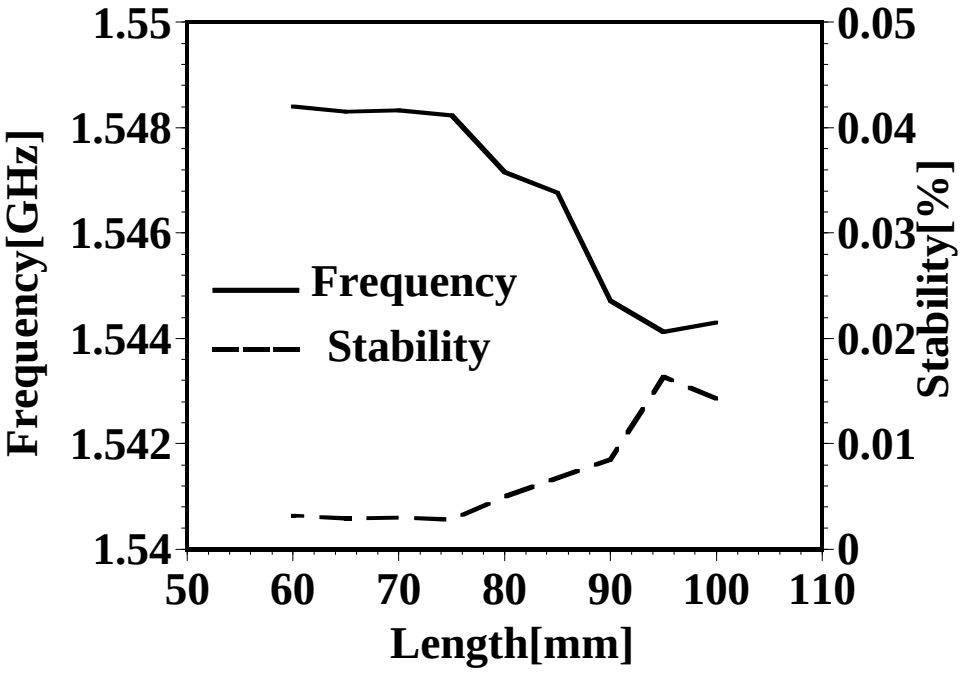

Fig. 4-20: Stability of oscillation versus length of parasitic element.

Lg = Ld= 43.5 mm, Ls = 30.0mm, h = 10.0 mm, Vds = 3.0 V, temperature = 20° C.

4.6. Self-oscillating Mixer Using Active Antenna With Parasitic Elements

This coplanar waveguide-fed active antenna using parasitic element is applied to self-oscillating mixer. To demonstrate the mixer operation, the dipole antenna placed above the active oscillator with parasitic element is fed by RF signal (f = 1.9 GHz) through coaxial cable on Fig. 4-21. The FET oscillator works as self-oscillating mixer and the IF signal is outputted from its gate in Fig. 4-21.

We discuss a change of the IF gain versus a position of parasitic element (x, y, z) in Fig. 4-22. The vertical axis is the relative gain (dB) that is compared only oscillator (no parasitic element). The x, y, z are parallel in gate and drain, above gate and drain and height of parasitic element, respectively. When the parasitic element is arranged in above of gate and drain, the IF gain is the highest. If the parasitic element is arranged in above of gate and drain, the IF gain does not change much. Accordingly, a strong electric field rises by a parallel course in gate and drain. When the parasitic element is arranged in near to an oscillator, the IF gain is the highest. But this oscillator cannot work mixer when distance of parasitic element and an oscillator is less than 10 mm. The IF gain versus length of parasitic element: L is shown Fig. 4-23. When the length of parasitic element is about 70 mm, the IF gain is the highest (up to about 15 dB). Then, the length of parasitic element (about 70 mm) is near to a half wavelength of the RF signal (f = 1.9 GHz).

In this active antenna, the IF signal can be outputted from the ground board. The parasitic element is connected to IF output and arrange by L-shaped in parallelism to the gate and drain is shown Fig. 4-24. When the length of this parasitic element is about 42 mm, the IF gain is the highest. Then, the length of parasitic element (about 42 mm) is near to a quarter wavelength of RF signal (f = 1.9 GHz). A change of the IF gain versus RF is shown Fig. 4-25. When the parasitic element is arranged, compared with only oscillator, the IF gain improves about 35 dB.

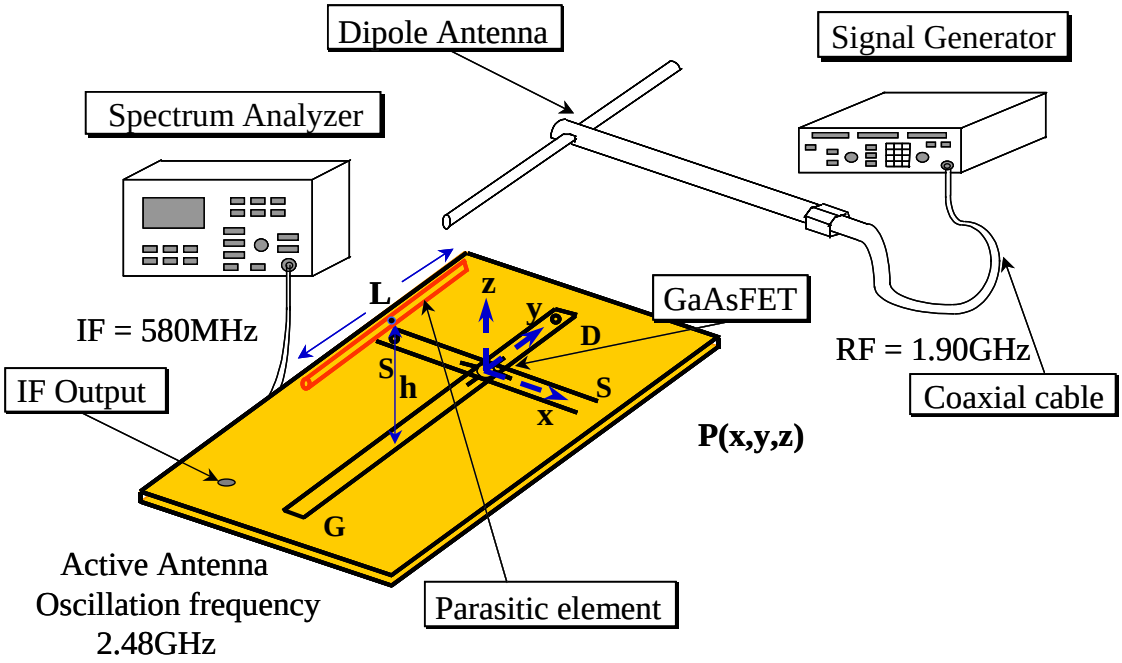

Fig. 4-21: Measurement setup for self-oscillating mixer

Lg = Ld = 37.0 mm, Ls = 25.0 mm, Oscillation frequency = 2.48 GHz

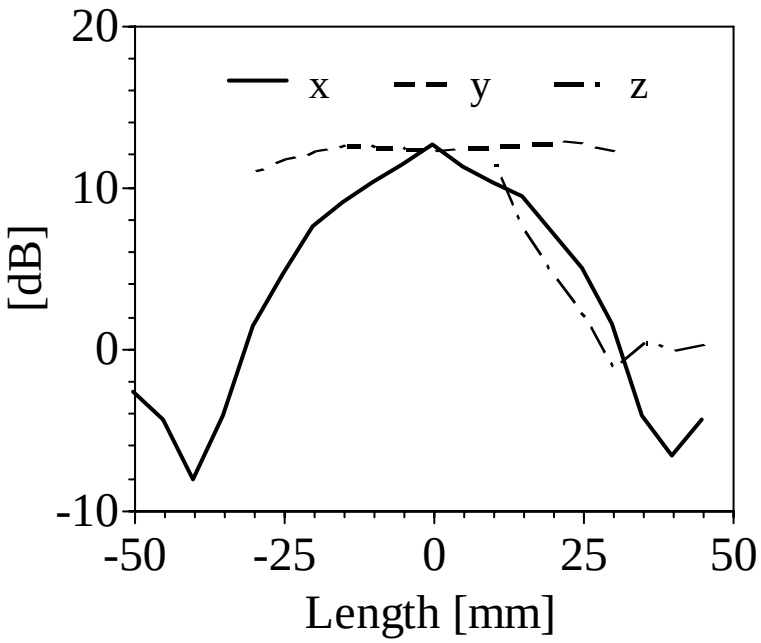

Fig. 4-22: IF Gain versus position of parasitic element

x = 0 mm, y = 10 mm, z = 1 mm, L = 70mm

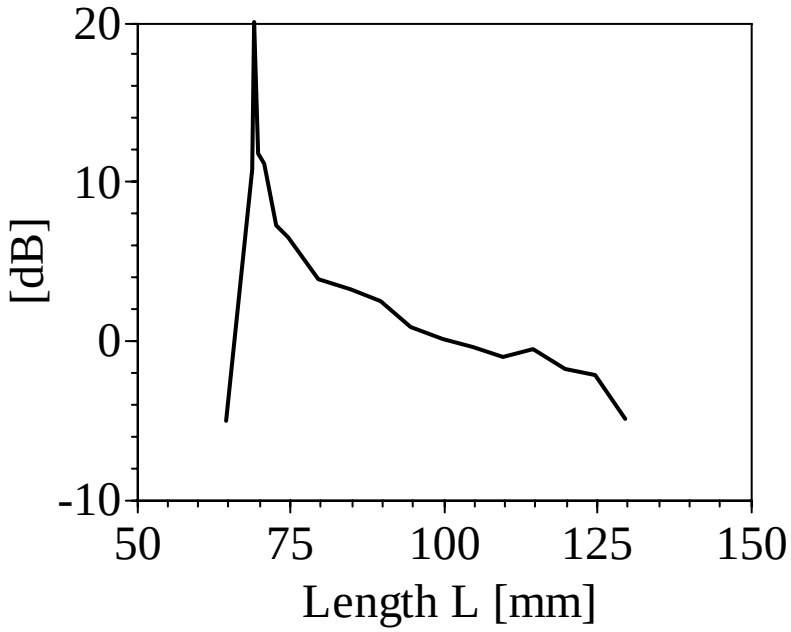

Fig. 4-23: IF Gain versus length of parasitic element

x = 0 mm, y = 10 mm, z = 1 mm

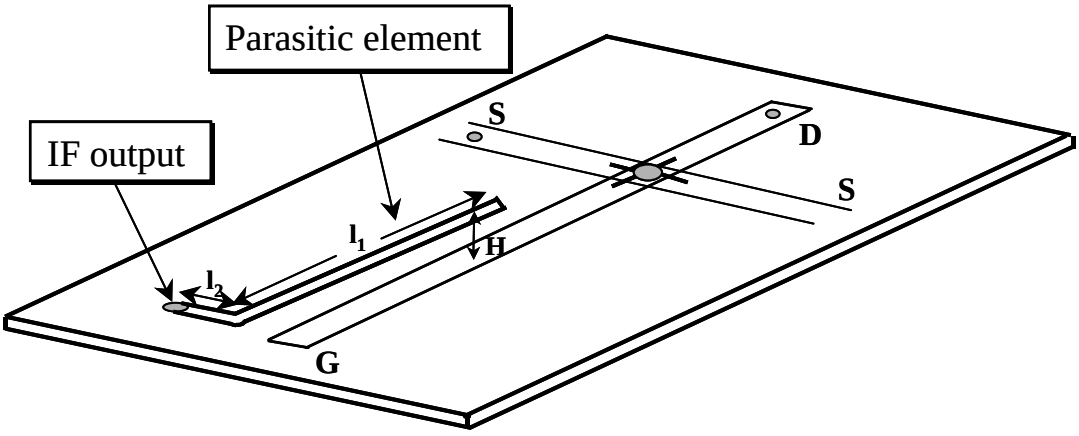

Fig. 4-24: Active antenna with quarter wavelength parasitic element for self-oscillating mixer

l_1 = 15.0 mm, l_2 = 32.0 mm, L = 42.0 mm, H = 5.0 mm

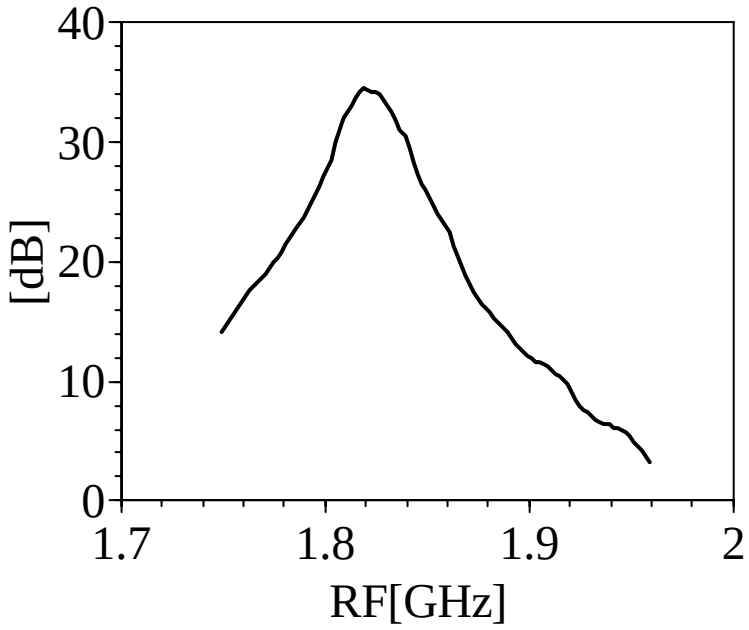

Fig. 4-25: IF Gain versus RF
Oscillation frequency = 2.49 GHz

4.7. Summary

Regarding the stability of the single active antenna, this chapter proposed an FET active antenna using a coplanar waveguide and an active antenna with a parasitic element in which a half-wave dipole parasitic resonator is placed above the gate-to-drain. By providing the parasitic resonator, the frequency stability was improved fourfold over the single oscillator and the active antenna combined with a patch antenna, without modifying the active antenna. It is confirmed that the parasitic resonator can improve the radiation pattern.

This chapter also proposed the self-oscillating mixer using the active oscillator with the parasitic element of half-wavelength dipole. The IF gain of this self-oscillating mixer was increased about 35 dB by the parasitic element, compared only oscillator.

References

[21] J.Lin, T.Itoh, “Low-Cost Adaptive Arrays for Analysis of Wireless Systems”, IEEE Trans Microwave Theory Tech Vol.42, p2186-2194, 1994.

[22] M.Kim, E.Sovero, J.Hacker, M.Lisio, J.Chiao, S.Lie, D.Gagnon, J.Rosenberg, “A 100-element HBT grid amplifier”, IEEE Trans Microwave Theory Tech Vol.41, p1762-1771, 1993.

[23] K.Cha, S.Kawasaki, T.Itoh, “Transponder using self oscillating mixer and active antenna”, 1994 IEEE MTT-S, TU3F-57, p425-428, 1994.

[24] W.K.Leverich, I.Wu, K.Chang, “FET active slotline notch antenna for quasi-optical power combining”, IEEE Trans Microwave Theory Tech Vol.41, p1515-1517, 1993

[25] T.Itsui, K.Hayata, Y.Tomioka, M.Tanaka, S.Kawasaki, “Active integrated antenna using a planar slot antenna miniaturized by the use of two layers”, Tech Rep IEICE AP96-86, p31-34, 1996.

[26] J.M.Laheurte, G.Forma, “CPW-fed oscillating microstrip antennas”, Electron letter, Vol.32, p85-86, 1996.

[27] A.Matsui, S.Okamura, “On the radiation characteristics of an active antenna element using a microstrip antenna ”, Tech Rep IEICE AP96-83, p13-18, 1996.

[28] T.Tsutsumi, N.Gaya, W.Chujo, H.Shimakage, C.Wang, “Experiment of a coplanar feed active antenna using a half wave slot and FET oscillator”, Tech Rep IEICE AP95-17, p9-14, 1995.

[29] M.kaneko, T.Goi, A.Tanaka, S.Kawasaki, “3×3 strong coupling quasi-optical array with the stable in-phase mode by dielectric resonators ”, ISAP’96, p133-133, 1996.

[30] JW.Boyles, “The oscillator as a reflection amplifier: An intuitive approach to oscillator design”, Microwave Journal, p83-98, 1986.

5. Conclusions

This thesis described smart antennas which are high function antennas to the demand of high-speed mobile communications. Investigation and verification of smart antennas were performed from three different viewpoints. One is sector antenna, anther is digital beam forming array antenna, and the other is active antenna.

In chapter2, this thesis presented 6-sector beam antenna using proximity coupled taper slot antenna in order to aim at low cost and simple manufacturing process of sector beam antennas. By arranging reflection board of parasitic element, side lobe level is suppressed. 6-sector beam antenna has uni-directional pattern and its half power beam width is about 60° in H plane. Therefore this antenna is suited for delay profile measurement in high frequency band. This chapter also presented a delay profile was measurement by using the PCTSA sector antenna at outdoor. The 6-sector antenna used could reduce a delay spread many times than omni directional antenna used in almost fixed points and movement environment. Therefore, the sector antenna is suited for high-speed wireless data transmission, because this sector antenna can reduce effectively a delay spread at outdoor.

In chapter3, this thesis proposed 2.6 GHz low cost DBF array antenna system and reported its evaluation based on our experimental results. The proposed system was partially constructed by digital devices for the simplification of hardware, and employs some techniques for the resolution improvement. The system was evaluated through the DOA estimation by the MUSIC algorithm inside a radio anechoic chamber. As a result, we found that the proposed system estimates the DOA with the highest accuracy at which MUSIC algorithm could perform. Moreover, this thesis discussed on the estimation errors. We also found that the estimation error was particularly affected from the inaccurate element interval. This chapter also proposed the calibration method for restraint of phase and amplitude unbalance among the array branches by using reference antenna. We also demonstrated near zero IF receiver. The conversion gain of this receiver was about 5 dB. We also examined this proposed receiver’s ability to function as a digital beam former. As a result, we found that the ability of receiver is almost same that of common receivers using isotopic antenna.

In chapter4, regarding the stability of the single active antenna, this thesis proposed an FET active antenna using a coplanar waveguide and an active antenna with a parasitic element in which a half-wave dipole parasitic resonator is placed above the gate-to-drain. By providing the parasitic resonator, the frequency stability is improved fourfold over the single oscillator and the active antenna combined with a patch antenna, without modifying the active antenna. It is confirmed that

the parasitic resonator can improve the radiation pattern. This chapter also proposed the self-oscillating mixer using the active oscillator with the parasitic element of half-wavelength dipole. The IF gain of this self-oscillating mixer is increased by the parasitic element, compared only active oscillator.

The foundation materials to realize high-speed wireless communications by showing the example of these smart antennas were provided. The common point of these antennas is raising the performance of the communication equipment not only combining antenna technology but also combining other technology (signal processing, microwave circuit, etc.). In order to realize high-speed wireless communications, it is indispensable to unite with two or more technology like smart antennas.

Acknowledgements

I wish to express my gratitude to my sincerest acknowledgment to my supervisor Associate Professor Hiroyuki Arai for his continuous guidance throughout this work. I am grateful to Professor Masahiro Toki, Professor Yasuo Hirose, Professor Yasuo Kokubun, and Associate Professor Toshihiko Baba with Yokohama National University for their useful discussions and the critical reading of manuscript. I am indebted to Dr. Yoshio Ebine of NTT DoCoMo Co. Ltd, Professor Tatsuo Itoh of University of California, Los Angeles, Dr Yongxi Qian of National Semiconductor Co. Ltd, Professor Shigeki Kawasaki of Tokai University, and Dr. Koichi Ichige with Yokohama National University for his useful and fruitful discussions. I am grateful to Mr. Kiyoshi Yamasaki with ASTEC Co. Ltd., Dr. Masahiro Karikome, with Nihon Dengyokousaku Co. Ltd., for their useful discussion and encouragement. I acknowledge SCAT (Support Center Advanced Telecommunication) for their scholarship. Thanks are also due to the members of Associate Professor Arai's group, Yokohama National University.

Finally, I acknowledge my parents and my family for their mental support.

Publication List

Following lists contain the related publications of this dissertation.

Papers

1. K.Mori, H.Arai, “Active antenna Using a Parasitic element”, IEICEJ Transaction B Vol.J82-B, No.9, pp.1722-1729, September 1999 (in Japanese).
2. K.Mori, H.Arai, “Study of Active antenna Receivers and Calibration Method for Digital Beamforming”, IEICEJ Transaction B, 2002 (in Japanese, submitted in 2001).

Letters

1. K.Mori, Y.Inoue, K.Ichige, H.Arai, ”DOA Estimation by DBF Array Antenna Experiments of DOA Estimation by DBF Array Antenna at 2.6GHz ”, IEICE Trans. Comm., vol. E-84-B, No.7, pp1871-1875, July 2001.

International Conferences

1. K.Mori, H.Arai, “Active Antenna Using Parasitic Elements”, IEEE Antennas and Propagation International Symposium (APS’98), pp.1636-1639, Atlanta, U.S.A, June 1998.
2. K.Mori, H.Arai, Y.Ebine, “A Method of Radiation Pattern Enhancement for 6-Sector Antenna Using Proximity Coupled Taper Slot”, KJJC-AP/EMC/EMT'98, pp.177-180, Pusan, Korea, Sep 1998.
3. K.Mori, H.Arai, Y.Ebine, “The Delay Profile Measurement By 6-Sector Proximity Toper Slot Antenna”, WPMC'98, pp.385-388, Yokosuka, Japan, Nov 1998.
4. K.Mori, H.Arai, Y.Ebine “A 12-Sector Antenna Using Proximity Coupled Taper Slot”, IEEE Antennas and Propagation International Symposium (APS’99), pp.2412-2415, Orland, U.S.A, July 1999.
5. K.Mori, M.Jittoh, H.Arai, “Self-oscillating Mixer Using Active Antenna With Parasitic Element”, Asia-Pacific Microwave Conference (APMC’99), pp.84-87, Singapore, Dec 1999.
6. K.Mori, H.Arai, Y.Ebine, “Delay Profile Measurement by the Sector Antenna at the Outdoor”, Antennas and Propagation Symposium, 2P7, Davos, Switzerland, Apr 2000.
7. K.Mori, H.Arai, Y.Ebine, “The DOA Estimation by Delay Profile Measurement Using the

Sector Antenna", IEEE Antennas and Propagation International Symposium (APS'00), pp.454-457, Salt Lake City, U.S.A, July 2000.

8. K.Mori, Y.Inoue, H.Arai, "The DOA Estimation Using The Low Cost DBF Array Antenna", International Symposium on Antennas and Propagation (ISAP'00), pp.1645-1648, Fukuoka, Japan, Aug 2000.
9. K.Mori, Y.Inoue, H.Arai, "A digital beam forming by using low cost receiver at 2.6 GHz", IEE International Conference on Antennas and Propagation (ICAP'01), pp.24-27, Manchester, UK, Apr, 2001.
10. K.Mori, H.Arai, Y.Qian, T.Itoh, "Direct Conversion Receiver for Digital Beamforming at 8.45GHz", IEEE MTT-S International Microwave Symposium, WEIF-45, Phoenix, U.S.A, May 2001.
11. K.Mori, Y.Inoue, H.Arai, "DBF array antenna systems at 8.45 GHz", IEEE Antennas and Propagation International Symposium (APS'01), Boston, U.S.A, Jul 2001.

IEICE Technical Reports

1. K.Mori, H.Arai, Y.Ebine, "Delay Profile Measurement by the Sector Antenna at the Outdoor", IEICE technical report. Antennas and propagation, AP99-267, Aug, 1999.

General Conference and Society Conference of IEICE (in Japanese)

1. K.Mori, H.Arai, "An Active Antenna Using Tapered Slot Antenna", Society Conference of IEICE, B-1-123, Sep 1997.
2. K.Mori, H.Arai, " An Active Antenna with Parasitic element", General Conference of IEICE, B-1-109, Mar 1998.
3. K.Mori, H.Arai, Y.Ebine, "Broadband Frequency Characteristics of 6-Sector Antenna Using PCTSA", Society Conference of IEICE, B-1-105, Oct 1998.
4. K.Mori, H.Arai, Y.Ebine, "An antenna element for 12-Sector using PCTSA", General Conference of IEICE, B-1-154, Mar 1999.
5. K.Mori, H.Arai, K.Watanabe, I.Yoshii, R.Kohno, "A Trial Production of Digital Beam Forming Array Antenna at 2.6 GHz", Society Conference of IEICE, B-1-93, Sep 1999.
6. K.Mori, H.Arai, Y.Ebine, "Direction of Arrival by Delay Profile Measurement Using Sector Antenna", General Conference of IEICE, B-1-42, Mar 2000.
7. K.Mori, Y.Inoue, H.Arai, K.Watanaba, R.Kohno," A DOA Estimation by using a low cost

DBF receiver in an indoor environment", Society Conference of IEICE, B-1-26, Sep 2000.

8. K.Mori, H.Arai, Y.Qian, T.Itoh, "Prototype of Direct Conversion Receiver for Digital Beamforming at 8.45GHz", General Conference of IEICE, C-2-16, Mar 2001.
9. K.Mori, H.Arai, "Calibration method of DBF receiver by using a reference antenna", Society Conference of IEICE, B-1-150, Sep 2001.
10. K.Mori, H.Arai, "Active antenna Receiver for Digital Beamforming at 8.45GHz", General Conference of IEICE, SBC-1-5, Mar 2002.

Joint work

International Conferences

1. Y.Inoue, K.Mori, H.Arai, "DOA error estimation using 2.6GHz DBF array antenna", Asia-Pacific Microwave Conference (APMC'01), pp.701-704, Taipei, Dec 2001.
2. Y.Inoue, K.Mori, H.Arai, "DOA Estimation in Consideration of the Array Element Pattern", VTC'02 Spring, Birmingham, U.S.A, May 2002.

IEICE Technical Reports

1. Y.Inoue, K.Mori, H.Arai, "Study of DOA Estimation Error and Correction Methods using 2.6GHz and 8.45GHz Band DBF Array Antennas", IEICE technical report. Antennas and propagation, AP2001-231, Aug 2001.

General Conference and Society Conference of IEICE (in Japanese)

1. I.Yoshii, T.Yamada, K.Watanabe, R.Kohno, K.Mori, K.Fujimori, H.Arai, "DOA Estimation for 8GHz 6-Sector Antenna", Society Conference of IEICE, SB-1-6, Oct 1998.
2. T.Yamada, I.Yoshii, K.Watanabe, R.Kohno, K.Mori, K.Fujimori, H.Arai, "Adaptive Array Antennas Using 8GHz 6-Sector Antenna", Society Conference of IEICE, SB-1-12, Oct 1998.
3. K.Watanabe, T.Yamada, I.Yoshii, R.Kohno, K.Mori, K.Fujimori, H.Arai, "An Implementation of a Simplified Type of Digital Beam Forming Antenna Array System at 2.5GHz", General Conference of IEICE, B-5-38, Mar 1999.
4. Y.Inoue, K.Mori, H.Arai, K.Watanaba, R.Kohno, "A model of standard propagation using

low cost DBF receiver in a radio anechoic chamber", Society Conference of IEICE, B-1-27, Sep 2000.

5. Y.Inoue, K.Mori, H.Arai, "Error of The DOA Estimation with A DBF Array Antenna", General Conference of IEICE, B-1-44, Mar 2001.
6. Y.Inoue, K.Mori, H.Arai, "DOA Estimation Error and the Steering Vector of the DBF Array Antenna", Society Conference of IEICE, B-1-33, Sep 2001.
7. Y.Inoue, K.Mori, H.Arai, "The Effect of Minute Change of a Linear Array Element Interval for DOA Estimation Error", General Conference of IEICE, B-1-147, Mar 2002.